

DESIGN AND CHARACTERIZATION OF L-PROBE
REFLECTARRAY AND TRANSMITARRAY

NG WAI HAU

MASTER OF ENGINEERING SCIENCE

LEE KONG CHIAN FACULTY OF ENGINEERING AND
SCIENCE
UNIVERSITI TUNKU ABDUL RAHMAN
MARCH 2017

**DESIGN AND CHARACTERIZATION OF L-PROBE
REFLECTARRAY AND TRANSMITARRAY**

By

NG WAI HAU

A dissertation submitted to the Department of Electrical and Electronic
Engineering,
Lee Kong Chian Faculty of Engineering and Science,
Universiti Tunku Abdul Rahman,
in partial fulfillment of the requirements for the degree of
Master of Engineering Science
March 2017

ABSTRACT

DESIGN AND CHARACTERIZATION OF L-PROBE REFLECTARRAY AND TRANSMITARRAY

Ng Wai Hau

Reflectarray and transmitarray are two popular antenna arrays which have been widely used in many wireless applications such as the satellite communication transmissions, and radar systems due to their capability of providing high antenna gain in a certain direction. The two antenna arrays consist of an array of radiating elements illuminated by a feeding source. The working principle of reflectarray is similar to parabolic dish whereas transmitarray is akin to lens. For the case of reflectarray, oblique source illumination is often desirable as the blockage of main radiation beam by the feed can be reduced. For the case of transmitarray, the feed antenna can be placed directly at the center of the aperture. Similar to the conventional antenna array, active devices such as varactor and diode can be incorporated into the reflectarray and transmitarray to enable beam scanning.

In the first project, the L-shaped probes have been deployed for designing a broadband reflectarray, working at the center frequency of 7.1 GHz. The unit element is first simulated using the unit cell boundary conditions to extract the S-curve. Simulation shows that a linear reflection phase range of 454.2° is achievable. With the use of S-curve, the unit element

is then designed into a full-fledged reflectarray which consists of 121 elements. The proposed reflectarray has been fabricated, and measured. Measurement shows that the proposed reflectarray can achieve an antenna gain of 20.4 dBi with a broad -1 dB gain bandwidth of 15.38%.

For the second project, the L-shaped probes are further deployed for designing two transmitarrays for realizing two different linear polarization operations in the C-band. One transmitarray has its transmitting wave polarized vertically and the other horizontally. The polarization of the transmitting wave can be manipulated by adjusting the probes orientation at the transmitting side of transmitarray. To demonstrate the idea, the transmitarray elements are simulated using the Floquet method. Linear phase curves with phase ranges of more than 360° were achieved. When designed into 9×9 full transmitarrays, the vertically polarized transmitarray has an antenna gain of ~ 21 dBi with a broad -1 dB gain bandwidth of 11.62% at the operating frequency of 7.8 GHz, whereas the horizontally polarized transmitarray has an antenna gain of ~ 19 dBi with a wide -1 dB gain bandwidth of 10.39% at the center frequency of 7.4 GHz.

ACKNOWLEDGEMENTS

First of all, I would like to express my utmost gratitude to Dr. Lee Kim Yee and Dr. Lim Eng Hock for their patience in guiding me throughout the research. Without their guidance and advices, I would not have able to complete my research projects. Their stimulating conversations and discussions are the key factors that lead to the development of the new devices.

Next, I would like to thank our department lab officer, Mr. Ho for guiding me in the fabrication of printed circuit board. I would also like to extend my gratitude to my friends: Lee Shin Rou and Mr. Phua, for their assistances during antenna measurements.

Finally, I would like to express my appreciation to UTAR for funding me and providing the necessary equipment, materials, and facilities. Online databases such as IEEE Xplore and Microwave Optical and Technology (MOTL) subscribed by UTAR have been useful and helpful to me as all the important literatures which are related to my research area can be accessed seamlessly.

APPROVAL SHEET

This dissertation entitled “**DESIGN AND CHARACTERIZATION OF L-PROBE REFLECTARRAY AND TRANSMITARRAY**” was prepared by NG WAI HAU and submitted as partial fulfillment of the requirements for the degree of Master of Engineering Science at Universiti Tunku Abdul Rahman.

Approved by:

(Dr. Lee Kim Yee)

Date:.....

Supervisor

Department of Electrical and Electronic Engineering
Lee Kong Chian Faculty of Engineering and Science
Universiti Tunku Abdul Rahman

(Assoc. Prof. Dr. Lim Eng Hock)

Date:.....

Co-supervisor

Department of Electrical and Electronic Engineering
Lee Kong Chian Faculty of Engineering and Science
Universiti Tunku Abdul Rahman

LEE KONG CHIAN FACULTY OF ENGINEERING AND SCIENCE
UNIVERSITI TUNKU ABDUL RAHMAN

Date: 15 March 2017

SUBMISSION OF DISSERTATION

It is hereby certified that NG WAI HAU (ID No: 14UEM07939) has completed this dissertation entitled "DESIGN AND CHARACTERIZATION OF L-PROBE REFLECTARRAY AND TRANSMITARRAY" under the supervision of Dr. Le Kim Yee (Supervisor) from the Department of Electrical and Electronic Engineering, Lee Kong Chian Faculty of Engineering and Science (FES), and Dr. Lim Eng Hock (Co-Supervisor) from the Department of Electrical and Electronic Engineering, Lee Kong Chian Faculty of Engineering and Science (FES).

I understand that University will upload softcopy of my dissertation in pdf format into UTAR Institutional Repository, which may be made accessible to UTAR community and public.

Yours truly,

(NG WAI HAU)

DECLARATION

I hereby declare that the dissertation is based on my original work except for citations and quotations which have been duly acknowledged. I also declare that it has not been previously or concurrently submitted for any other degree at UTAR or other institutions.

(NG WAI HAU)

Date _____

TABLE OF CONTENTS

| | Page |
|--|-------------|
| ABSTRACT | ii |
| ACKNOWLEDGEMENTS | iv |
| APPROVAL SHEET | v |
| PERMISSION SHEET | vi |
| DECLARATION | vii |
| LIST OF TABLES | xi |
| LIST OF FIGURES | xii |
| | |
| CHAPTER | |
| | |
| 1 INTRODUCTION | 1 |
| 1.1 Backgrounds and Issues | 1 |
| 1.2 Key Performance Indicators for Reflectarray and Transmitarray Unit Elements | 5 |
| 1.2.1 Reflection Magnitude and Transmission Magnitude | 6 |
| 1.2.2 Reflection Phase and Transmission Phase | 7 |
| 1.3 Key Performance Indicators for Reflectarray and Transmitarray | 7 |
| 1.3.1 Antenna Gain | 7 |
| 1.3.2 Aperture Efficiency | 8 |
| 1.3.3 Gain Bandwidth | 9 |
| 1.4 Research Objectives and Motivation | 10 |
| 1.5 Thesis Overview | 11 |
| | |
| 2 BACKGROUND AND DEVELOPMENT | 13 |
| 2.1 Development History | 13 |

| | | |
|----------|---|-----------|
| 2.2 | Design Procedures of Reflectarray and Transmitarray | 17 |
| 2.3 | Unit Element Simulation | 20 |
| 2.3.1 | Waveguide Method | 20 |
| 2.3.2 | Floquet Method | 21 |
| 3 | BROADRANGE L-PROBE REFLECTARRAY | 24 |
| 3.1 | Introduction | 24 |
| 3.2 | Unit Element Configuration and Analysis | 26 |
| 3.3 | Reflectarray Configuration | 30 |
| 3.4 | Measurement Setup | 34 |
| 3.5 | Simulated and Experimental Results of Reflectarray | 35 |
| 3.6 | Parametric Analysis | 37 |
| 3.6.1 | Comparison of Single and Double L Probe Elements | 37 |
| 3.6.2 | Length Difference between Long and Short Probes | 39 |
| 3.6.3 | Feeding Angle | 40 |
| 3.6.4 | Unit Cell Size | 42 |
| 3.6.5 | Probe Height | 44 |
| 3.6.6 | Probe Diameter | 46 |
| 3.6.7 | f/D Ratio | 48 |
| 3.7 | Conclusion | 50 |
| 4 | CO-JOINED L PROBES FOR TWO BROADBAND TRANSMITARRAYS WITH DIFFERENT POLARIZATIONS | 51 |
| 4.1 | Introduction | 51 |
| 4.2 | Unit Element Configuration and Analysis | 53 |
| 4.3 | Transmitarray Configuration | 61 |
| 4.4 | Measurement Setup | 64 |
| 4.5 | Simulated and Experimental Results of Transmitarray | 65 |
| 4.6 | Parametric Analysis for Vertically Polarized Transmitarray | 69 |

| | | |
|----------|---|------------|
| 4.6.1 | Comparison of Single and Double L Probe Elements | 69 |
| 4.6.2 | Length Difference between Long and Short Probes | 71 |
| 4.6.3 | Probe Diameter | 73 |
| 4.6.4 | Probe Height | 75 |
| 4.6.5 | Separation Distance between Long and Short Probes in x -direction | 77 |
| 4.6.6 | Unit Cell Size | 79 |
| 4.6.7 | f/D Ratio | 81 |
| 4.7 | Parametric Analysis for Horizontally Polarized Transmitarray | 82 |
| 4.7.1 | Comparison of Single and Double L Probe Elements | 82 |
| 4.7.2 | Length Difference between Long and Short Probes | 84 |
| 4.7.3 | Probe Height | 86 |
| 4.7.4 | Probe Diameter | 87 |
| 4.7.5 | Separation Distance between Long and Short Probes in y -direction | 89 |
| 4.7.6 | Separation Distance between Long and Short Probes | 91 |
| 4.7.7 | Unit Cell Size | 93 |
| 4.7.8 | f/D Ratio | 96 |
| 4.8 | Conclusion | 97 |
| 5 | SUMMARY AND DISCUSSION | 99 |
| | BIBLIOGRAPHY | 100 |
| | APPENDICES | 109 |

LIST OF TABLES

| Table | | Page |
|--------------|--|-------------|
| 4.1 | Comparison of the proposed transmitarrays with the recently published works. | 69 |

LIST OF FIGURES

| Figure | | Page |
|--------|--|------|
| 1.1 | A parabolic reflector. | 2 |
| 1.2 | Reconfigurable phased array. | 3 |
| 1.3 | The configuration of a typical reflectarray. (a) Center-fed (b) offset-fed. | 4 |
| 1.4 | The configuration of a typical transmitarray. | 5 |
| 2.1 | Different types of microstrip reflectarray elements, (a) identical patches with phase delay lines of different lengths, (b) dipoles with variable dipole lengths, (c) patches of variable sizes. | 14 |
| 2.2 | A thin lens. | 15 |
| 2.3 | Various transmitarray elements, (a) dipole lens, (b) aperture coupled microstrip patches. | 16 |
| 2.4 | Design procedure of the reflectarray and transmitarray by using the phase-only optimization technique (POT). | 19 |
| 2.5 | Waveguide model of a transmitarray element. | 21 |
| 2.6 | An infinite array with identical elements. | 22 |
| 2.7 | Floquet model of a transmitarray element. | 22 |
| 2.8 | Electric fields generated along the z -direction for different Floquet boundary conditions. (a) TE_{00} mode, (b) TM_{00} mode. | 23 |
| 3.1 | One-port Floquet cell for simulating the co-joined L-probe reflectarray unit element. | 28 |
| 3.2 | Reflection magnitude and reflection phase of the reflectarray unit element. | 28 |
| 3.3 | Electric field distributions around the (a) long L-probe, (b) short L-probe at the frequency of 7.1 GHz for the case of $l_1 = 20$ mm. | 29 |

| | | |
|------|---|----|
| 3.4 | Configuration of the proposed linearly polarized reflectarray. | 31 |
| 3.5 | Prototype of the linearly polarized reflectarray. | 31 |
| 3.6 | Path length for the electromagnetic waves travelling from the feeding horn to the reference element (element (6, 1)). | 33 |
| 3.7 | Measurement setup for the reflectarray ($R = 11.5$ m). | 35 |
| 3.8 | Measured and simulated (a) E - and (b) H - planes radiation patterns of the proposed reflectarray at 6.9 GHz. | 36 |
| 3.9 | Measured and simulated antenna gains of the proposed reflectarray as a function of frequency. | 37 |
| 3.10 | Comparison of the reflection magnitudes and reflection phases of the reflectarray unit elements with single and double L probes. | 38 |
| 3.11 | Effects of the length difference (x) between the long and the short probes on the reflection magnitude and reflection phase of the reflectarray unit element. | 39 |
| 3.12 | Effects of the feeding horn incident angle (θ_o) on the reflection magnitude and reflection phase of the reflectarray unit element. | 40 |
| 3.13 | Radiation patterns of the proposed reflectarray for different feeding horn incident angles (θ_o) at 6.9 GHz. (a) E - and (b) H - planes. | 41 |
| 3.14 | Effects of the unit element dimension (L) on the reflection magnitude and reflection phase of the reflectarray unit element. | 43 |
| 3.15 | Radiation patterns of the proposed reflectarray for different separation distances (L) at 6.9 GHz. (a) E - and (b) H - planes. | 44 |
| 3.16 | Effects of the probe height (h) on the reflection magnitude and reflection phase of the reflectarray unit element. | 45 |

| | | |
|------|---|----|
| 3.17 | Radiation patterns of the proposed reflectarray for different probe heights (h) at 6.9 GHz. (a) E - and (b) H - planes. | 46 |
| 3.18 | Effects of the probe diameter (d) on the reflection magnitude and reflection phase of the reflectarray unit element. | 47 |
| 3.19 | Radiation patterns of the proposed reflectarray for different probe diameters (d) at 6.9 GHz. (a) E - and (b) H - planes. | 48 |
| 3.20 | Radiation patterns of the proposed reflectarray for different f/D ratios. (a) E - and (b) H - planes. | 49 |
| 4.1 | (a) Perspective view, (b) Floquet periodic boundary conditions of the vertically polarized unit element. | 55 |
| 4.2 | (a) Perspective view, (b) Floquet periodic boundary conditions of the horizontally polarized unit element. | 57 |
| 4.3 | Transmission magnitudes and transmission phases of the transmitarray elements which generate (a) y -polarized wave, (b) x -polarized wave. | 59 |
| 4.4 | Electric field distributions around the (a) long probe, (b) short probe at the frequency of 7.8 GHz with $l_1 = 20$ mm for the vertically polarized unit element. | 60 |
| 4.5 | Configurations of the proposed (a) vertically, (b) horizontally polarized transmitarrays. | 62 |
| 4.6 | Prototypes of the (a) vertically, (b) horizontally polarized transmitarrays. | 63 |
| 4.7 | Measurement setup for the transmitarray. | 64 |
| 4.8 | Measured and simulated (a) E - and (b) H - plane radiation patterns of the vertically polarized transmitarray. | 66 |
| 4.9 | Measured and simulated (a) E - and (b) H - plane radiation patterns of the horizontally polarized transmitarray. | 67 |
| 4.10 | Measured and simulated antenna gains of the vertically and horizontally polarized transmitarrays. | 68 |

| | | |
|------|---|----|
| 4.11 | Configuration of the vertically polarized transmitarray unit element with single L probe. | 70 |
| 4.12 | Comparison of the transmission magnitudes and transmission phases of the vertically polarized transmitarray unit elements with single and double L probes. | 70 |
| 4.13 | Effects of the length difference (x) between the long and the short probes on the transmission magnitude and transmission phase of the vertically polarized transmitarray unit element. | 71 |
| 4.14 | Radiation patterns of the proposed vertically polarized transmitarray for different length differences (x) between the long and the short probes at 7.8 GHz. (a) E - and (b) H - planes. | 72 |
| 4.15 | Effects of the probe diameter (d) on the transmission magnitude and transmission phase of the vertically polarized transmitarray unit element. | 73 |
| 4.16 | Radiation patterns of the proposed vertically polarized transmitarray for different probe diameters (d) at 7.8 GHz. (a) E - and (b) H - planes. | 74 |
| 4.17 | Effects of the probe height (h) on the transmission magnitude and transmission phase of the vertically polarized transmitarray unit element. | 75 |
| 4.18 | Radiation patterns of the proposed vertically polarized transmitarray for different probe heights (h) at 7.8 GHz. (a) E - and (b) H - planes. | 76 |
| 4.19 | Effects of the separation distance between the long and the short probes in the x -direction (G_x) on the transmission magnitude and transmission phase of the vertically polarized transmitarray unit element. | 77 |
| 4.20 | Radiation patterns of the proposed vertically polarized transmitarray for different probe separations in the x -direction (G_x) at 7.8 GHz. (a) E - and (b) H - planes. | 78 |
| 4.21 | Effects of the unit element dimension (L) on the transmission magnitude and transmission phase of the vertically polarized transmitarray unit element. | 79 |

| | | |
|------|---|----|
| 4.22 | Radiation patterns of the proposed vertically polarized transmitarray for different separation distances (L) at 7.8 GHz. (a) E - and (b) H - planes. | 80 |
| 4.23 | Radiation patterns of the proposed vertically polarized transmitarray for different f/D ratios. (a) E - and (b) H - planes. | 82 |
| 4.24 | Configuration of the horizontally polarized transmitarray unit element with single L probe. | 83 |
| 4.25 | Comparison of the transmission magnitudes and transmission phases of the horizontally polarized transmitarray unit elements with single and double L probes. | 83 |
| 4.26 | Effects of the length difference (x) between the long and the short probes on the transmission magnitude and transmission phase of the horizontally polarized transmitarray unit element. | 84 |
| 4.27 | Radiation patterns of the proposed horizontally polarized transmitarray for different length differences (x) between the long and the short probes at 7.3 GHz. (a) E - and (b) H - planes. | 85 |
| 4.28 | Effects of the probe height (h) on the transmission magnitude and transmission phase of the horizontally polarized transmitarray unit element. | 86 |
| 4.29 | Effects of the probe diameter (d) on the transmission magnitude and transmission phase of the horizontally polarized transmitarray unit element. | 87 |
| 4.30 | Radiation patterns of the proposed horizontally polarized transmitarray for different probe diameters (d) at 7.3 GHz. (a) E - and (b) H - planes. | 88 |
| 4.31 | Effects of the separation distance between the long and the short probes in the y -direction (G_y) on the transmission magnitude and transmission phase of the horizontally polarized transmitarray unit element. | 90 |
| 4.32 | Radiation patterns of the proposed horizontally polarized transmitarray for different probe separations in the y -direction (G_y) at 7.3 GHz. (a) E - and (b) H - planes. | 91 |

| | | |
|------|---|----|
| 4.33 | Effects of the separation distance between the long and the short probes ($G_x = G_y$) on the transmission magnitude and transmission phase of the horizontally polarized transmitarray unit element. | 92 |
| 4.34 | Radiation patterns of the proposed horizontally polarized transmitarray for different probe separations ($G_x = G_y$) at 7.3 GHz. (a) E - and (b) H -planes. | 93 |
| 4.35 | Effects of the unit element dimension (L) on the transmission magnitude and transmission phase of the horizontally polarized transmitarray unit element. | 94 |
| 4.36 | Radiation patterns of the proposed horizontally polarized transmitarray for different separation distances (L) at 7.3 GHz. (a) E - and (b) H - planes. | 95 |
| 4.37 | Radiation patterns of the proposed horizontally polarized transmitarray for different f/D ratios. (a) E - and (b) H - planes. | 97 |

CHAPTER 1

INTRODUCTION

1.1 Backgrounds and Issues

Antenna is a vital part of all wireless communication systems for transmitting or receiving electromagnetic wave signals. Basically, antennas can be categorized into two major types of radiators: the omnidirectional antenna and the directional antenna. The omnidirectional antenna is commonly used when a wireless system needs to cover a moderately large area in all directions and the gain of the antenna is not of concern. The directional antenna, on the other hand, is utilized when antenna gain is of paramount importance as it can focus and direct electromagnetic energy to a specific direction. The directional antenna is usually used for long range communications such as the satellite communications and radar systems.

Parabolic reflector, as illustrated in Figure 1.1, is a type of directional antenna which has been extensively relied upon in the past for long range communications. However, the parabolic reflectors come with several disadvantages. First of all, the reflecting disc of the parabolic reflector is usually made of metallic materials, making it heavy and bulky. For this reason, it is unsuitable for space-borne applications (Huang, 1995). Next, fabrication of the reflecting disc which is curved in shape is usually challenging and difficult, leading to a costly manufacturing process. Although a mechanical

rotator can be integrated into the parabolic reflector for introducing beam-scanning functionality, it is only suitable for capturing slow-changing wireless signals.

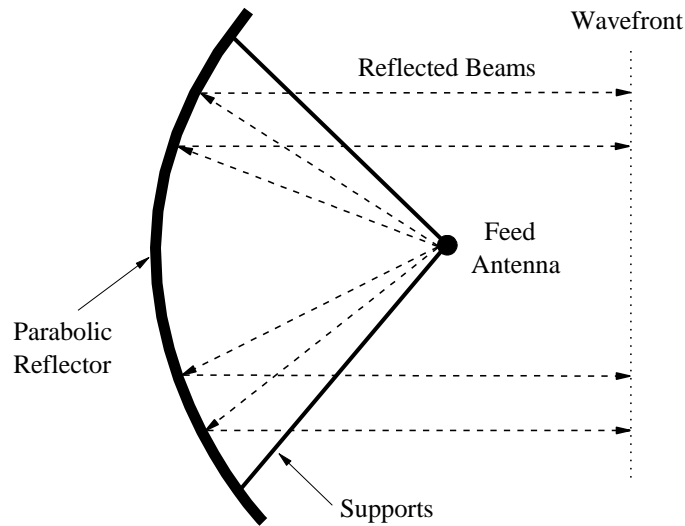


Figure 1.1: A parabolic reflector.

The phased array is another type of conventional antenna for use in high-gain applications. It is a combination of multiple antennas to achieve high antenna gain. Figure 1.2 shows the schematic of a typical phased array. It is composed of three modules: the power dividers, the phase shifters and the antenna elements. The power dividers split and distribute the input signal and the phase shifters provide different phases to each of the antenna elements for enabling beam scanning. Although the limitations of the parabolic reflector have been overcome in the phased array, the phased array suffers high insertion losses from the power divider and the phased shifter modules.

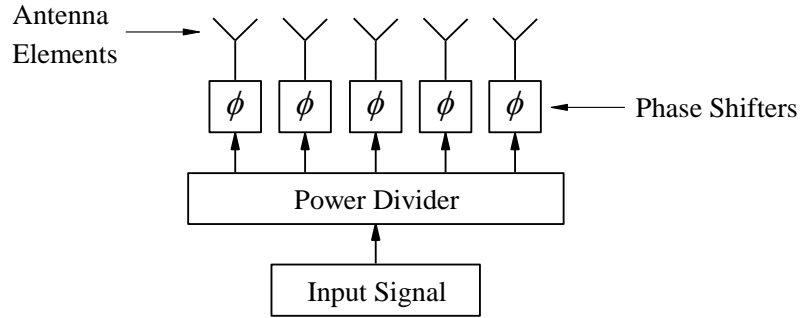


Figure 1.2: Reconfigurable phased array.

A new type of antenna array, which is known as the reflectarray, is introduced to overcome the shortcomings of the parabolic reflector and the phased array. Essential features of the parabolic reflector and the phased array are also possessed by the reflectarray (Mener et al., 2013). The configuration of a typical reflectarray is depicted in Figure 1.3. It consists of an array of radiating elements printed on a substrate and the radiating elements are spatially illuminated by a feeding source. Unlike the parabolic reflector, the reflectarray has a flat reflecting surface, making it lighter and easier to manufacture. In addition, unlike the phased array, the reflectarray does not require any power dividing networks to feed each of the radiating elements (Pan et al., 2012). As a result, losses in the reflectarray are lower than the phased array. There are two feeding schemes in reflectarrays: center-fed and offset-fed. A center-fed reflectarray will have its feeding source placed at the boresight of the antenna while an offset-fed reflectarray has the feed antenna positioned at an oblique angle. Reflectarray with center-fed scheme often exhibits poorer radiation performances due to the blockage of the feed antenna, which interrupts and scatters the reflected waves of the reflectarray. Although an offset-fed reflectarray does not suffer from the feed blocking loss, the

reflectarray will obtain undesirable effects such as higher cross polarization, beam squinting, and feed image (Almajali et al., 2014; Shaker et al., 2014).

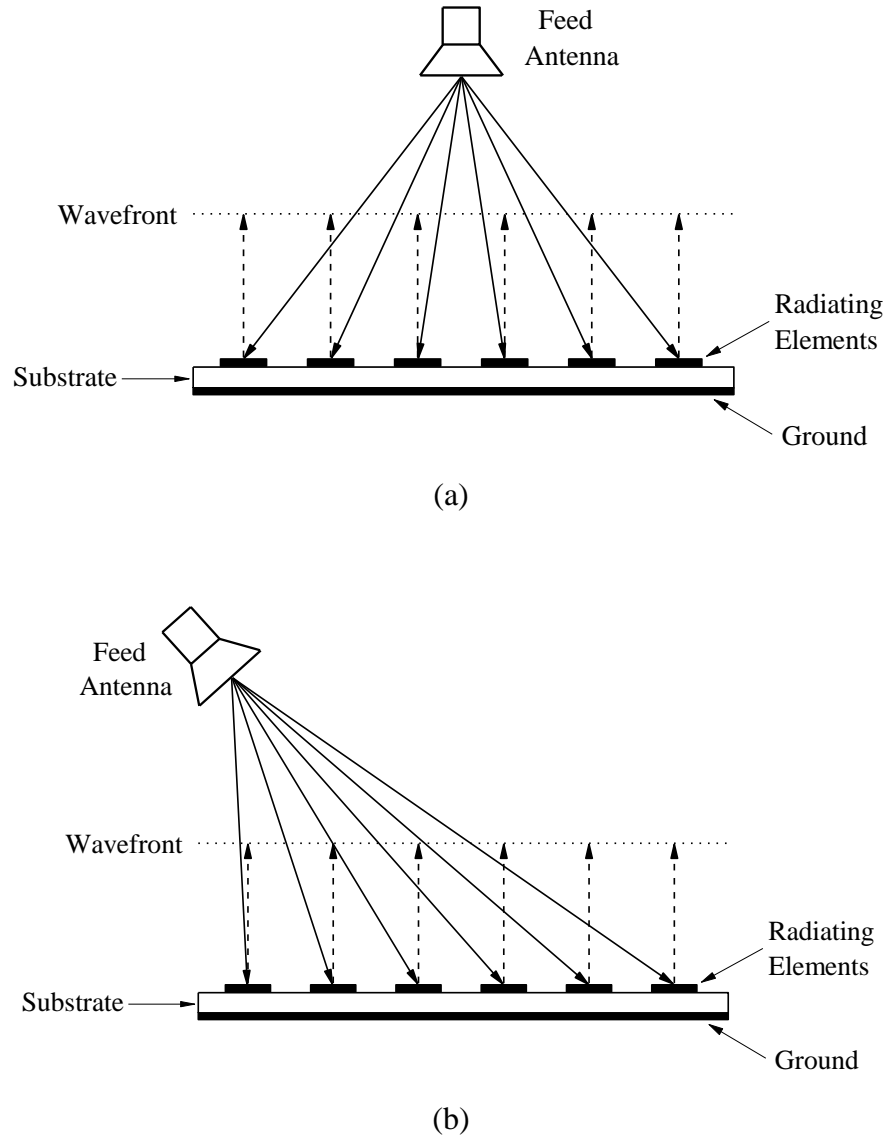


Figure 1.3: The configuration of a typical reflectarray. (a) Center-fed (b) offset-fed.

An alternative to the reflectarray is the transmitarray, which has the features of the phased array and the dielectric lens. A transmitarray usually consists of multiple stacks of conducting layers illuminated by a feeding source, as illustrated in Figure 1.4. To achieve best radiation performances, the

feed antenna is usually placed at the center of the aperture without any inclination angle. Electromagnetic energy illuminated from the feed antenna is received at one end and re-radiated from the other end of the transmitarray. Hence, problems encountered in the center-fed and offset-fed reflectarrays are alleviated for transmitarrays. By incorporating active elements such as diodes, a transmitarray can be made steerable which favors applications such as satellite-based communication systems.

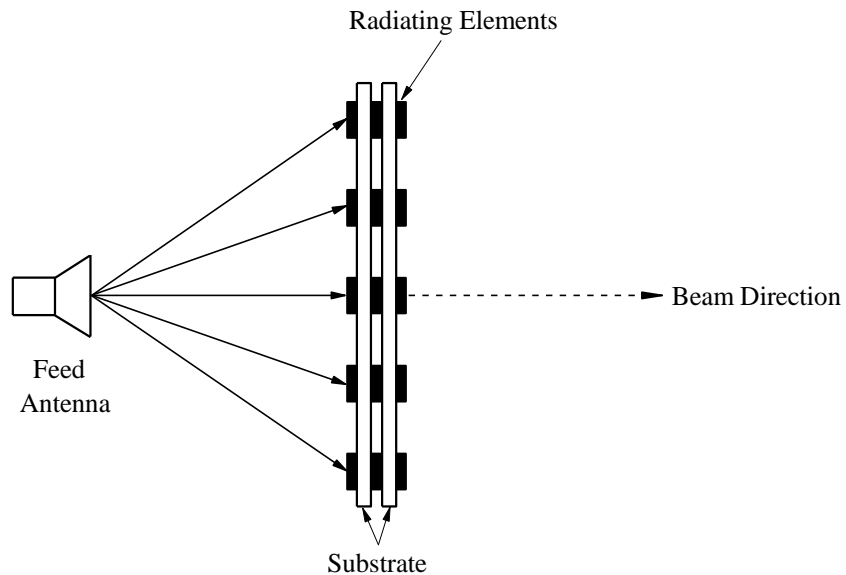


Figure 1.4: The configuration of a typical transmitarray.

1.2 Key Performance Indicators for Reflectarray and Transmitarray Unit Elements

In this section, the key performance parameters which are used for describing the performances of the unit elements of the reflectarray and the transmitarray are discussed.

1.2.1 Reflection Magnitude and Transmission Magnitude

Reflection magnitude ($|S_{11}|$) and transmission magnitude ($|S_{21}|$) are denoted as the amount of electromagnetic waves reflected and transmitted away from the radiating elements of the reflectarray and the transmitarray, respectively. They are expressed in decibel (dB). For a unit element to radiate effectively, it is important to ensure the reflection magnitude of the reflectarray element and the transmission magnitude of the transmitarray element are close to 0 dB. For both of the parameters, the acceptable amplitude level is -3 dB.

For the reflectarray elements, the reflection magnitude is affected by factors such as the substrate thickness of the unit element and the losses within the unit element. According to Karnati et al. (2013), the reflection magnitude of a reflectarray element can be made higher by increasing the substrate thickness. It was reported in (Bozzi et al., 2004) that a reflectarray element exhibits two types of losses, namely, metal loss and dielectric loss. Metal loss is the loss contributed by conductor that exists in the unit element; whereas dielectric loss is the loss caused by the substrate of the unit element. Any increase of these two losses will result in a lower reflection magnitude. It was also report in (Bozzi et al., 2004) that the reflection magnitude of a unit element is also affected by the shape of the unit element.

1.2.2 Reflection Phase and Transmission Phase

Reflection phase (also known as S-curve - $\angle S_{11}$) and transmission phase ($\angle S_{21}$) are referred as the phases generated at a particular frequency by varying one of the geometrical phase-shifting parameters of the reflectarray element and the transmitarray element, respectively. They are useful for compensating the propagation paths of the propagating electromagnetic waves, travelling from the feeding source to the radiating elements. When designing the unit element, it is crucial to ensure a minimum phase range of 360° is achievable so that arrays of any sizes can be designed. Other than that, it is also important to make sure the gradient of the phase curve to be slow and linear so that the dimensions between the adjacent elements are distinguishable.

1.3 Key Performance Indicators for Reflectarray and Transmitarray

In this section, the three important parameters - antenna gain, aperture efficiency, and gain bandwidth are described for evaluating the performances of the reflectarray and the transmitarray.

1.3.1 Antenna Gain

Antenna gain is a measure of the capability of an antenna to direct electromagnetic waves to certain directions. It is usually compared with the

isotropic antenna, which is a theoretical antenna that radiates equally in all directions. Therefore, it is expressed in dBi. The gain of an antenna can be found using equation (1.1). Based on the equation, it can be noted that the antenna gain is always lower than its directivity due to the fact that the radiation efficiency of an antenna is always less than unity in practical.

$$\text{Antenna Gain} = \text{Radiation Efficiency} \times \text{Directivity} \quad (1.1)$$

Several factors are affecting the antenna gain of a reflectarray and a transmitarray. The first factor is the number of unit elements that exist in the antenna array. Antenna arrays with more unit elements will usually achieve a higher antenna gain. The gain of the antenna array is also affected by the separation distance between the elements. For a microstrip antenna array, the unit elements are typically separated by 0.5λ to 0.6λ to reduce the unwanted side lobes. Losses such as the taper loss, quantization loss, and spillover loss can significantly reduce the antenna gain. However, such losses can be easily mitigated by optimizing the ratio between the focal length and the size of the antenna array (f/D ratio) (Kaouach et al., 2011; Clemente et al., 2012; Jiang et al., 2013).

1.3.2 Aperture Efficiency

Aperture efficiency is a measure of how effective the physical area of a reflectarray and a transmitarray is utilized. It can be calculated using equation

(1.2). The typical aperture efficiency of a reflectarray and a transmitarray is in the range of 0.4 to 0.6.

$$n_a = \frac{G\lambda^2}{4\pi A} \quad (1.2)$$

where

n_a = aperture efficiency of the reflectarray or transmitarray

G = antenna gain

λ = wavelength at the center frequency of the reflectarray or transmitarray, m

A = aperture area of the reflectarray or transmitarray, m²

1.3.3 Gain Bandwidth

There are two common values for measuring the bandwidth of a reflectarray and a transmitarray: -1 dB and -3 dB gain bandwidths. For stricter requirement, -1 dB gain bandwidth is usually selected. It is defined as the range of frequencies at which the drop in the antenna gain to be 1 dB. It is widely known that the bandwidth of an antenna array is greatly restrained by the properties of the unit element. The f/D ratio is another parameter that affects the bandwidth of the antenna arrays.

1.4 Research Objectives and Motivation

In this dissertation, a type of resonator formed by the L-shaped probe is explored for designing the reflectarray and transmitarray. There are three main aims for conducting this research. The first aim of this research is to investigate the use of the L-shaped probes for achieving linear phase curve in the design of the reflectarray and transmitarray elements. The characteristics of the L-shaped probes are further investigated for designing the broadband reflectarray and transmitarray with minimal number of layers. The L-shaped probes are also explored for realizing two different linear polarization operations in the transmitarray.

To meet all the research objectives, two projects have been conducted. The first project goes to designing a reflectarray while the second project is devoted to designing two transmitarrays. In both projects, by co-joining two L-shaped probes of different lengths side-by-side, linear phase curves with phase ranges of more than 360° are obtained. With the use of only a layer of low cost FR4 substrate as the base support for the L-shaped probes, the proposed reflectarray and transmitarrays are able to provide high antenna gain and broad -1 dB gain bandwidth of not less than 10%. It was found that the proposed transmitarray can generate the vertically and horizontally polarized waves by adjusting the orientation of the L-shaped probes on the transmitting side of the transmitarray. To demonstrate the ideas, the prototypes of the antenna arrays have been designed, fabricated, and measured. Parametric analysis has been conducted to analyze the effects of the design parameters.

1.5 Thesis Overview

This dissertation is consisted of five chapters. The first chapter is started with discussions on the backgrounds and issues of the conventional antennas and the introduction of the two new antenna arrays: the reflectarray and the transmitarray. The key performance indicators of the reflectarray and the transmitarray are presented. In the last part of the chapter, the research objectives and motivation are clearly projected.

In the second chapter, the developments of the reflectarray and transmitarray are elaborated, followed by detailed explanations on the design methodologies and design procedures. The design limitations are also discussed.

In the third chapter, the reflectarray which is designed using the L-shaped probes is presented. Details of the configurations, fabrication, and measurement setup as well as the simulation and measurement results are included. Parametric analysis has been conducted to study the characteristics of the design parameters.

In the fourth chapter, the concept of dual linear polarization is presented with the design of two L-probe transmitarrays. The configurations and fabrication, along with results from simulation and measurement are presented. Other findings such as the effects of the design parameters are also demonstrated.

In the fifth chapter, the research works are summarized and concluded.
The key findings of the research are discussed.

CHAPTER 2

BACKGROUND AND DEVELOPMENT

2.1 Development History

The idea of reflectarray was first conceived by Berry et al. (1963) in the early 1960s. The first reflectarray was designed and constructed using 426 open-waveguides cascaded in array, which are fed by a horn antenna. Due to the heaviness and bulkiness of the waveguide especially when designed at lower frequency, the waveguide-based reflectarray was hindered from further development. Later, Phelan (1977) proposed the active spiraphase reflectarray where switching diodes were incorporated in between the four spiral arms for achieving circularly polarized and beam steering at the same time. The spiraphase reflectarray did not get great attention as the structure was still relatively huge and heavy.

In the late 1970s, microstrip technology began to emerge and it had enabled the advancement of the reflectarray. The first microstrip reflectarray was proposed by Malagisi (1978) and the microstrip element was analyzed by Montgomery (1978) using finite array approach. To further reduce the size and mass of the reflectarray, different types of microstrip elements have been introduced. Examples of the unit element configurations are identical patches with phase delay lines of different lengths (Chang and Huang, 1995), dipoles with variable dipole lengths (Kelkar, 1991), and patches of variable sizes

(Pozar and Metzler, 1993; Pozar et al., 1997), as illustrated in Figure 2.1 (a), (b), and (c), respectively.

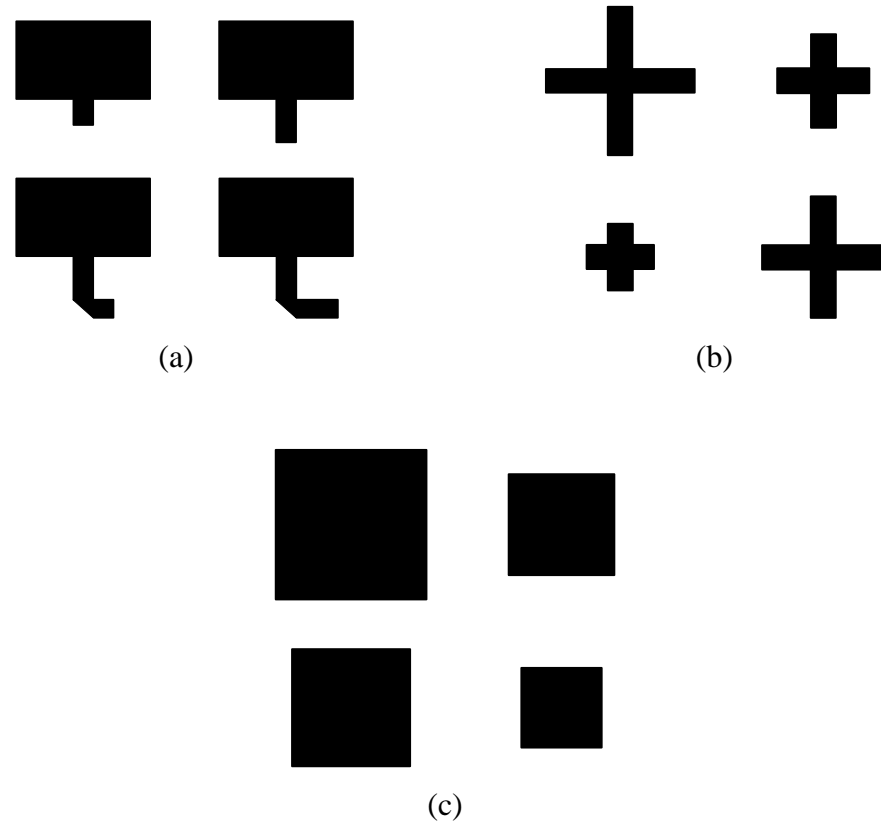


Figure 2.1: Different types of microstrip reflectarray elements, (a) identical patches with phase delay lines of different lengths, (b) dipoles with variable dipole lengths, (c) patches of variable sizes.

Due to inherent narrow bandwidth of the microstrip reflectarray, several approaches have been made in order to overcome the bandwidth limitation. The initial method was using a thick substrate for designing a single layer reflectarray (Sze and Shafai, 1999). Such method was proven to be able to improve the bandwidth of the reflectarray, but at the expense of reducing the attainable phase range. Later, multilayer reflectarray (Encinar, 2001) was introduced to enhance the bandwidth of the reflectarray. Recently, the single-layered multi-resonant element (Cadoret et al., 2005) and the

subwavelength coupled-resonant element (Nayeri et al., 2011) were proposed to achieve wideband operation.

The concept of transmitarray was originated from the dielectric lens. The transmitarray has working principle similar to that for the dielectric lens, which is illustrated in Figure 2.2 where the incoming electromagnetic waves that pass through the dielectric lens are refracted and converged at the focal point. One of the earliest developments of dielectric lens was found in 1946, where the dielectric lens was capable of providing wide-angle beam scanning capability (Friedlander, 1946). Although the dielectric lens does not have aperture blockage issue as encountered in the parabolic reflector, it is bulky when designed at lower frequency, and the complexities in the design and fabrication often require sophisticated tooling, which results in a higher manufacturing cost.

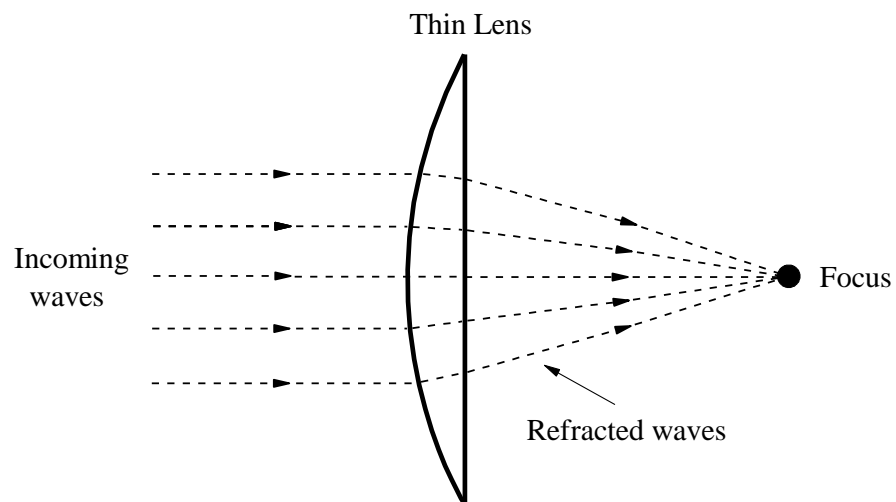


Figure 2.2: A thin lens.

Planar lens antenna, also known as microstrip transmitarray, has the features of low profile, light weight and easy to manufacture while mitigating

the shortcomings of the dielectric lens. Due to the attractive attributes of the microstrip transmitarray, it has lured the attention and interest of many researchers. Some of the early developed microstrip transmitarrays were dipole array lens antenna (Milne, 1982), planar three-dimensional constrained lenses (McGrath, 1986), and flat lens antenna using aperture coupled microstrip patches (Pozar, 1996), which are depicted in Figure 2.3. One of the main challenges in designing the transmitarray is that the unit element itself must provide sufficient transmission phase range, while maintaining good transmission at the operating frequency passband. Since a single-layered transmitarray element can only provide a phase range of not more than 90° (Abdelrahman et al., 2014a), most of the transmitarray elements were proposed in multilayer configurations for achieving larger phase range (Shibayama et al., 2010; Wang et al., 2012; Chen et al., 2013b; Liu et al., 2015; Abdelrahman et al., 2015).

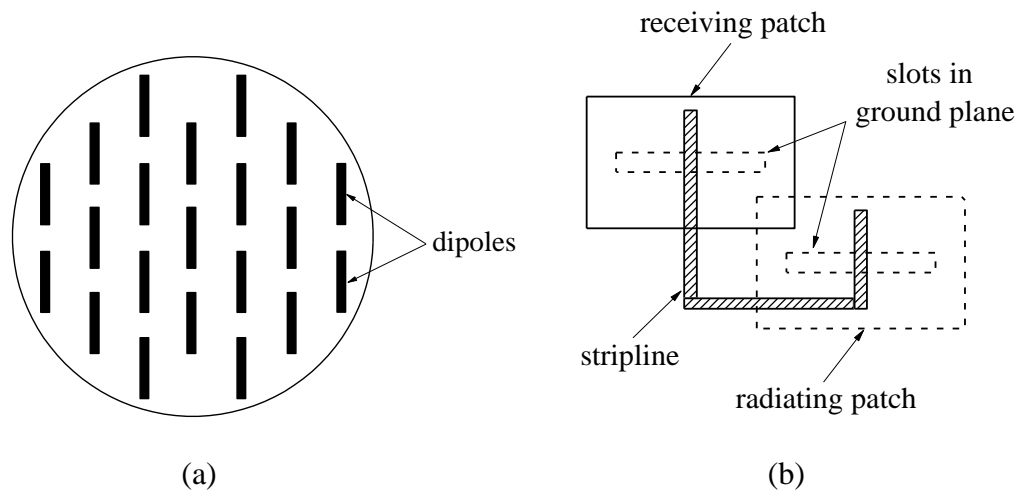


Figure 2.3: Various transmitarray elements, (a) dipole lens, (b) aperture coupled microstrip patches.

2.2 Design Procedures of Reflectarray and Transmitarray

In general, there are two methods that can be employed when designing the reflectarray and the transmitarray. The first method is known as direct optimization technique (DOT), where all the unit elements of the antenna array are optimized concurrently. This technique is based on spectral domain method of moment (SDMoM) and local periodicity is presumed, where the antenna array element is expanded into an infinite array of identical elements. It was demonstrated by Zhou et al. (2013) for designing reflectarrays. The technique is highly advantageous and useful when the unit elements are positioned randomly on the radiating aperture, the unit elements are of arbitrary shapes, or a much optimal design of antenna array is required. Nevertheless, the DOT requires high computational resources and a lot of time in simulating, analyzing, and optimizing in order to obtain the optimized design.

The second method is called phase-only optimization technique (POT), which also employs SDMoM and assuming local periodicity. In the POT, the antenna array elements are optimized one by one to match the phase distribution on the array surface. It is suitable for antenna array which is designed either in square or circular grid with equal or unequal element spacing. In contrast to the DOT, the POT is much straightforward, more efficient in terms of computation time and, at the same time, most optimal in design with accurate results. In fact, the POT is a popular choice and it has been extensively applied by many researchers in the past for designing different types of reflectarrays and transmitarrays (Encinar and Zornoza, 2004;

Carrasco et al., 2008; Encinar et al., 2011; Ryan et al., 2010; Shaker et al., 2014).

In this dissertation, the proposed L-probe reflectarray and transmitarray are designed using the POT. The design procedure is summarized in a flowchart, as illustrated in Figure 2.4. Firstly, the L-probe reflectarray and transmitarray elements are simulated in the Floquet cell using the CST Microwave Studio for the purposes of obtaining the S-curve for the reflectarray and the transmission phase curve for the transmitarray. To generate the phase curves, the phase-changing parameters of the unit elements are identified and varied. Next, the size and constellation of the full antenna arrays are determined and the propagation path length for each of the array elements from the feed horn is calculated. After that, by choosing one of the unit elements as the reference, the path differences between the reference element and all other unit elements are calculated in terms of phase angles, which represent the phase distributions on the array surfaces. Then, the dimensions for all unit elements are extracted by mapping the acquired phase angle of each unit element to the phase-shifting geometrical parameter in the S-curve and transmission phase curves of the L-probe reflectarray and transmitarray, respectively. Finally, the full-fledged L-probe reflectarray and transmitarray are constructed and simulated using the full-wave simulation procedure provided by the CST Microwave Studio. To validate the simulation results, prototypes are fabricated and measured in free space.

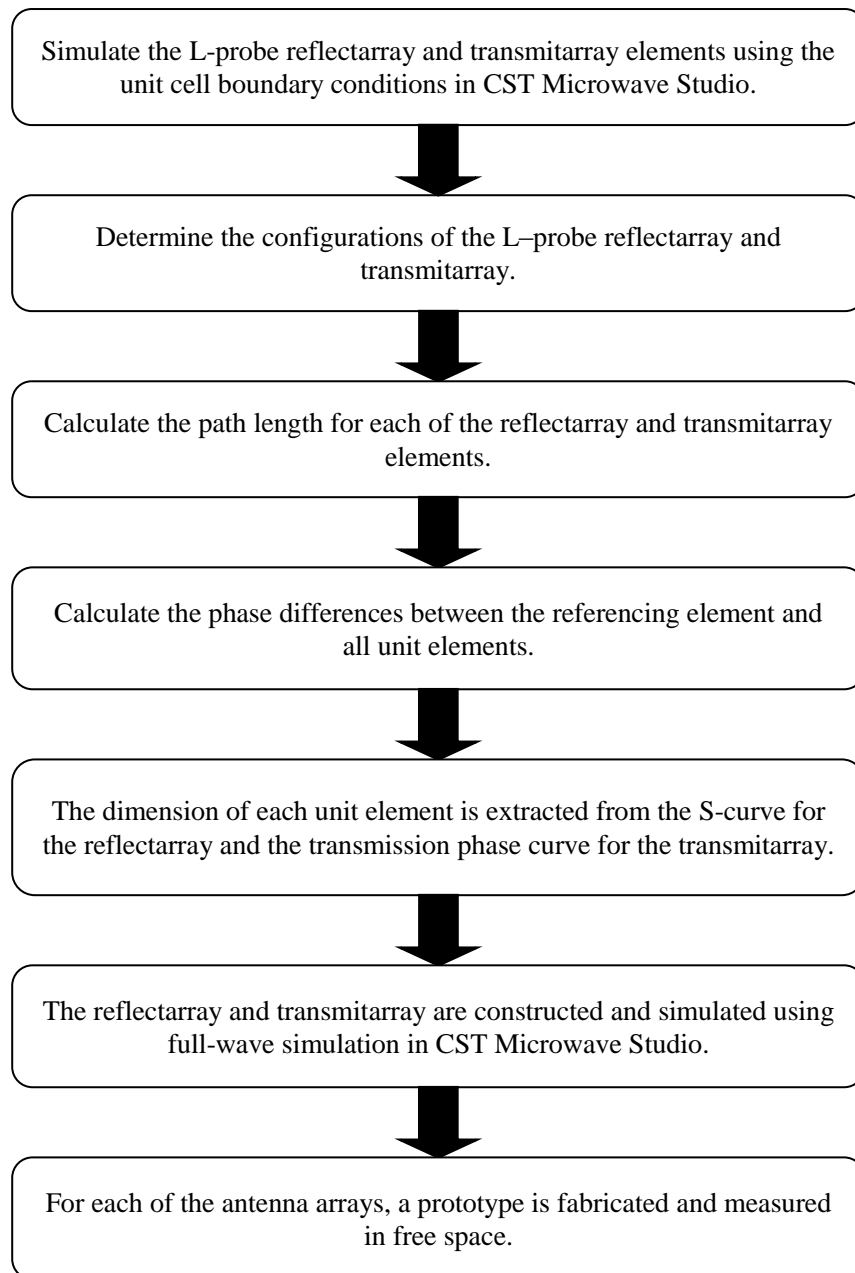


Figure 2.4: Design procedure of the reflectarray and transmitarray by using the phase-only optimization technique (POT).

2.3 Unit Element Simulation

Prior to designing the reflectarray and transmitarray, the unit elements have to be first analyzed and simulated for ensuring that a sufficient phase range is obtained. There are two possible methods for simulating the unit element - the Waveguide method and the Floquet method. Detailed explanations will be given in the following subsections.

2.3.1 Waveguide Method

As the name implies, the waveguide method is a technique in which the unit element is simulated in waveguide sections, as can be seen in Figure 2.5. With reference to the figure, the transmitarray element is embedded in between two sections of waveguides, with Port 1 defined as the input port where electromagnetic wave is launched; whereas Port 2 is set as the output port for receiving signal. To imitate the waveguides, the four boundaries are defined as perfect electrical conductor (PEC) in the CST Microwave Studio. Unit element simulated using this method can be verified experimentally. However, the size of the unit element has to follow the dimensions of the waveguide and the incident angle of the incoming wave is highly dependent on waveguide's operating and cut-off frequencies, making it a less popular method for designing the full-fledged antenna arrays. It is worth pointing out that the waveguide model of a reflectarray element involves only one waveguide section and a port (Port 1).

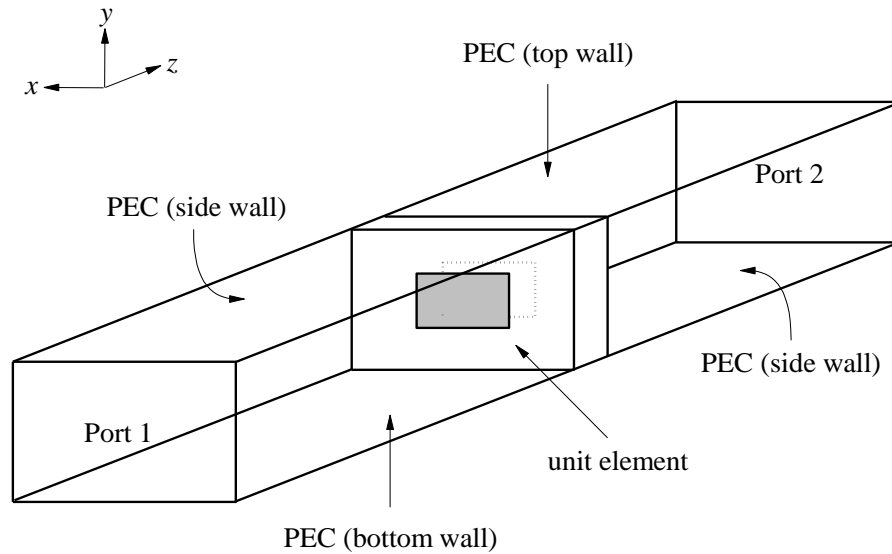


Figure 2.5: Waveguide model of a transmitarray element.

2.3.2 Floquet Method

The Floquet method is a popular and commonly applied technique for designing the reflectarrays and transmitarrays. Unit element which is placed inside a Floquet cell is virtually duplicated into multiple identical elements which imitate an infinite array with mutual coupling between the elements considered, as depicted in Figure 2.6. To realize the infinite array approach, the four walls around the unit element have to be set as periodic boundaries in the CST Microwave Studio. An example of the Floquet model is illustrated in Figure 2.7. In Floquet method, there are two modes which represent the plane waves, namely, the TE_{00} and TM_{00} modes. With reference to Figure 2.8, the E-fields of the TE_{00} and TM_{00} modes are directing in the y - and x -directions, respectively.

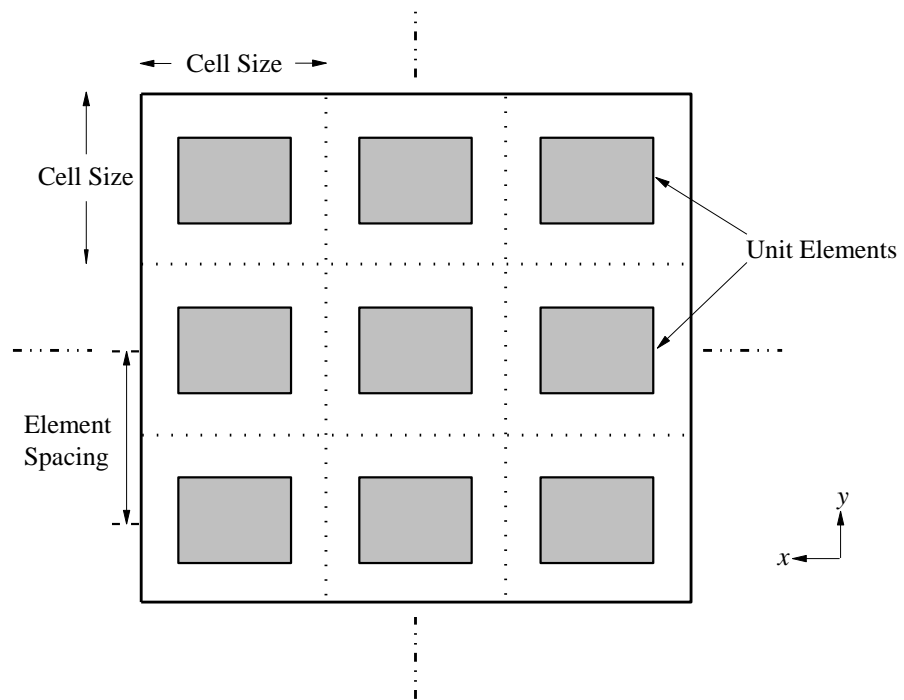


Figure 2.6: An infinite array with identical elements.

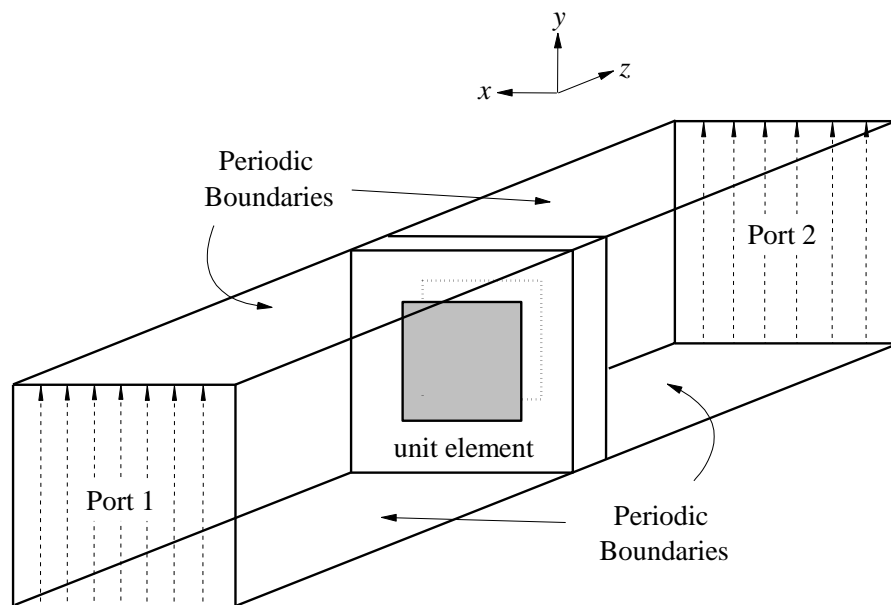


Figure 2.7: Floquet model of a transmitarray element.

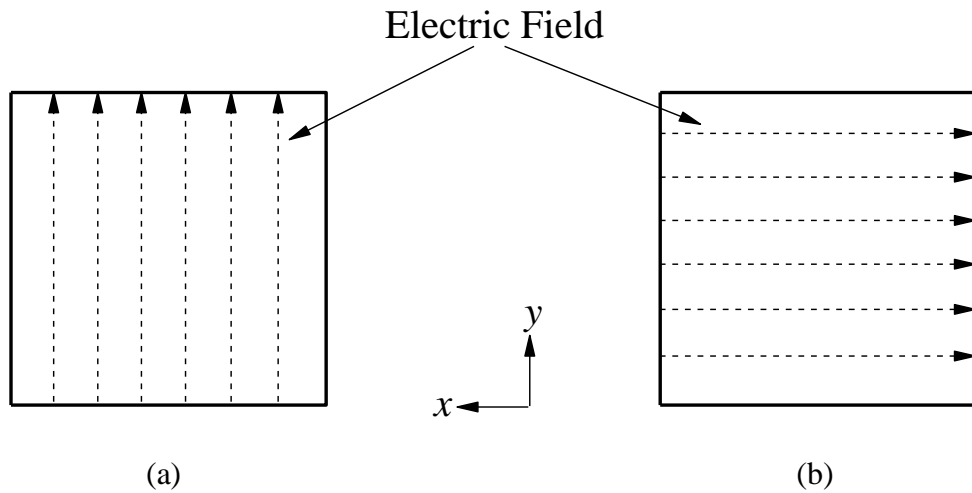


Figure 2.8: Electric fields generated along the z -direction for different Floquet boundary conditions. (a) TE_{00} mode, (b) TM_{00} mode.

In contrast to the waveguide method, the Floquet method allows any sizes of unit elements to be designed. In addition, it also enables the operating frequency of the unit element and the illuminating angle of the incident wave to be chosen freely. Nonetheless, the Floquet method also comes with several disadvantages. Firstly, unlike the waveguide method, unit element simulated using the Floquet method cannot be verified by experiment. Secondly, the mutual coupling between adjacent elements is assumed to be equal for all identical unit elements. This supposition is not accurate as the shapes of all unit elements are different in practical. Thirdly, the reflectarray and the transmitarray are not infinite in practice. Diffraction effect due to finite edges is not accounted for in Floquet model.

CHAPTER 3

BROADRANGE L-PROBE REFLECTARRAY

3.1 Introduction

Reflectarray is one type of antenna array which consists of an array of radiating elements illuminated by a feeding source. Its working principle is similar to that for the parabolic reflector where the spherical wavefront of the feeding source is converted to a planar one. The concept of reflectarray was first introduced by Berry et al. (1963) in the early 1960's where multiple truncated waveguides were used as the phase-shifting elements. The proposed structure was non-planar and bulky. In 1991, microstrip reflectarray was introduced (Huang, 1991). It has many advantages such as light weight, flat surface, and easy to manufacture. Owing to the well accepted advantages of microstrip technology, various designs of reflectarray unit elements have been proposed. Some of the early proposed reflectarray unit elements include patches with variable stub lengths (Chang and Huang, 1992), patches of variable sizes (Pozar and Metzler, 1993), and crossed dipoles (Pozar and Targonski, 1998).

Narrow bandwidth is a well-known factor that impedes microstrip structure from uses in designing broadband reflectarrays. Over the years, many research works have been conducted to broaden the bandwidth of the reflectarray. In the early 2000's, multilayer structures with stacked patches of variable size

(Encinar, 2001; Encinar and Zornoza, 2003) were proposed to mitigate the bandwidth limitation of the microstrip reflectarray. In order to alleviate the error due to misalignment between the multiple layers, a single-layered reflectarray is introduced. The single-layered reflectarrays that use multi-resonant elements such as circular rings connected to open-circuited stubs (Li et al., 2012), I-shaped dipole enclosed with a circular ring (Chen et al., 2013a), and multiple parallel dipole elements (Yoon et al., 2015) have been discovered to be able to achieve broad bandwidth. By controlling the separation distance of the elements to be smaller than half-wavelength, subwavelength coupled-resonant element (Zhao et al., 2010; Zhang et al., 2013; Qin et al., 2016) is another viable way for enhancing the bandwidth of reflectarray.

It has long been known that wire is an efficient electromagnetic radiator. It was first presented by Nakano et al. (1995) that an L-shaped wire can be used for exciting the C-shaped loop antenna to provide broadside radiation. Later, Luk et al. (1998) introduced a low profile L-probe-fed suspended patch antenna which is able to achieve a broad impedance bandwidth of 35%. In recent years, the L-shaped probe has also been utilized to attain dual (Wong et al., 2004; Lau and Luk, 2007; Liu et al., 2014) and circular polarization (Lau and Luk, 2005) operations. Due to the light weight feature, the L-shaped probe has also been used for designing antenna array (Lim et al., 2012).

In this chapter, the L-shaped probe is utilized for designing a linearly polarized broadband reflectarray. By varying the horizontal lengths of the two

L-probes, a linear phase range of 454.2° is attainable. An 11×11 reflectarray is designed, simulated, and experimentally verified. The designed reflectarray is able to provide a measured antenna gain of 20.4 dBi and a -1 dB gain bandwidth of 15.38%, with frequency range from 6.6 GHz to 7.7 GHz.

3.2 Unit Element Configuration and Analysis

For the first time, two L-shaped probes are co-joined for designing a reflectarray. The electromagnetic characteristics of the reflectarray unit element are first analyzed. Figure 3.1 shows the configuration of the element, which is placed inside a one-port Floquet cell. It is composed of two conductive L-shaped probes which are constructed side-by-side in parallel and with a gap of $G_x = 5$ mm on a square-shaped ($L = 30$ mm) FR4 substrate that has a thickness of $t = 1.7$ mm, a dielectric constant of $\epsilon_r = 4.3$, and loss tangent of $\tan \delta = 0.025$. To erect the L probes, the substrate is drilled with two holes with a diameter of $d = 1$ mm at a distance of 4 mm away from its edge, and the two probes are then properly soldered through the top and bottom copper layers. The main function of the substrate, with both surfaces laminated with copper layers, is the base support for the L probes. The vertical lengths of both of the long and short probes are fixed at a constant height of $h = 10$ mm. The horizontal length of the long probe (l_1) is always $x = 7$ mm more than the short probe, and the two probes are varied simultaneously to function as phase-shifting geometrical parameter.

With reference to Figure 3.1, the unit element is placed inside the Floquet cell. The unit cell is set to have periodic boundaries. In simulation, the cell is automatically expanded into an infinite array with considering mutual coupling between the adjacent elements. The position of the waveguide port (Port 1) is located at a distance of 152 mm from the horizontal parts of the probes. A y -polarized plane wave (Floquet mode TE_{00}) with an incident angle of $\phi = 0^\circ$, $\theta = 15^\circ$, propagating to the direction of the probes, is launched from the port. After the execution of simulation, the reference plane is further de-embedded from the port to horizontal probes. As a result, the length between the port and the unit element can be neglected as it does not contribute to the reflection magnitude and phase range.

Figure 3.2 shows the reflection magnitude ($|S_{11}|$) and reflection phase ($\angle S_{11}$) of the unit element at the operating frequency of 7.1 GHz when l_1 is varied from 9.5 to 26.4 mm, with a linear phase range 454.2° obtained. It is worth mentioning that the reflection magnitude can be well kept above -0.1 dB in this range. For the case of $l_1 = 20$ mm, electric field distributions around the long probe (20 mm) and short probe (13 mm) are illustrated in Figure 3.3 (a) and (b), respectively. One and half standing wave is found on the long probe, and the vertical and horizontal wires add up to be 0.71λ , which is quite close to 0.75λ (31.7 mm). There is one standing wave formed on the short probe, and the total wire length is $\sim 0.54\lambda$.

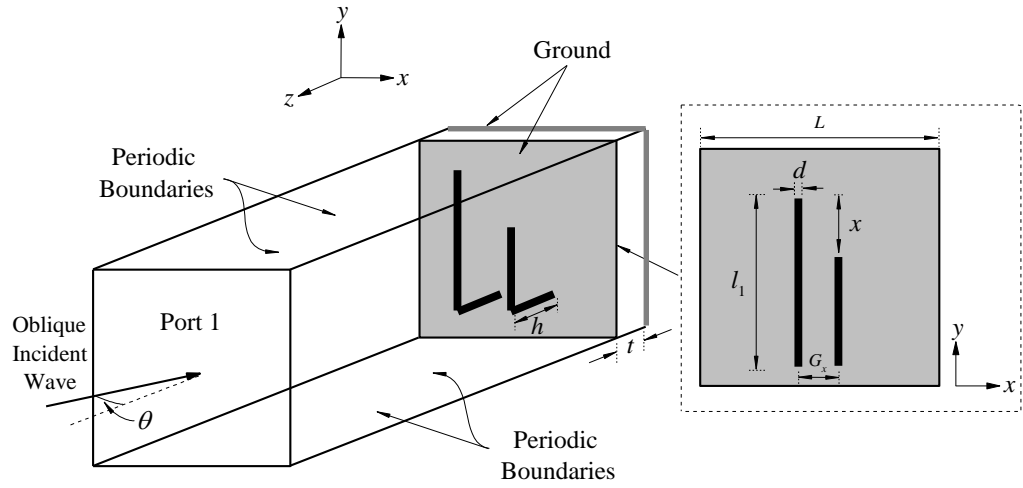


Figure 3.1: One-port Floquet cell for simulating the co-joined L-probe reflectarray unit element.

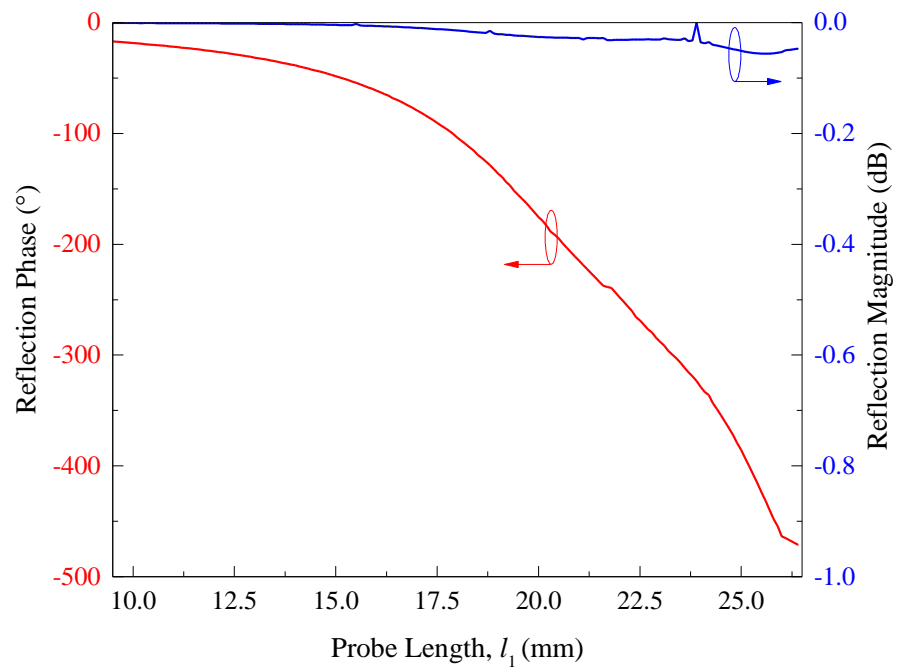
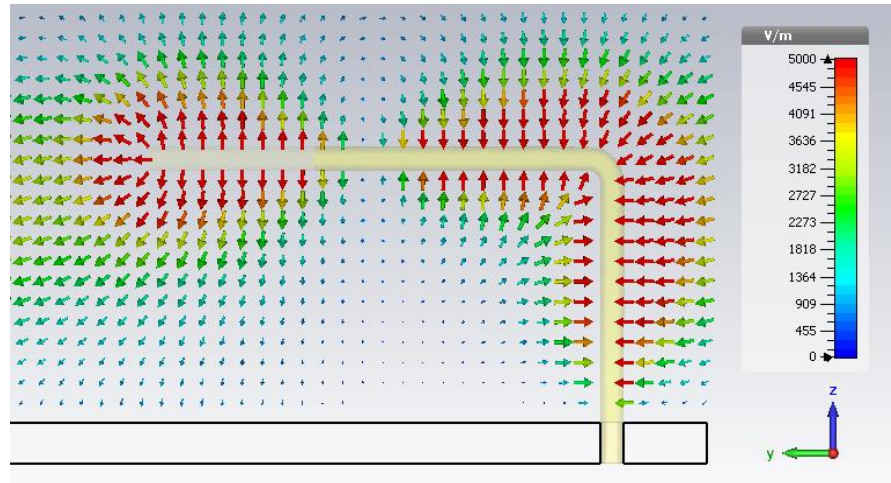
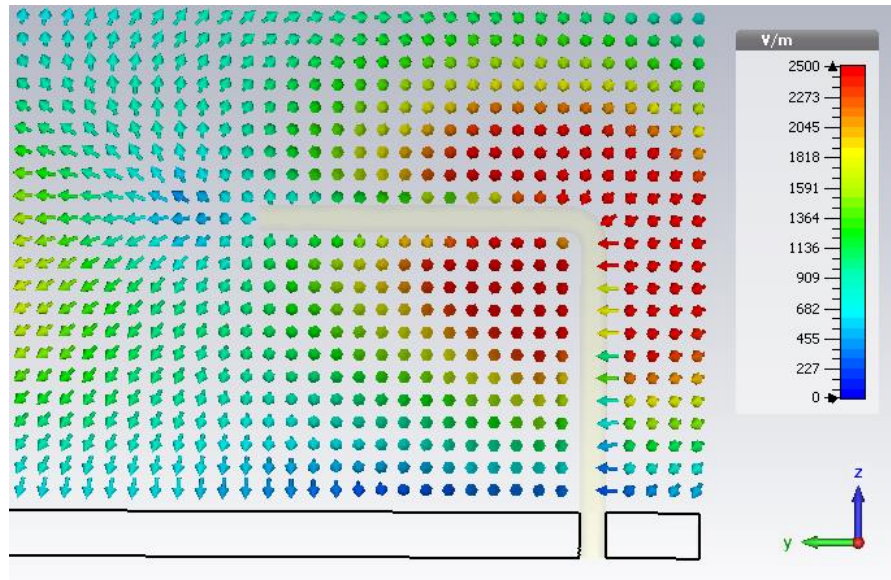


Figure 3.2: Reflection magnitude and reflection phase of the reflectarray unit element.



(a)



(b)

Figure 3.3: Electric field distributions around the (a) long L-probe, (b) short L-probe at the frequency of 7.1 GHz for the case of $l_1 = 20$ mm.

3.3 Reflectarray Configuration

The unit element is designed into a full-fledged linearly polarized (LP) reflectarray as shown in Figure 3.4. The reflectarray consists of 121 elements (11×11). Each element is separated by $L = 0.71\lambda = 30$ mm which contributes to the board size of $D = 330$ mm. A C-band (5.85 – 8.2 GHz) pyramidal horn is used as the source for exciting the reflectarray elements. The feeding horn is placed at a far-field distance of $f = 264$ mm, with an incident angle of $\theta_o = 15^\circ$ pointing to the center element of the reflectarray. In this case, the f/D ratio is calculated to be 0.8. The prototype of the LP reflectarray is shown in Figure 3.5. The design procedure is elaborated now. To commence with, a reference element, which can be any one of the reflectarray elements, is selected. Referring to the red curve in Figure 3.2, the reference element is first set to be a random phase (ϕ_o) on the y -axis which corresponds to a probe length l_1 , ranging from 9.5 to 26.4 mm on the x -axis. Path lengths for the waves propagating from the feeding horn to the reference element and the N^{th} elements are denoted as P_o and P_N , and the phase difference (δ_ϕ) between the two paths can be easily calculated as $\delta_\phi = (P_N - P_o) \times (2\pi/\lambda)$. This is the additional phase ($\phi_N = \phi_o + \delta_\phi \pm 2n\pi$) that is required by the N^{th} element such that the wave is reflected in phase with the reference element. With the use of the red curve, the probe length can be determined by mapping ϕ_N to the geometrical parameter on the x -axis.

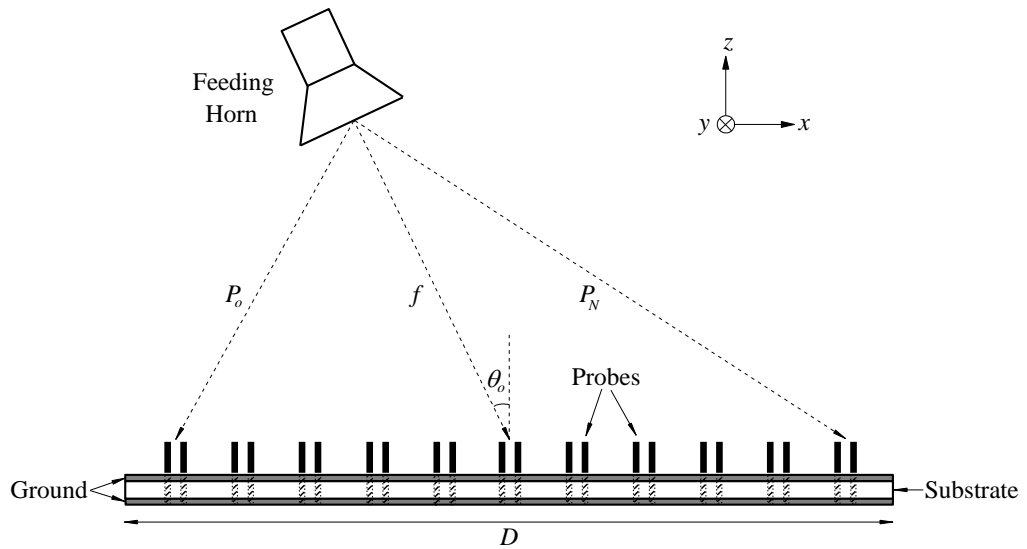


Figure 3.4: Configuration of the proposed linearly polarized reflectarray.

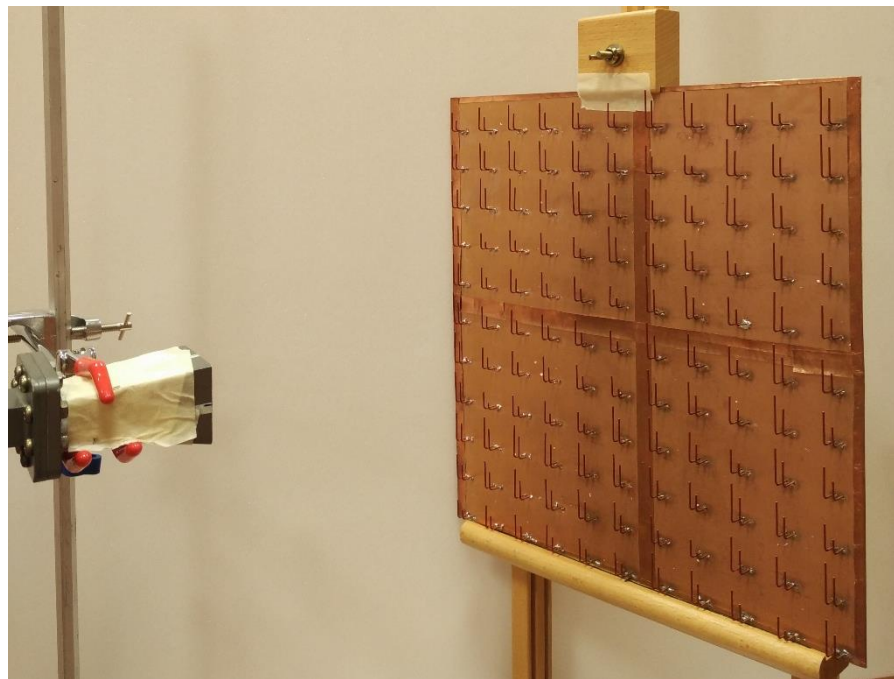


Figure 3.5: Prototype of the linearly polarized reflectarray.

The design procedure for one unit element is now delineated. To begin, with reference to Figure 3.6, the detailed steps for calculating the additional phase required by the element on the sixth row sixth column of the proposed reflectarray, denoted as (6, 6), are shown below. Then, the phase distributions

of the radiating elements on the proposed reflectarray and their corresponding probe lengths are tabulated in the table, as shown in Appendix A.

- 1) The reference element, in this case, element (6, 1) is selected. The reference element is given a phase of $\phi_o = -385.5^\circ$ from the S-curve, which is mapped to the probe length, l_1 of 23.5 mm.
- 2) The path length for the electromagnetic waves, travelling from the feeding horn to the reference element, P_o is calculated.

$$\begin{aligned} p &= P_{(6,6)} \times \sin \theta_o & H &= P_{(6,6)} \times \cos \theta_o \\ &= 264 \text{ mm} \times \sin 15^\circ & &= 264 \text{ mm} \times \cos 15^\circ \\ &= 68.33 \text{ mm} & &= 255 \text{ mm} \end{aligned}$$

$$\begin{aligned} a &= D/2 & q &= a - p - (30 \text{ mm} / 2) \\ &= 330 \text{ mm} / 2 & &= 165 \text{ mm} - 68.33 \text{ mm} - (30 \text{ mm} / 2) \\ &= 165 \text{ mm} & &= 81.67 \text{ mm} \end{aligned}$$

$$\begin{aligned} P_o &= \sqrt{q^2 + H^2} \\ &= \sqrt{(255 \text{ mm})^2 + (81.67 \text{ mm})^2} \\ &= 267.76 \text{ mm} \end{aligned}$$

- 3) The path lengths for P_o and $P_{(6,6)}$ are converted to propagation phases.

$$\begin{aligned} \lambda &= c / f_o \\ &= (3 \times 10^8) / (7.1 \times 10^9) \\ &= 42.25 \text{ mm} \end{aligned}$$

$$\begin{aligned} \varphi_o &= P_o \times \frac{2\pi}{\lambda} \\ &= 267.76 \text{ mm} \times \frac{2\pi}{42.25 \text{ mm}} \times \frac{180^\circ}{\pi} \\ &= 2281.5^\circ \end{aligned}$$

$$\begin{aligned} \varphi_{(6,6)} &= P_{(6,6)} \times \frac{2\pi}{\lambda} \\ &= 264 \text{ mm} \times \frac{2\pi}{42.25 \text{ mm}} \times \frac{180^\circ}{\pi} \\ &= 2249.5^\circ \end{aligned}$$

4) The phase difference between element (6, 6) and the reference element is calculated.

$$\begin{aligned}\delta_{\phi(6,6)} &= \varphi_{(6,6)} - \varphi_o \\ &= 2249.5^\circ - 2281.5^\circ \\ &= -32^\circ\end{aligned}$$

5) The additional phase that is required by element (6, 6) is calculated and mapped to its corresponding probe length in the S-curve. In this case, -57.5° is selected, and it is mapped to the probe length of $l_1 = 14.2$ mm in the S-curve.

$$\begin{aligned}\phi_{(6,6)} &= \phi_o + \delta_{\phi(6,6)} \pm 2n\pi \\ &= -385.5^\circ - 32^\circ \\ &= -417.5^\circ\end{aligned}\quad \text{OR} \quad \begin{aligned}\phi_{(6,6)} &= \phi_o + \delta_{\phi(6,6)} \pm 2n\pi \\ &= -385.5^\circ - 32^\circ + 360^\circ \\ &= -57.5^\circ\end{aligned}$$

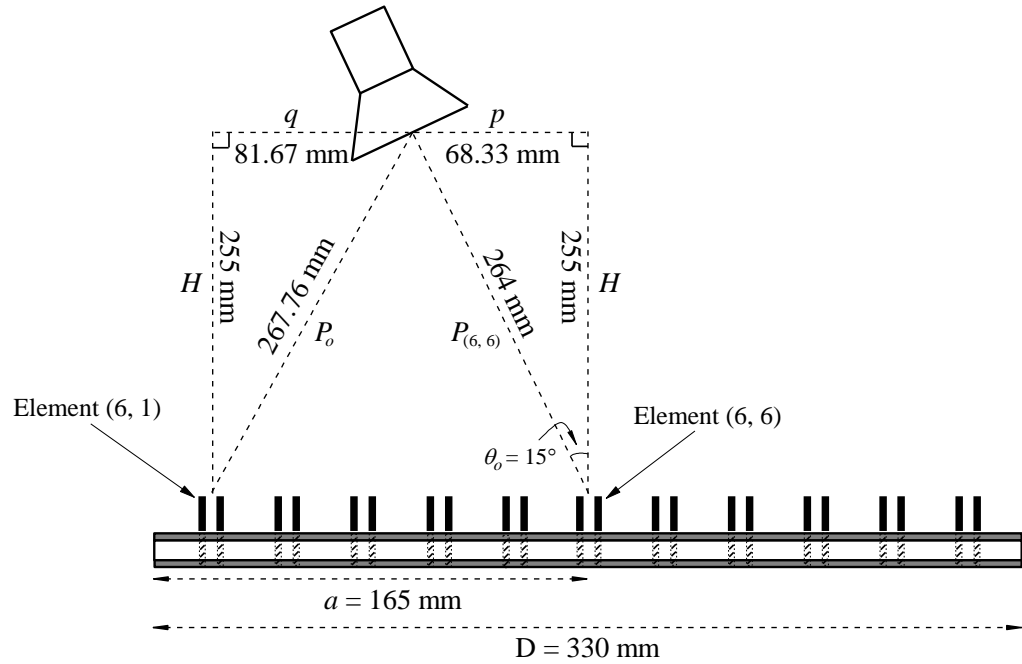


Figure 3.6: Path length for the electromagnetic waves travelling from the feeding horn to the reference element (element (6, 1)).

3.4 Measurement Setup

Figure 3.7 shows the free space experimental setup for measuring the antenna gain and radiation patterns of the antenna under test (reflectarray). The antenna under test (AUT), which is the transmitting antenna, is connected to a signal generator (Rohde & Schwarz SMB100A) for generating microwave signal. The signal generator is tuned to the operating frequency of the AUT. To capture the received power P_r , a C-band pyramidal horn (ATM PNR137-440-2, 5.85 GHz – 8.2 GHz), which is the receiving antenna, is connected to a spectrum analyzer (Advantest U3771). It is placed at a far field distance of $R > 2D^2/\lambda$, where D is the diagonal dimension of the AUT. In measurement, a power of $P_t = -10$ dBm is supplied from the signal generator, and the AUT is rotated on a turntable in the θ direction for a full cycle of 360° . For different elevation angles, the received powers are directly read from the spectrum analyzer. The gain of the AUT for each elevation angle is found by applying the Friss transmission formula. The antenna measurement is conducted at the 10th floor (concourse area) of the university, which is very spacious. The proposed reflectarray is able to provide high antenna gain, thus, the measured results are less affected by the environmental factors.

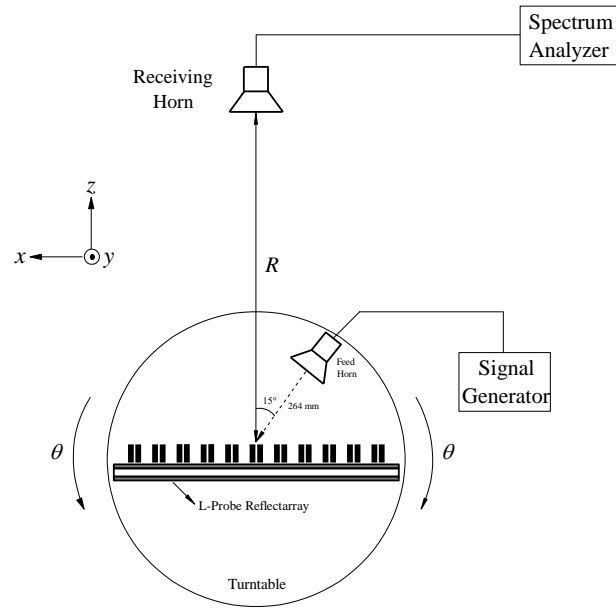
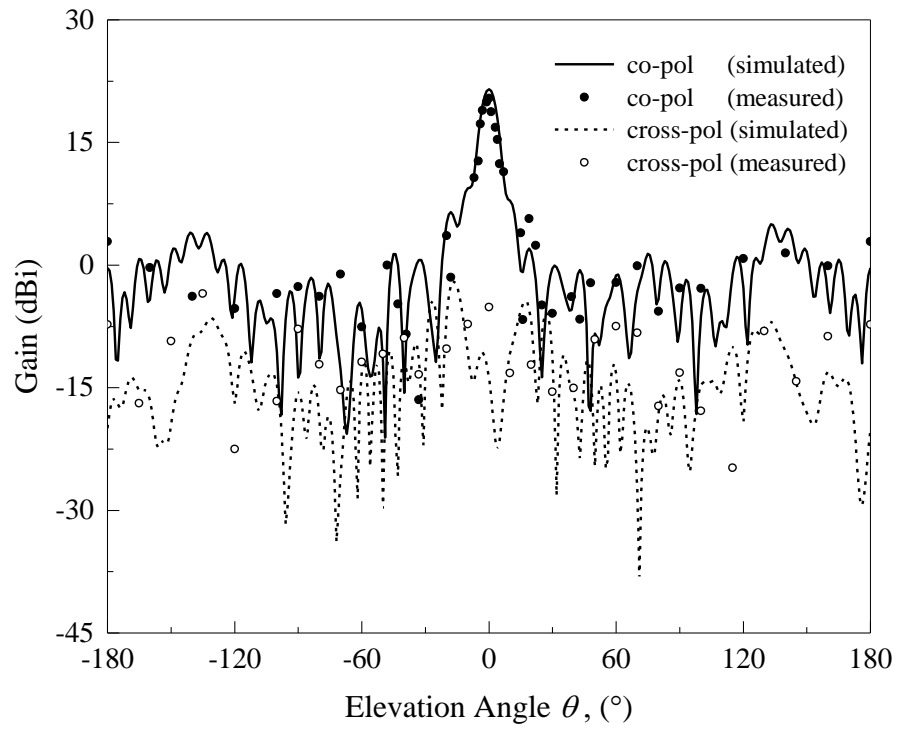


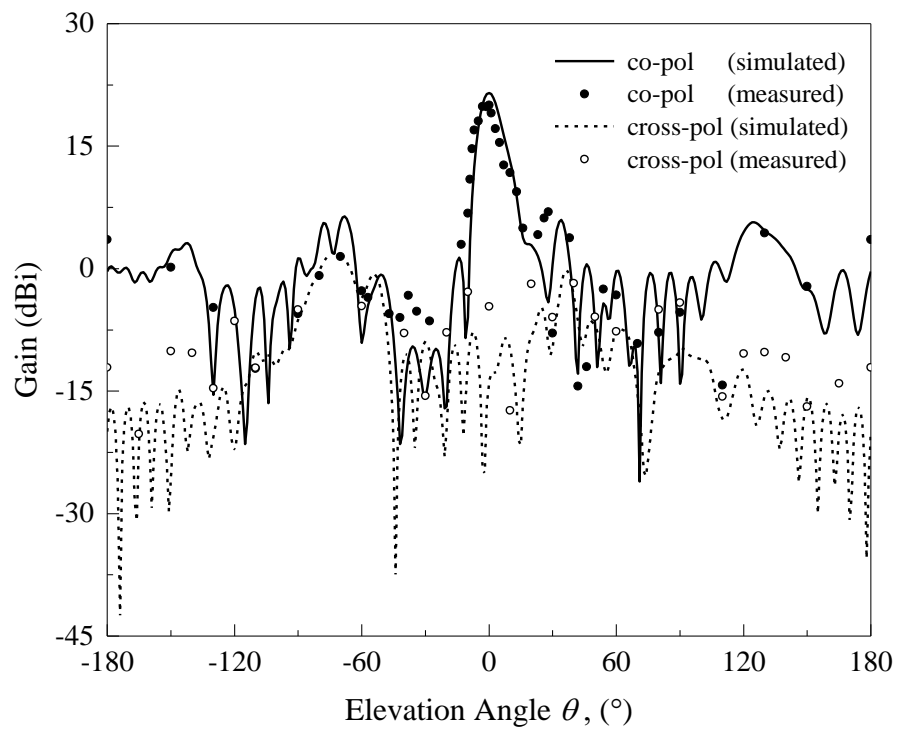
Figure 3.7: Measurement setup for the reflectarray ($R = 11.5$ m).

3.5 Simulated and Experimental Results of Reflectarray

The characteristics of the proposed reflectarray, shown in Figure 3.4, are now analyzed. Figure 3.8 shows the measured and simulated radiation patterns in the yz -plane (E -plane) and xz -plane (H -plane) of the proposed reflectarray at 6.9 GHz. Generally, the measurement results agree well with simulation. A measured peak gain of 20.4 dBi is obtained in the boresight direction ($\theta = 0^\circ$) while simulation reads 21.5 dBi. The difference between the measured co-polarized field and its cross-polarized field at $\theta = 0^\circ$ is at least 25 dB. The measured and simulated antenna gain against frequency is shown in Figure 3.9. From measurement, a -1 dB gain bandwidth of 15.38% is achievable, with frequency ranging from 6.6 GHz to 7.7 GHz.



(a)



(b)

Figure 3.8: Measured and simulated (a) *E*- and (b) *H*- planes radiation patterns of the proposed reflectarray at 6.9 GHz.

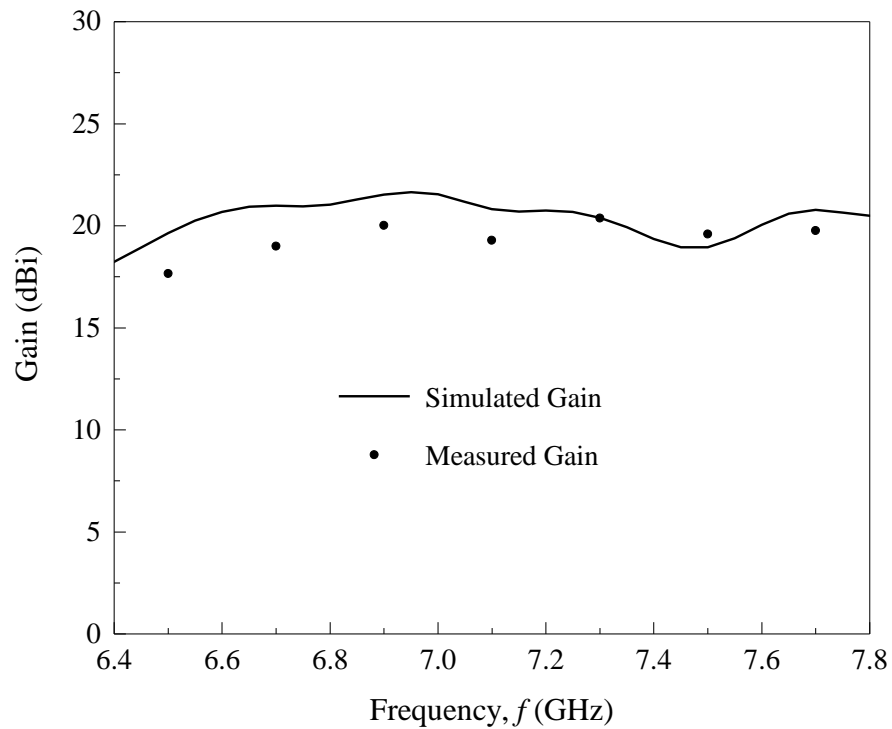


Figure 3.9: Measured and simulated antenna gains of the proposed reflectarray as a function of frequency.

3.6 Parametric Analysis

Parametric analysis has been performed on some of the key design parameters in order to study the reflection characteristics of the unit element and their effects on the radiation performances when the unit element is designed into a full-fledged reflectarray.

3.6.1 Comparison of Single and Double L Probe Elements

To begin, the reflectarray unit element which consists of a single L probe is compared with the one with two L probes, where the short probe is always shorter than the long probe by $x = 7$ mm and their corresponding

reflection characteristics are shown in Figure 3.10. It is apparent that the reflectarray unit element with single L probe is unsuitable for designing the full-fledged reflectarray as the element is only able to provide a phase range of up to 276.1° . On the other hand, the reflectarray unit element which consists of two L probes is capable of achieving a broad phase range of 454.2° and, therefore, it is chosen for the reflectarray design. The broadening of phase range is due to the long and the short probes which resonate simultaneously at the design frequency of 7.8 GHz.

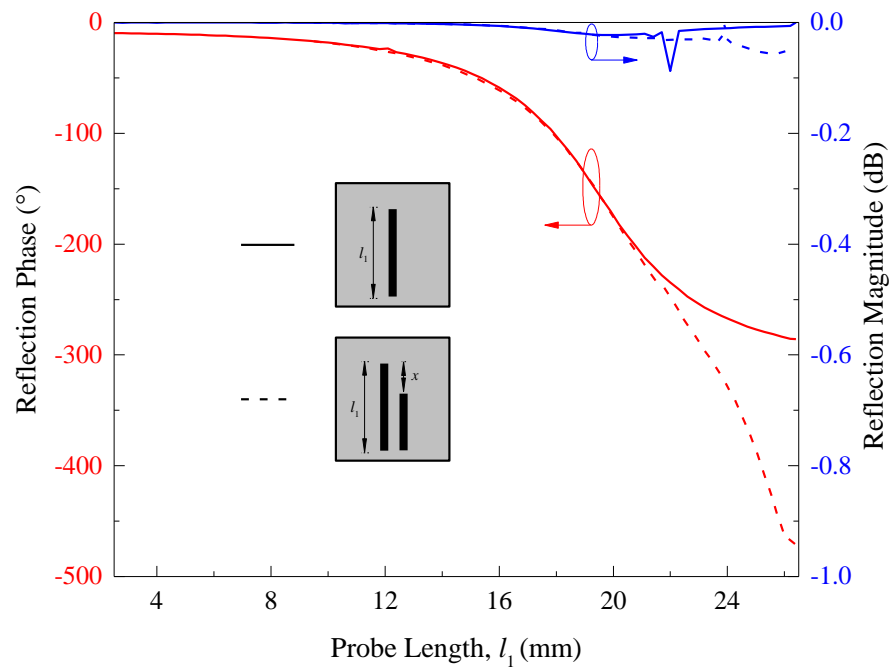


Figure 3.10: Comparison of the reflection magnitudes and reflection phases of the reflectarray unit elements with single and double L probes.

3.6.2 Length Difference between Long and Short Probes

The difference in length (x) between the long and the short probes is varied from 0 mm to 9 mm and the element responses are shown in Figure 3.11. It is observed that the changing rate of phase curve becomes slower and the phase range narrows down when the length difference is increased. For the case of $x = 0$ mm, the long and the short probes have the same length. The combination of the same resonating mode of the two probes has contributed to the abrupt change in phase around the probe length of $l_1 = 19$ mm to 20 mm. In our experiment, the length difference between two probes is selected to be 7 mm because the gradient of its reflection phase is the slowest among all and it provides sufficient phase range for designing the full-fledged reflectarray.

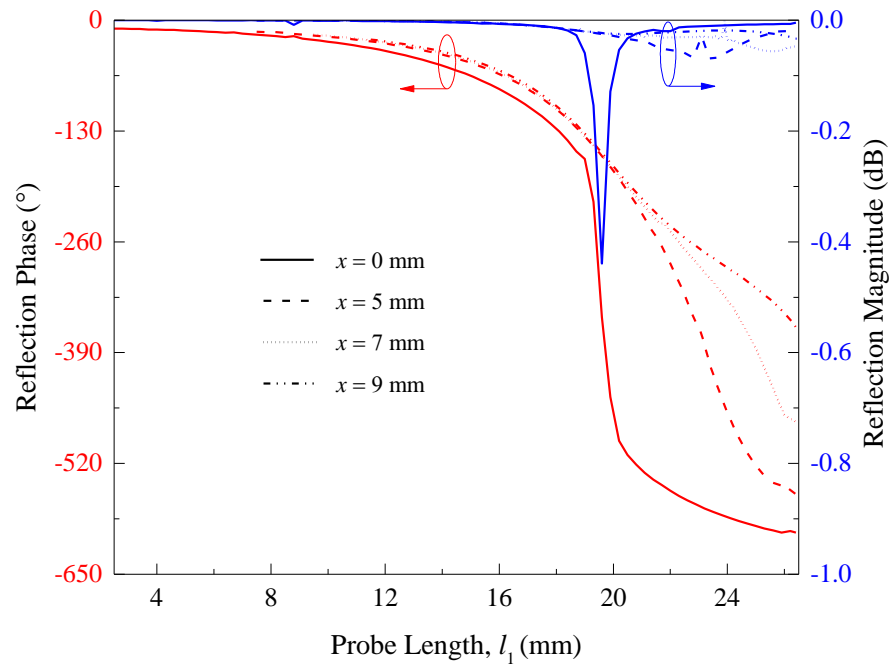


Figure 3.11: Effects of the length difference (x) between the long and the short probes on the reflection magnitude and reflection phase of the reflectarray unit element.

3.6.3 Feeding Angle

The feeding angle (θ_o) is now studied. In the proposed unit element, a steeper reflection phase slope is obtained with the feeding angle varied from $\theta_o = 10^\circ$ to 20° , as illustrated in Figure 3.12. For all feeding angles, a phase range of $\sim 440^\circ$ is achievable. In the full-fledged reflectarray, as can be seen in Figure 3.13, higher side lobe level is observed when the reflectarray element is excited with a larger feeding angle. Significant reduction in the boresight ($\theta = 0^\circ$) antenna gain is also observed when the feeding angle goes beyond $\theta_o = 15^\circ$. This is because some of the elements are not properly reachable by the feeding beam in this case.

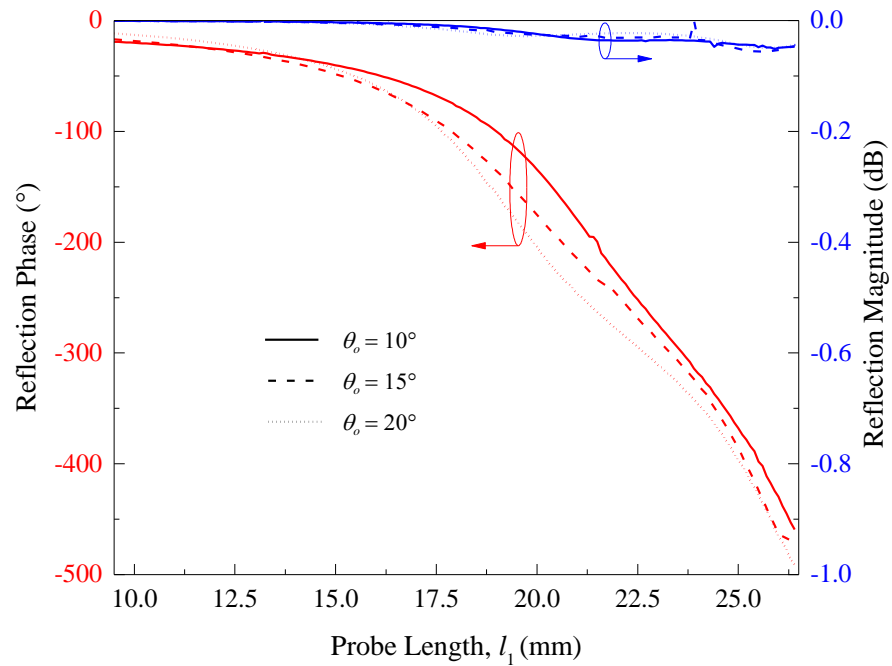
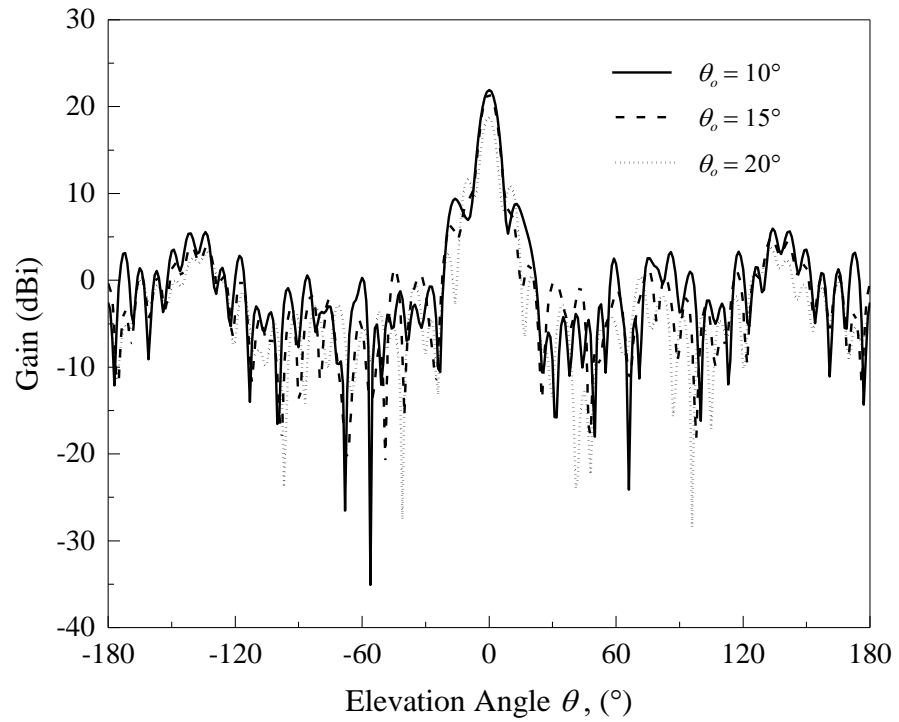
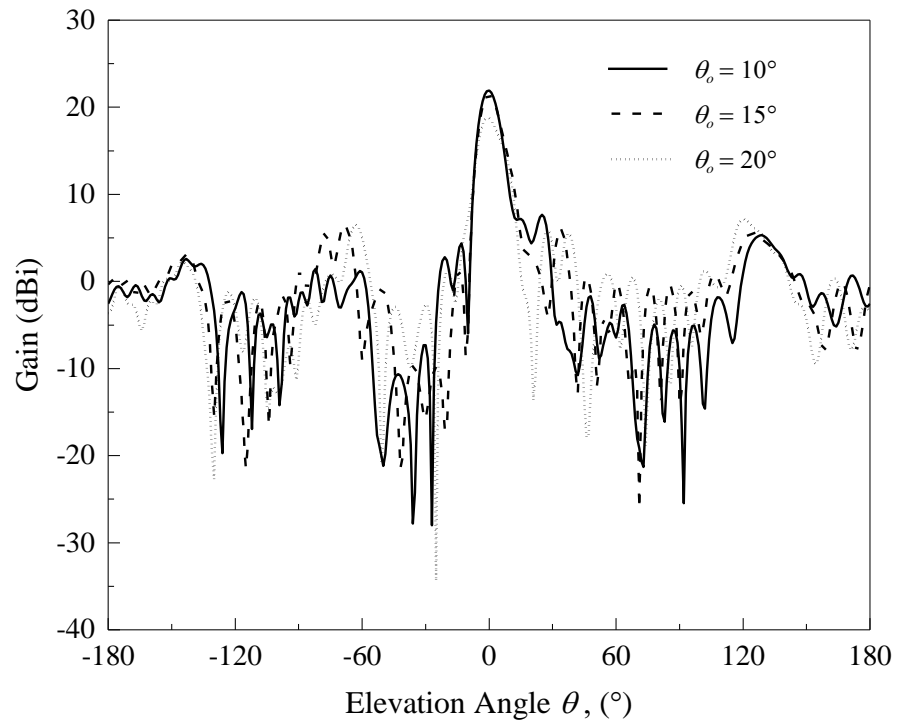


Figure 3.12: Effects of the feeding horn incident angle (θ_o) on the reflection magnitude and reflection phase of the reflectarray unit element.



(a)



(b)

Figure 3.13: Radiation patterns of the proposed reflectarray for different feeding horn incident angles (θ_o) at 6.9 GHz. (a) *E*- and (b) *H*-planes.

3.6.4 Unit Cell Size

Next, the effects of unit cell size (L), which is also the separation distance between elements in full reflectarray, are analyzed. Figure 3.14 illustrates the reflection characteristics of the unit element when the cell size is varied from $L = 0.71\lambda$ to 0.805λ at 7.1 GHz. A larger unit cell is observed to be able to provide a broader reflection phase range as the probes are extendable further. However, increasing the cell size comes with the price of steeper reflection phase slope. Varying the cell size, however, does not affect the reflection magnitude much. Figure 3.15 shows the radiation patterns of the reflectarray at 6.9 GHz. Significant increase in the side lobe level around the elevation angle of $\theta = -90^\circ$ to $+90^\circ$ and notable reduction in the boresight antenna gain are inspected when the separation between reflectarray elements becomes greater. The enlargement of the unit cell size has caused the optimal radiation frequency of the reflectarray to shift lower than 6.9 GHz.

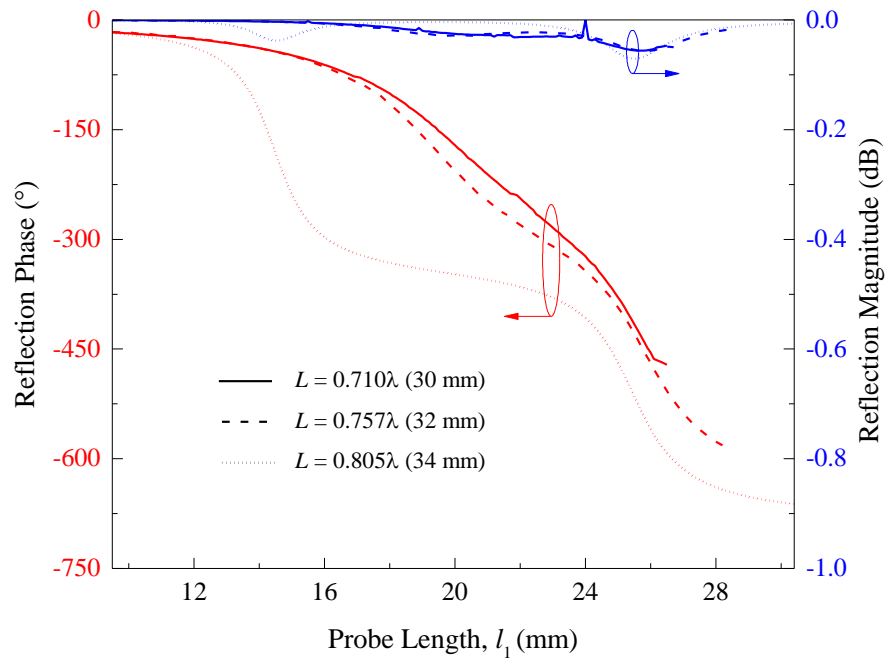
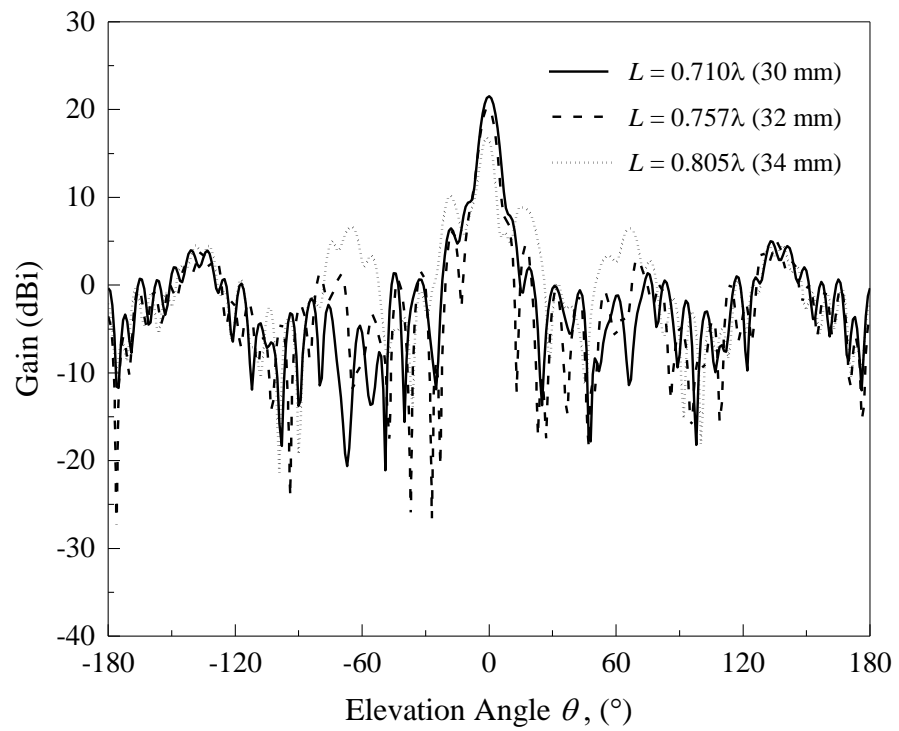


Figure 3.14: Effects of the unit element dimension (L) on the reflection magnitude and reflection phase of the reflectarray unit element.



(a)

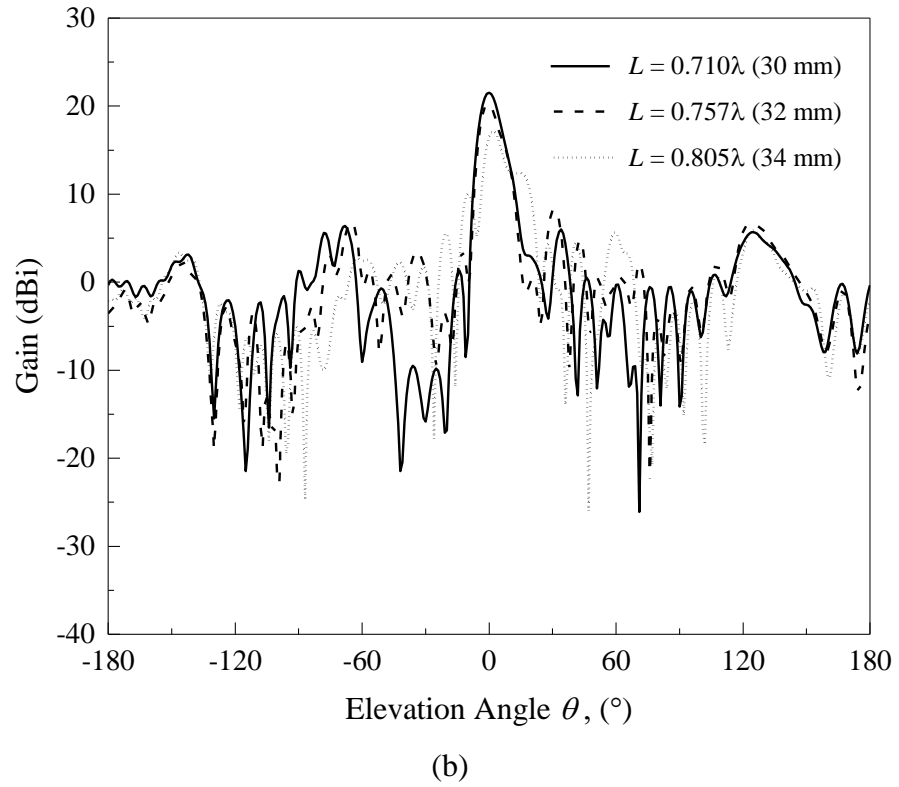


Figure 3.15: Radiation patterns of the proposed reflectarray for different separation distances (L) at 6.9 GHz. (a) E - and (b) H - planes.

3.6.5 Probe Height

By varying the probe height (h) from 10 mm to 14 mm, the reflection characteristics of the reflectarray unit element are shown in Figure 3.16. It can be deduced that varying the probe height does not change the linearity of the reflection phase curve much. For the probe height of $h = 10$ mm, 12 mm, and 14 mm, a phase range of 454.2° , 496.59° , and 508.22° can be obtained, respectively. Figure 3.17 shows the radiation patterns of the full-fledged reflectarrays for different probe heights. The reflectarrays with probe heights of $h = 12$ mm and 14 mm have antenna gains which are ~ 1 dB lower than the

one with probe height of $h = 10$ mm. Also, a side lobe level of ~ 8 dB around the elevation of $\theta = -30^\circ$ and $+30^\circ$ is observed for the case of $h = 14$ mm.

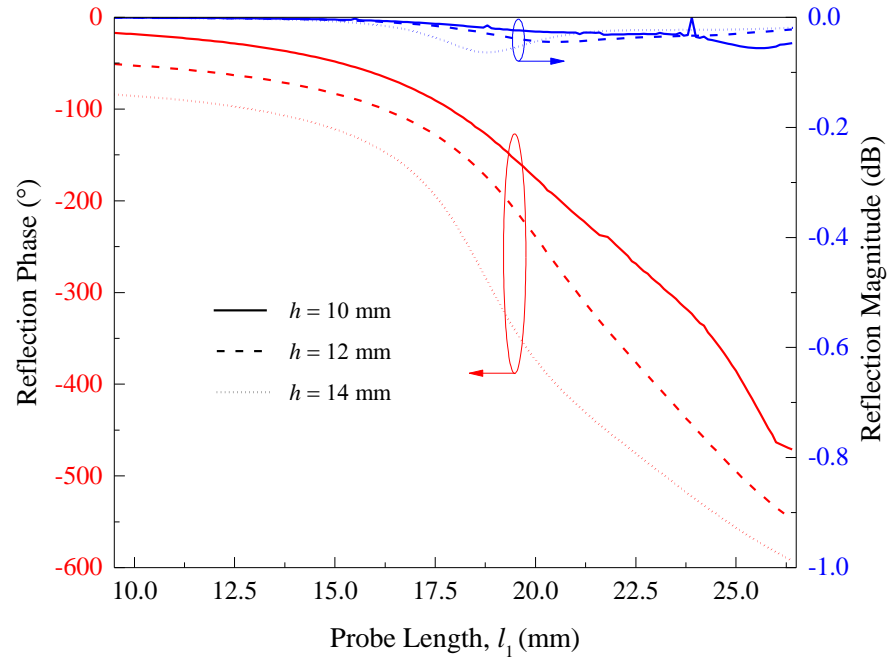
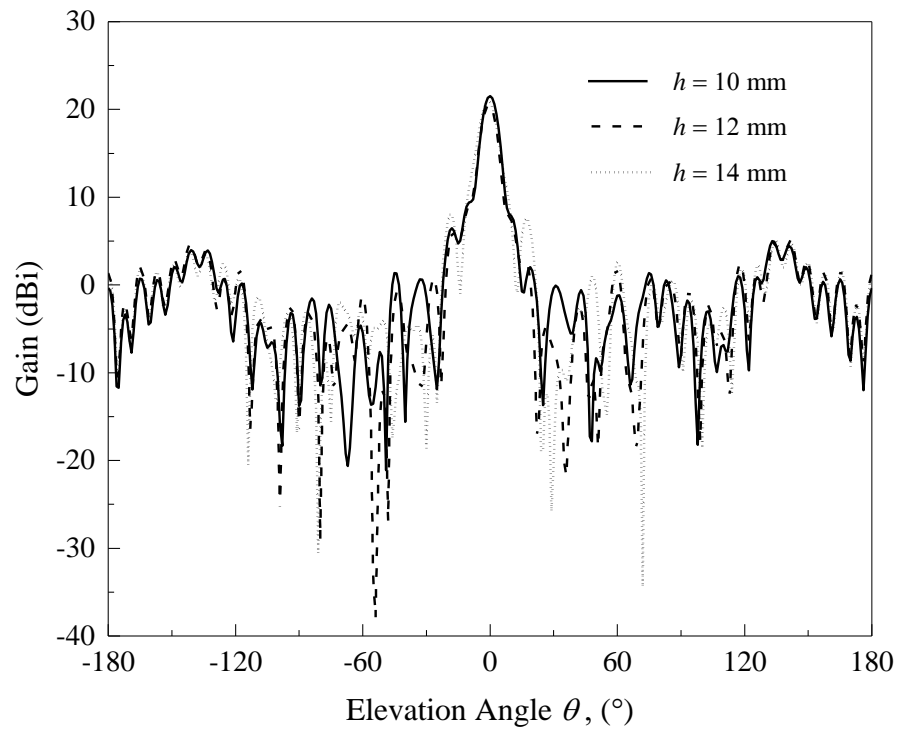


Figure 3.16: Effects of the probe height (h) on the reflection magnitude and reflection phase of the reflectarray unit element.



(a)

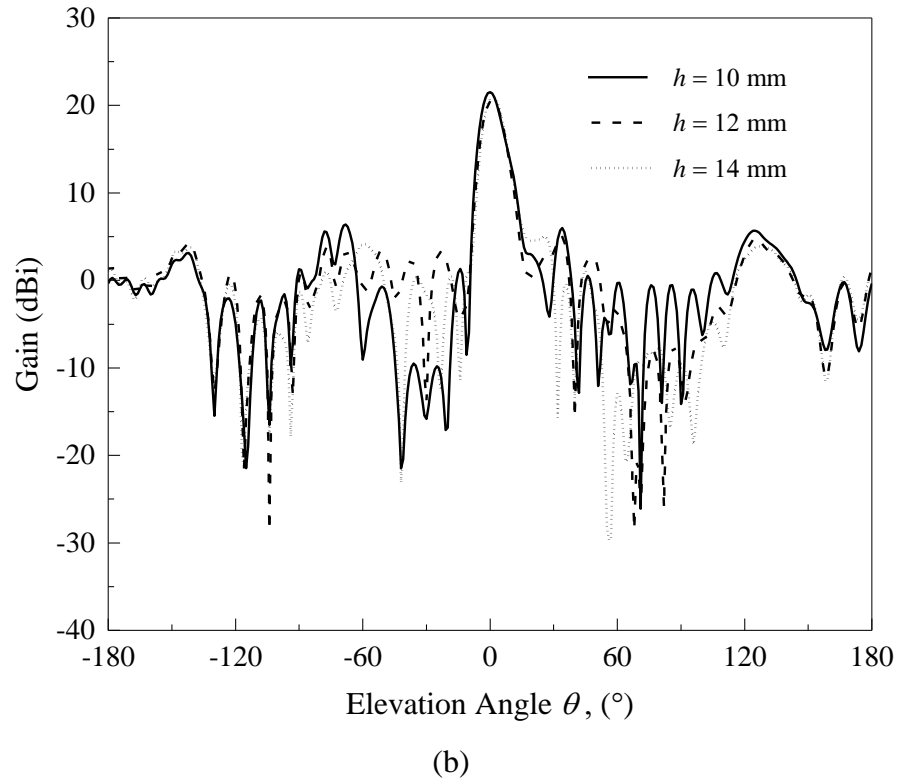


Figure 3.17: Radiation patterns of the proposed reflectarray for different probe heights (h) at 6.9 GHz. (a) E - and (b) H - planes.

3.6.6 Probe Diameter

Now, the effects of probe diameter (d) are studied. Figure 3.18 shows the reflection magnitude and reflection phase of the reflectarray unit element when the probe diameter is varied from 0.5 mm to 1.5 mm. A larger probe diameter has enabled a larger reflection phase range but with the price of steeper reflection phase slope. The performances of the reflectarray with different probe diameters are studied in Figure 3.19. For all probe diameters, the front-to-back ratios of the reflectarrays are maintained above 21.88 dB while the discrepancies between the main and side lobe levels are kept well beyond 14.82 dB.

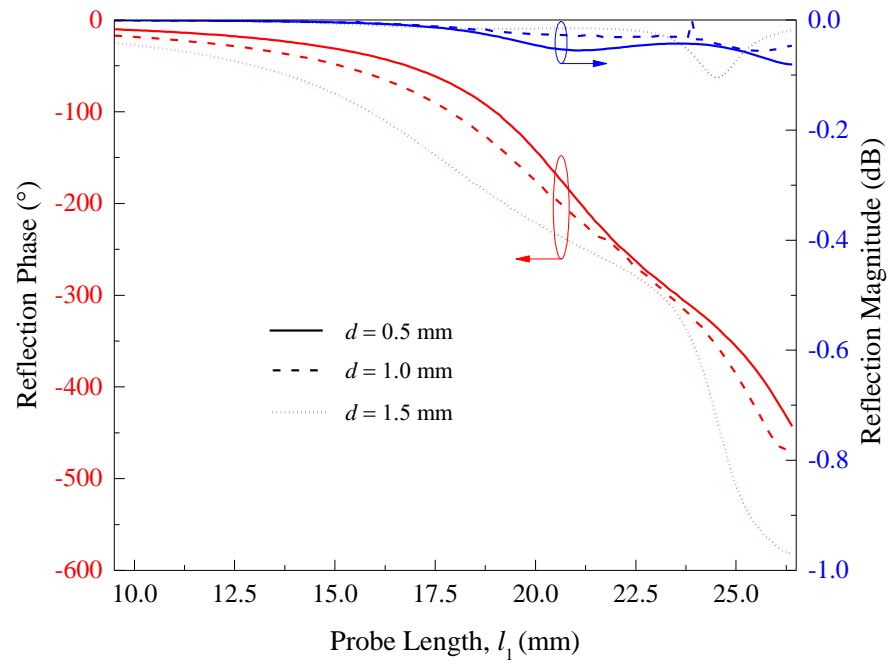
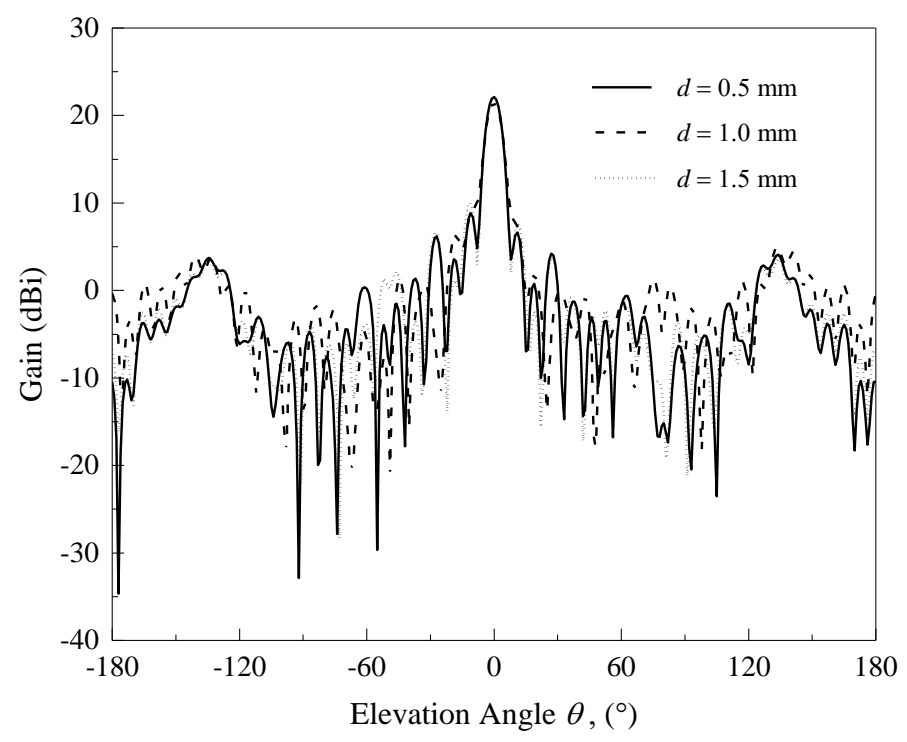


Figure 3.18: Effects of the probe diameter (d) on the reflection magnitude and reflection phase of the reflectarray unit element.



(a)

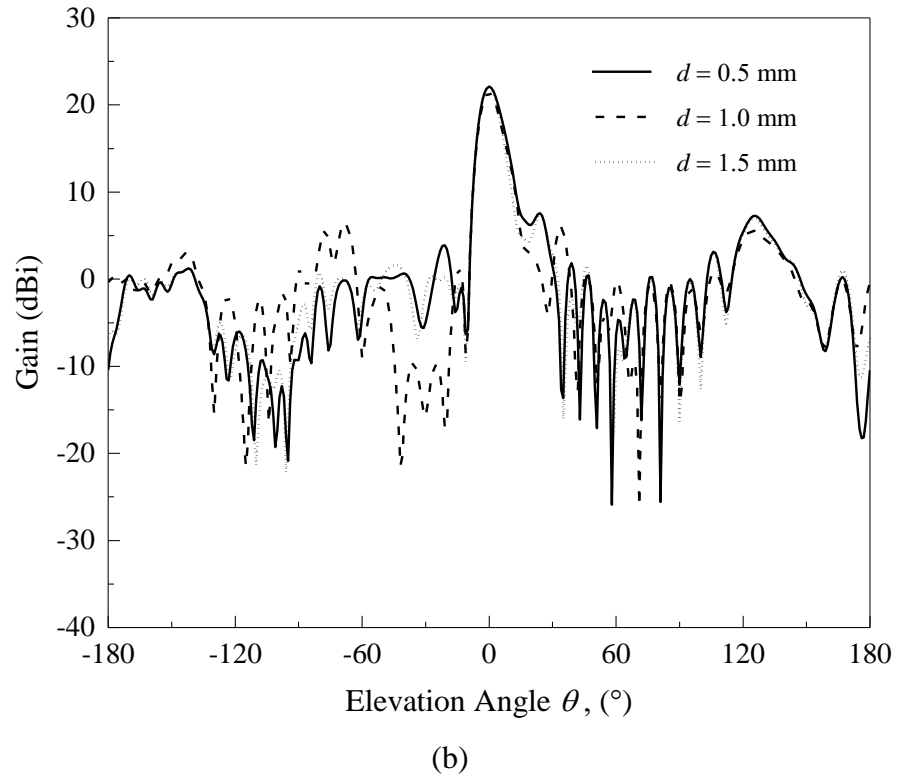
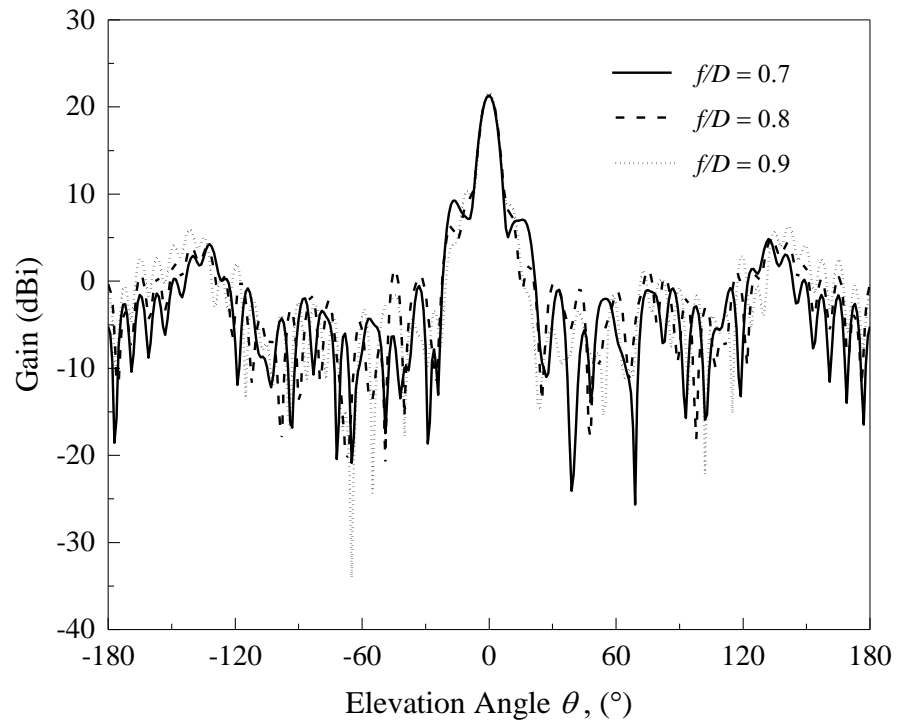


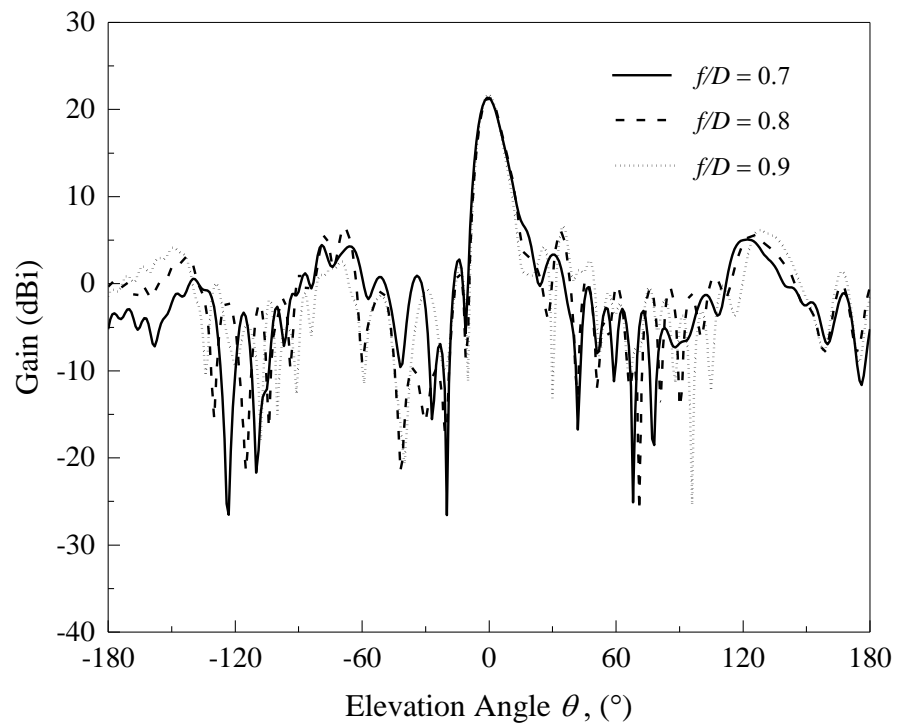
Figure 3.19: Radiation patterns of the proposed reflectarray for different probe diameters (d) at 6.9 GHz. (a) E - and (b) H - planes.

3.6.7 f/D Ratio

Finally, by maintaining the cell size at $L = 0.71\lambda$ (30 mm) and array dimension at $D = 330$ mm, the effects of f/D ratio are analyzed at 6.9 GHz. Referring to the radiation patterns in Figure 3.20, increase in the f/D ratio is jeopardizing the radiation performances by boosting up the side lobe level and pushing down the front-to-back ratio. High back lobe level of ~ 0 dBi is observed for f/D ratio of 0.9 because some of the signals from the feed antenna is spilled to the back of the reflectarray.



(a)



(b)

Figure 3.20: Radiation patterns of the proposed reflectarray for different f/D ratios. (a) E - and (b) H - planes.

3.7 Conclusion

Conductive L-shaped probes have been employed for designing a reflectarray for the first time. The electric field distribution around the L probes is presented and the procedures for designing the reflectarray are elucidated. The reflectarray unit element has been simulated using a one-port Floquet cell, where linear phase range of 454.2° is obtainable. An 11×11 reflectarray is designed and simulated, and a prototype is fabricated and measured. Measurement shows that the reflectarray has an antenna gain of 20.4 dBi and a -1 dB gain bandwidth of 15.38%, covering 6.6 GHz to 7.7 GHz. In general, measurement results agree well with simulation. The effects of some of the crucial geometrical design parameters have been investigated. It is found that the reflectarray unit element which consists of two L probes with one probe longer than the other can generate a linear phase curve with phase range of larger than 360° . It is also discovered that the feeding horn incident angle, the unit cell size, and the probe height must be properly selected in order to achieve good radiation performances in the reflectarray.

CHAPTER 4

CO-JOINED L PROBES FOR TWO BROADBAND TRANSMITARRAYS WITH DIFFERENT POLARIZATIONS

4.1 Introduction

Transmitarray consists of an array of planar radiating elements fed by a single source. It combines the features of the conventional lens and phase array. The working principle of the transmitarray is akin to lens and it has many advantages such as low profile, light weight, and easy to manufacture. Unlike reflectarray, the radiating elements of the transmitarray are not blocked by its feeding source. Multilayer frequency selective surface (M-FSS) approach is one of the most applied techniques for designing the transmitarray elements. The M-FSS approach requires the use of multiple identical dielectric/air gap layers, stacking on top of each other, for generating sufficient transmission phase range. It was reported in (Abdelrahman et al., 2014a) that a single-layer transmitarray element can usually generate phase range of up to 90° . Unit elements such as double square rings (Ryan et al., 2010), spiral dipole (Abdelrahman and Elsherbeni, 2014) and square slot loaded with stubs (Rahmati and Hassani, 2015a) are the resonators which have been utilized for designing transmitarrays. By sandwiching a PBG element between two annular ring slots (Rahmati and Hassani, 2015b), such multilayered structure was found to be able to provide a phase range of 360°

by involving only two thin dielectric layers. Nonetheless, a mere -1 dB gain bandwidth of 5.7% was achieved in this case.

Dual- and multi-polarization antenna arrays are always demanded by many wireless applications as they are not only able to generate high gain, but they can also provide different polarizations for a higher data transfer rate. With the use of the aperture-coupled patches, recently, a dual-polarized transmitarray (Plaza et al., 2014; Pham et al., 2016) was successfully designed owing to the good polarization isolation between its coupling slots. Later in (Zhong et al., 2016), rectangular ring slot element was employed for designing a transmitarray which is capable of generating radiation patterns with all types of polarizations. It has been demonstrated (Xu et al., 2016) that the twisted complementary dual-split ring resonator can also be used for designing a linear polarizer. In this case, the antenna array can function as a reflectarray at low frequency for producing vertically polarized radiation and a transmitarray at high frequency for generating horizontally polarized radiation. At the intermediate frequencies, it can radiate in both directions with different polarizations.

In 1995, the L-shaped wire was found to be useable as an efficient probe for exciting the C-shaped loop antennas (Nakano et al., 1995). Later, it was discovered in (Luk et al., 1998) that the bandwidth of a microstrip antenna can be broadened up to 35% by electromagnetically coupling the energy from an L-shaped probe to the patch. Since then, the L-shaped probe was widely used as proximity excitation source for many antennas such as the dielectric

resonator antennas (Kishk et al., 2006), the orthogonally slit cut annular ring microstrip antenna (Singh et al., 2013), and the E-shaped patch antenna (Zheng et al., 2014). Due to its advantages such as light weight, low profile, and ease of tuning, the L-shaped probe has also been used for constructing antenna array (Wong et al., 2004; Wang et al., 2013). Lately, circularly polarized wave with high axial ratio bandwidth is found achievable when the L-shaped probe is incorporated with a waveguide (Yamauchi and Fukusako, 2014, 2015) for designing the circularly polarized antenna.

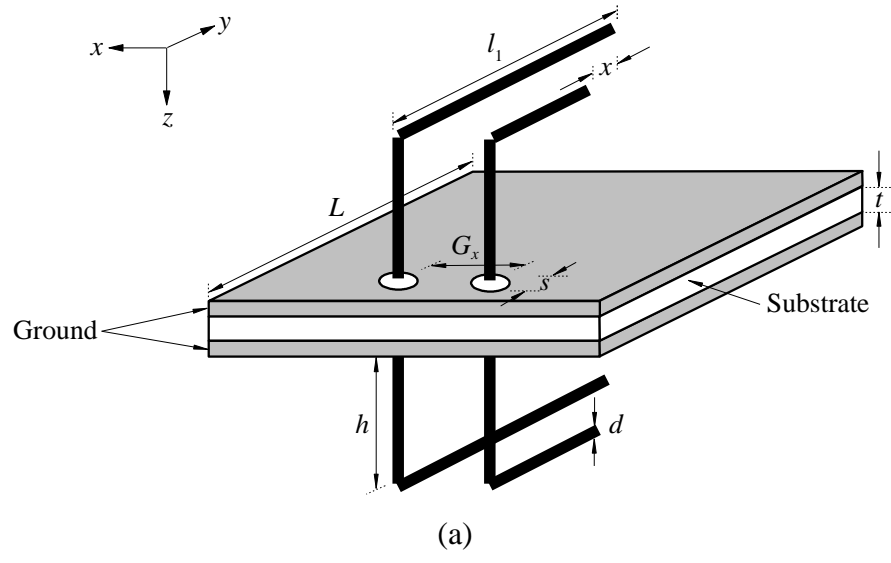
In this chapter, two L-shaped probes are co-joined for designing two broadband transmitarrays that can transmit with different polarizations. By changing the orientation of the L-shaped probes, the transmitting wave can be easily directed into either the horizontal or vertical direction. The configurations of the proposed transmitarray elements are first presented, where the elements are simulated using a Floquet cell for extracting their transmission properties. The configurations of the full transmitarrays are then elucidated. The two proposed transmitarrays are simulated and experimentally verified, and the array performances are demonstrated thereafter.

4.2 Unit Element Configuration and Analysis

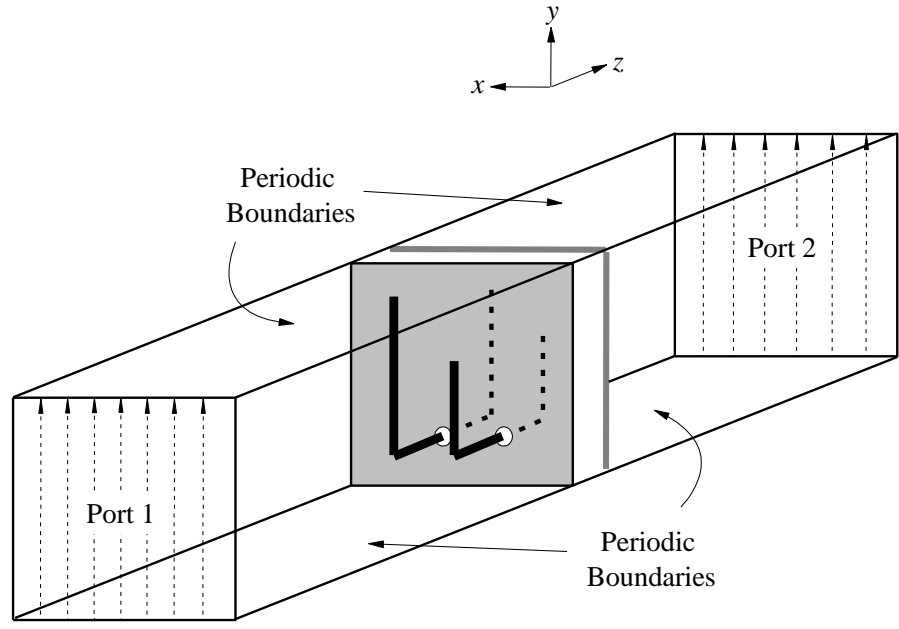
In this section, the configurations of the proposed transmitarray elements are studied. They are designed to generate vertically (y -) and horizontally (x -) polarized waves, as shown in Figure 4.1 and 4.2, respectively. The unit element in Figure 4.1 is described first. Referring to Figure 4.1 (a),

the unit element is composed of an FR4 substrate with thickness of $t = 1.7$ mm, dissipation factor of $\tan \delta = 0.025$, and dielectric constant of $\epsilon_r = 4.3$, along with two co-joined conductive probes. The substrate is the structural support for the L probes. In the design, the two probes with a diameter of $d = 1$ mm, which are penetrating through the FR4, are aligned in parallel but separated by a gap of $G_x = 5$ mm. At the height of $h = 10$ mm from the ground plate, the probes on both sides of the substrate are bent 90° into the y -direction. The probes are placed at 4 mm away from the edge of the substrate. Part of the copper, with diameter of $s = 3$ mm, is etched away around the probes for isolation. Two holes ($d = 1$ mm) are then drilled through the substrate for accommodating the probes, and non-conductive adhesive is applied around the probes for holding them. To generate phase change, with reference to Figure 4.1, the horizontal length l_1 of the long probes on the two sides is varied from 16 to 27.4 mm. The short probe is always shorter than the long probe by $x = 8$ mm, which is optimized by simulation.

For simulation, the unit element is placed in an $L \times L$ (31×31 mm²) Floquet cell as illustrated in Figure 4.1 (b). The unit cell is set to have periodic boundaries. Two wave ports, assigned as Port 1 and Port 2, are set as the transmitting and receiving ports, respectively, at a distance of 152 mm away from the horizontal parts of the probes. The distance can be of any value as the reference planes are de-embedded flushing with the horizontal probes. A y -polarized plane wave, with a normal incident angle of $\phi = 0^\circ$, $\theta = 0^\circ$, is launched from Port 1.



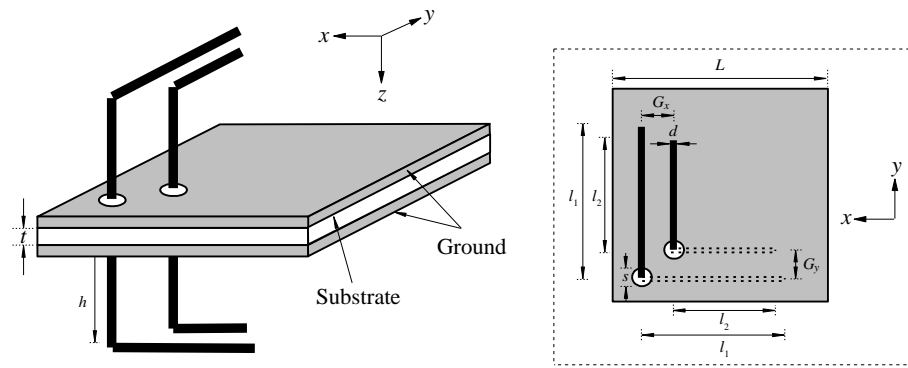
(a)



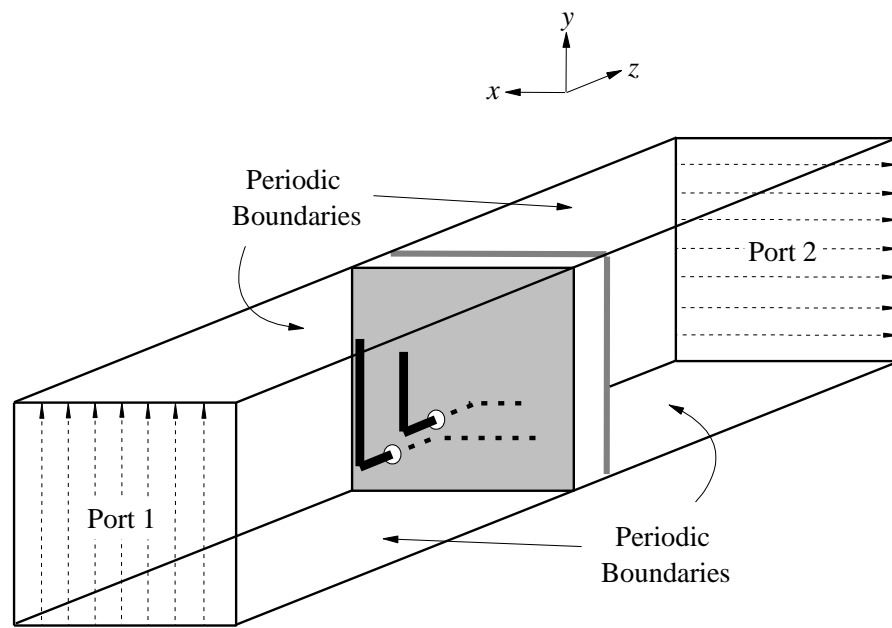
(b)

Figure 4.1: (a) Perspective view, (b) Floquet periodic boundary conditions of the vertically polarized unit element.

By changing the orientation of the horizontal probes, as shown in Figure 4.2, the unit element can be made to generate horizontally polarized (x -polarized) wave. This is done by, first, relocating the long probe to a location 4 mm away from the left bottom edge of the substrate while placing the short probe at a distance of $G_x = G_y = 5$ mm away from the long probe. Next, the probes on the transmitting side of unit element are bent 90° pointing to the x -direction. The probe length (l_2) is always shorter than l_1 by $x = 7$ mm ($x = l_1 - l_2$), as shown in Figure 4.2 (a). Again, the two probes on both sides of the substrate are varied simultaneously from $l_1 = 17$ to 27.4 mm to generate transmission phase shift. Other parameters are kept the same as those in Figure 4.1 (a). To enable propagation of the x -polarized wave in the transmitting side of the Floquet cell, the waveport polarization at Port 2 is set to be in the x -direction, as shown in Figure 4.2 (b).



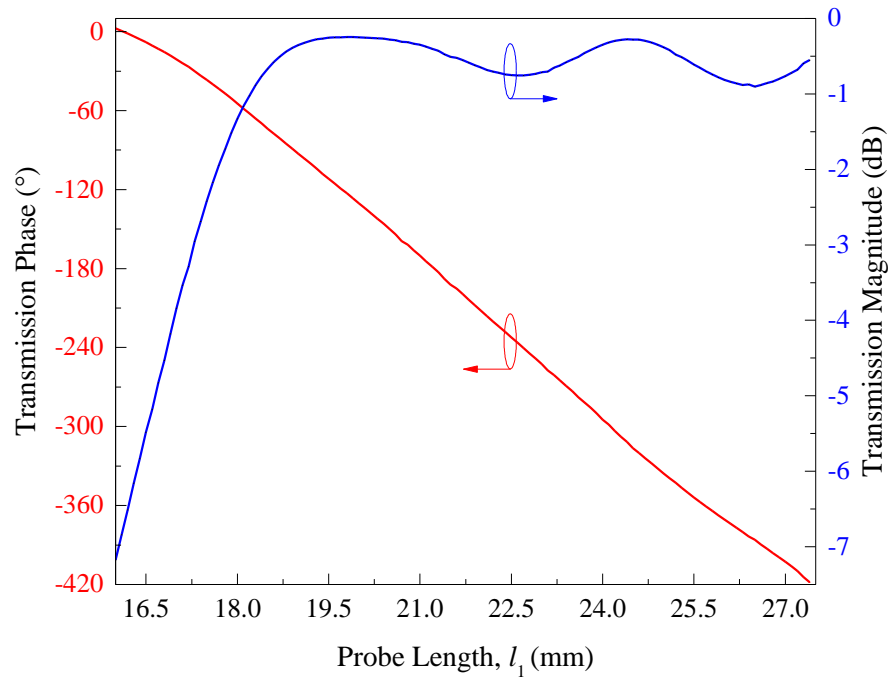
(a)



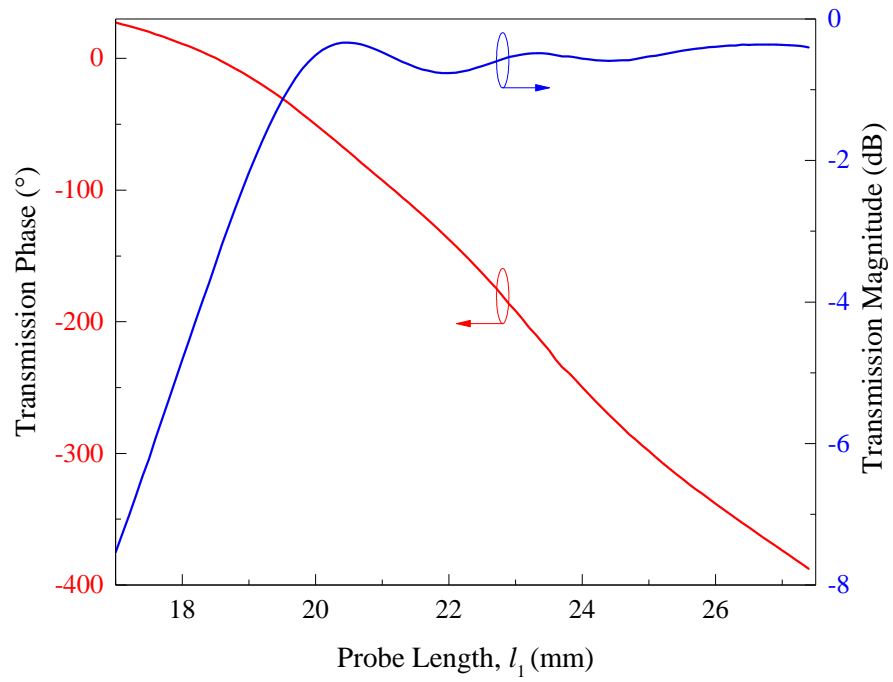
(b)

Figure 4.2: (a) Perspective view, (b) Floquet periodic boundary conditions of the horizontally polarized unit element.

Figure 4.3 (a) and (b) show the transmission magnitudes ($|S_{21}|$) and transmission phases ($\angle S_{21}$) of the transmitarray elements at the center frequency of 7.8 GHz and 7.4 GHz, as described in Figure 4.1 and 4.2, respectively. For transmission magnitude of higher than -3 dB, the vertically polarized element is able to produce a maximum phase range of 388° ; whereas the horizontally polarized element is generating 382.89° . Both curves are found to have linear phase slope. The electric field distributions around the long ($l_1 = 20$ mm) and short ($l_2 = 12$ mm) probes for the vertically polarized unit element are depicted in Figure 4.4 (a) and (b), respectively. Three standing waves (1.5λ) are formed on the long probe while two standing waves (1λ) are found on the short probe, corresponding fairly well with their respective physical lengths of 1.6λ (61.7 mm) and 1.19λ (45.7 mm). A similar phenomenon is found on the field distributions of the horizontally polarized element, and the discussion is omitted here.

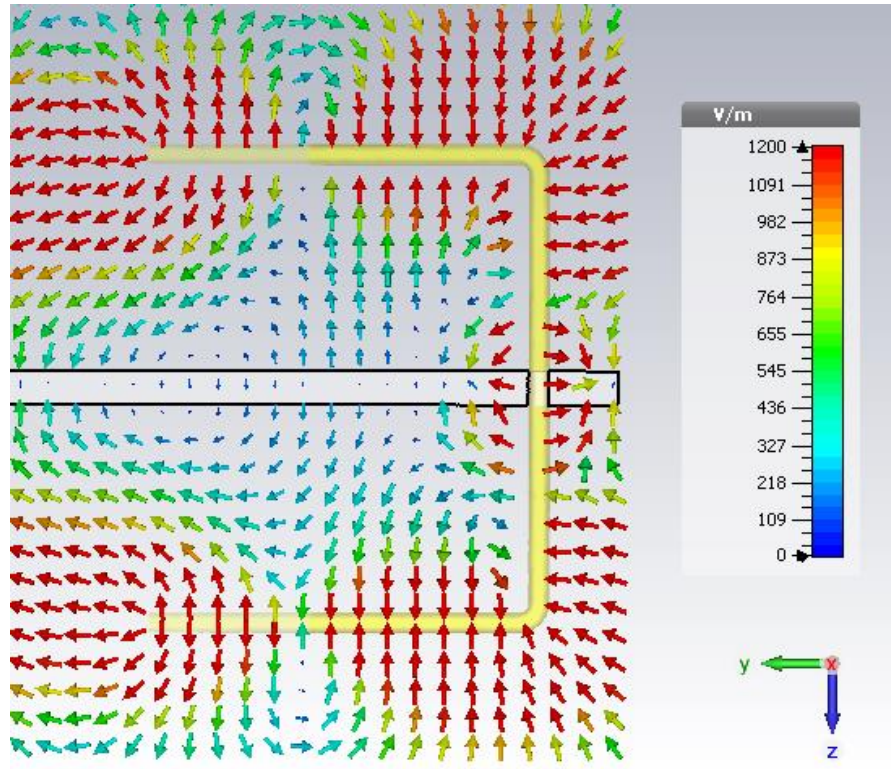


(a)

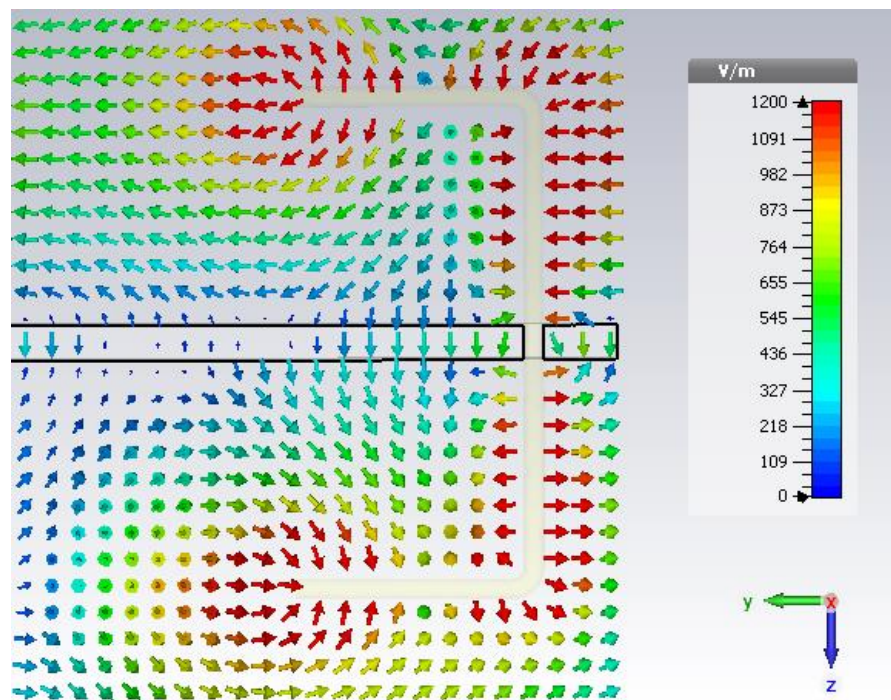


(b)

Figure 4.3: Transmission magnitudes and transmission phases of the transmitarray elements which generate (a) y-polarized wave, (b) x-polarized wave.



(a)

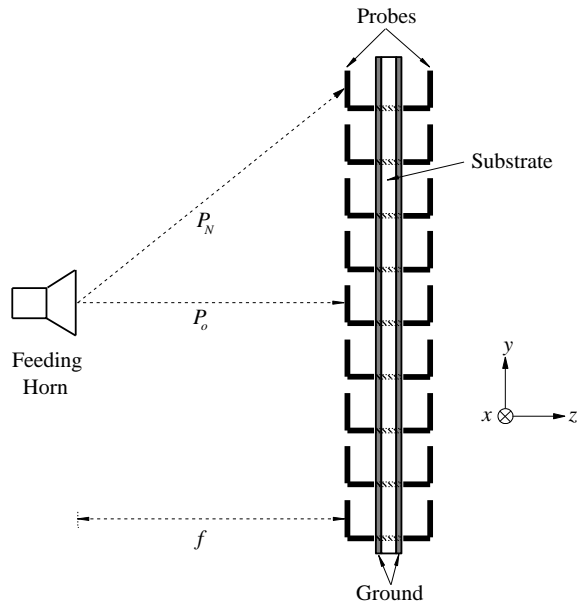


(b)

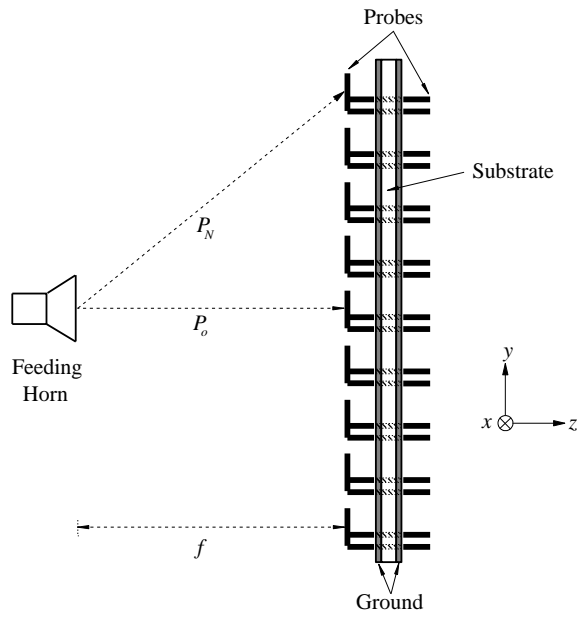
Figure 4.4: Electric field distributions around the (a) long probe, (b) short probe at the frequency of 7.8 GHz with $l_1 = 20$ mm for the vertically polarized unit element.

4.3 Transmitarray Configuration

With the use of the transmission phase curves in Figure 4.3, the unit elements are designed into the full-fledged transmitarrays shown in Figure 4.5. The phase distributions of all radiating elements on the antenna apertures and their corresponding probe lengths for the vertically and horizontally polarized transmitarrays are listed in the tables, which can be found in Appendix B, and C, respectively. By properly compensating the propagation path length for the N^{th} element (P_N) with respect to the reference (P_o), a cophasal re-radiated wave can be generated in the boresight direction. The design parameters of the two transmitarrays are described now. With reference to Figure 4.5 (a) and (b), the transmitarrays are assembled from 81 elements (9×9). For the vertically and horizontally polarized transmitarrays, the element sizes are set to be $L = 0.806\lambda = 31$ mm and $L = 0.765\lambda = 31$ mm, respectively. A C-band linearly polarized (5.85 – 8.2 GHz) pyramidal horn is used to excite the two transmitarray elements where the horn is placed at the focal length of $f = 223.2$ mm from the middle point. For both, the resulting f/D ratio is 0.8 where $D = 9L = 279$ mm. The prototypes of the transmitarrays are shown in Figure 4.6. The top and bottom ground layers are connected by 3M copper tapes so that they are equi-potential.



(a)



(b)

Figure 4.5: Configurations of the proposed (a) vertically, (b) horizontally polarized transmitarrays.



(a)



(b)

Figure 4.6: Prototypes of the (a) vertically, (b) horizontally polarized transmitarrays.

4.4 Measurement Setup

Measurements for the vertically polarized (y -polarized) and the horizontally polarized (x -polarized) transmitarray prototypes are conducted in free space for obtaining their antenna gains and radiation patterns. The experimental setup for both of the transmitarrays is illustrated in Figure 4.7. To capture the received power, a C-band pyramidal horn (ATM PNR137-440-2, 5.85GHz – 8.2GHz), which is the receiving antenna, is connected to a spectrum analyzer (Advantest U3771). It is placed at a far field distance of $R > 2D^2/\lambda$, where D is the diagonal dimension of the transmitarray.

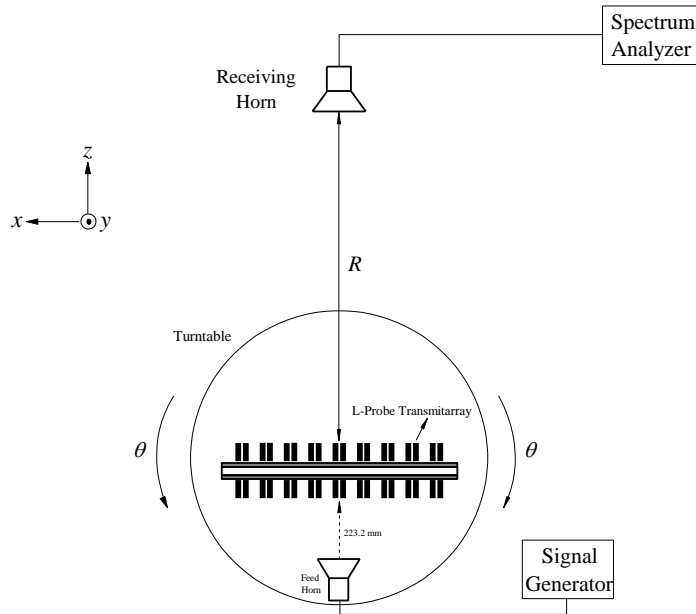
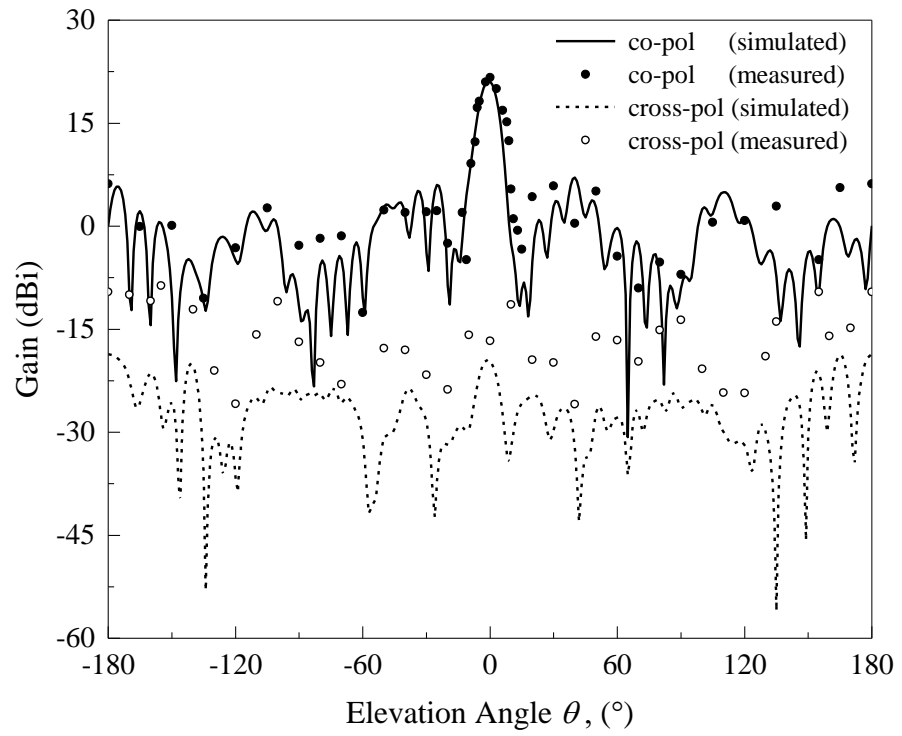


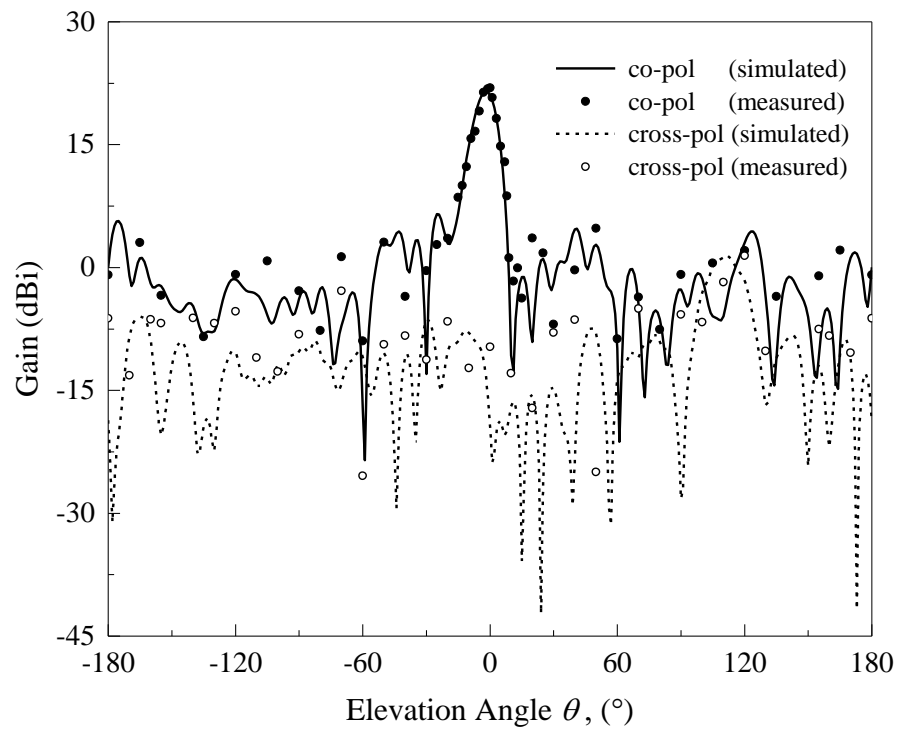
Figure 4.7: Measurement setup for the transmitarray.

4.5 Simulated and Experimental Results of Transmitarray

Figure 4.8 shows the measured and simulated radiation patterns of the vertically polarized (y -polarized) transmitarray in the yz -plane (E -plane) and xz -plane (H -plane). At the elevation angle of $\theta = 0^\circ$, it has a measured gain of 21.9 dBi (simulation: 21 dBi) at 7.8 GHz, which corresponds to an aperture efficiency of 23.4%. The cross-polarized field is at least 30 dB smaller than its co-polarized counterpart in the boresight direction ($\theta = 0^\circ$). For the horizontally polarized (x -polarized) transmitarray, it is observed from Figure 4.9 that broadside radiation pattern with a measured peak gain of 19.1 dBi (simulation 19.8 dBi) has been obtained. This corresponds to an aperture efficiency of 14% (simulation: 16.5%). It should be pointed out that the xz -plane is the E -plane while the yz -plane is the H -plane in this case. The co-polarized and cross-polarized fields at the elevation angle of $\theta = 0^\circ$ are different by 21.3 dB. The simulated radiation efficiencies of the vertically and horizontally polarized transmitarrays are found to be 92.4% and 89.5%, respectively. The antenna gains of both the proposed transmitarrays are shown in Figure 4.10. The vertically polarized transmitarray has a measured -1 dB gain bandwidth of 11.62% (simulation: 11.92%), covering 7.3 GHz - 8.2 GHz (simulation: 7.1 GHz - 8 GHz). And the horizontally polarized transmitarray has a measured -1 dB gain bandwidth of 10.39%, (covering 7.3 GHz - 8.1 GHz), being slightly lower than the simulated bandwidth of 12.79% (covering 6.95 GHz to 7.9 GHz).

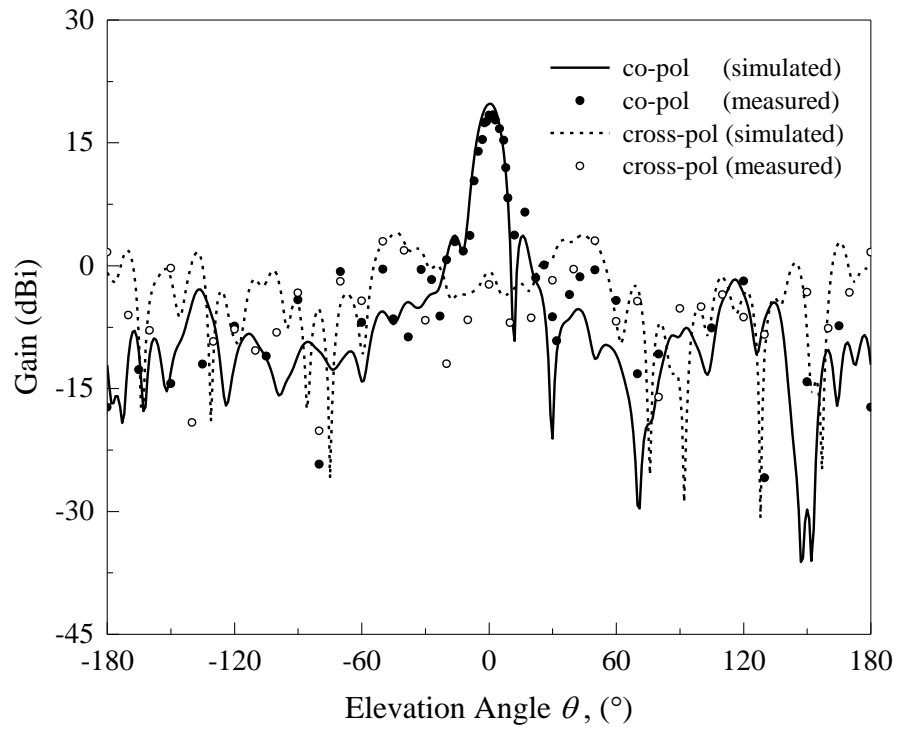


(a)

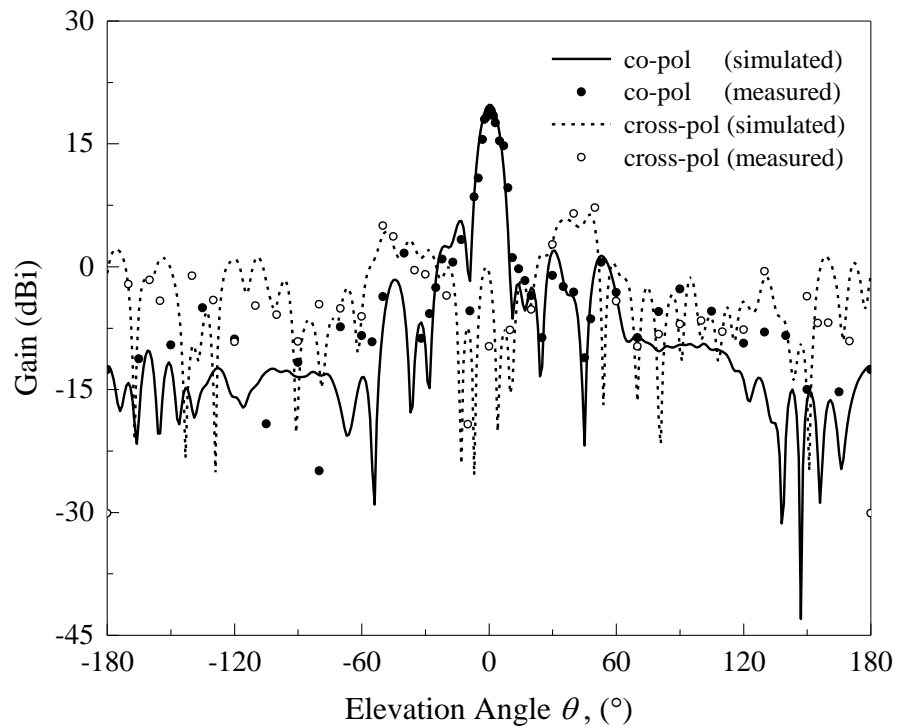


(b)

Figure 4.8: Measured and simulated (a) *E*- and (b) *H*- plane radiation patterns of the vertically polarized transmitarray.



(a)



(b)

Figure 4.9: Measured and simulated (a) E - and (b) H - plane radiation patterns of the horizontally polarized transmitarray.

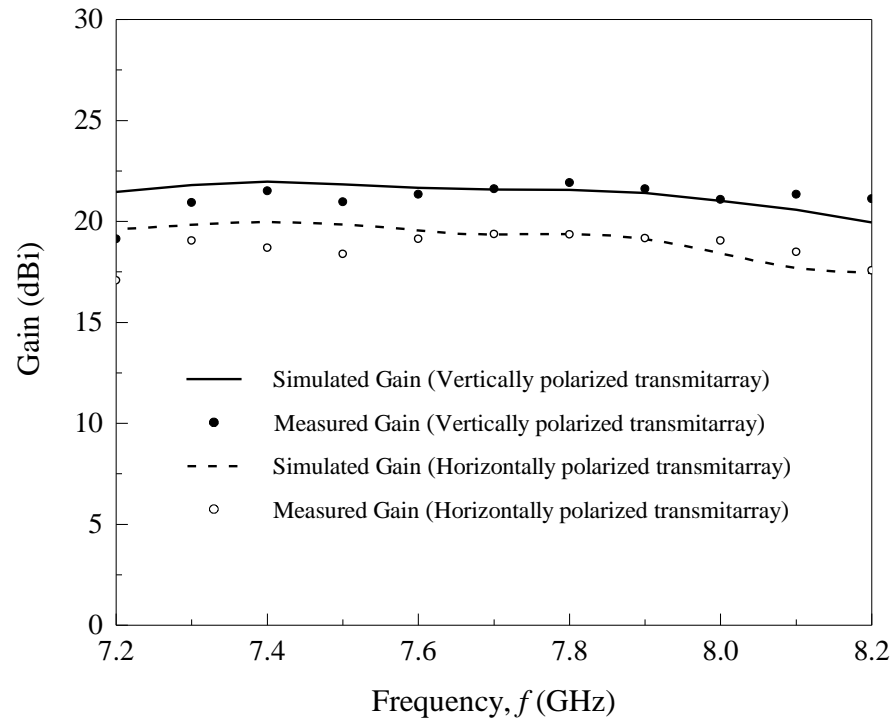


Figure 4.10: Measured and simulated antenna gains of the vertically and horizontally polarized transmitarrays.

Table 4.1 compares the performances of the proposed transmitarrays with some of the recently published works. It is observed that the proposed transmitarrays have reasonable antenna gains, aperture efficiencies, and -1 dB gain bandwidths.

Table 4.1: Comparison of the proposed transmitarrays with the recently published works.

| Reference | Number of Conducting Layer(s) | Gain (dBi) | Aperture Efficiency (%) | -1/-3*dB Gain Bandwidth (%) |
|-----------------------------|-------------------------------|------------|-------------------------|-----------------------------|
| Vertically polarized | - | 21.9 | 23.4 | 11.62 |
| Horizontally polarized | - | 19.1 | 14 | 10.39 |
| (This work) | | | | |
| (Pham et al., 2016) | 3 | 24.9 | 24.6 | 20* |
| (Zhong et al., 2016) | 3 | 20.1 | 27 | 8.3 |
| (Xu et al., 2016) | 3 | 18.5 | 28 | 6.7 |
| (Abdelrahman et al., 2014b) | 4 | 23.76 | 16 | 4.2 |
| (Yu et al., 2016) | 3 | 18.9 | 20.9 | 9.6 |

4.6 Parametric Analysis for Vertically Polarized Transmitarray

In this section, parametric analysis is performed on some of the crucial geometrical design parameters of the vertically polarized transmitarray for understanding their effects on the unit element and the full-fledged transmitarray performances.

4.6.1 Comparison of Single and Double L Probe Elements

Figure 4.11 shows the configuration of the vertically polarized transmitarray element which consists of a single L probe. It is compared with the unit element with double L probes shown in Figure 4.1 (a) and the transmission characteristics for both of the unit elements are illustrated in Figure 4.12. Obviously, the unit element with single L probe has poor

transmission across all probe lengths. Hence, it cannot be used for designing the full-fledged transmitarray.

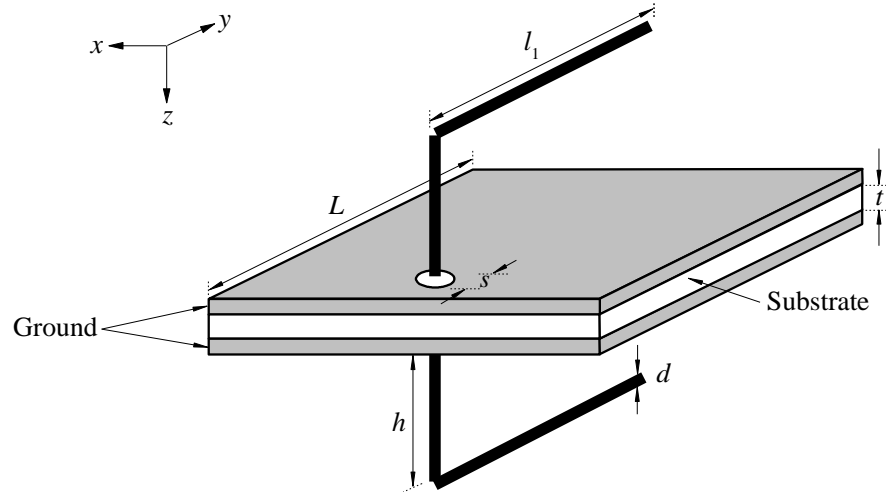


Figure 4.11: Configuration of the vertically polarized transmitarray unit element with single L probe.

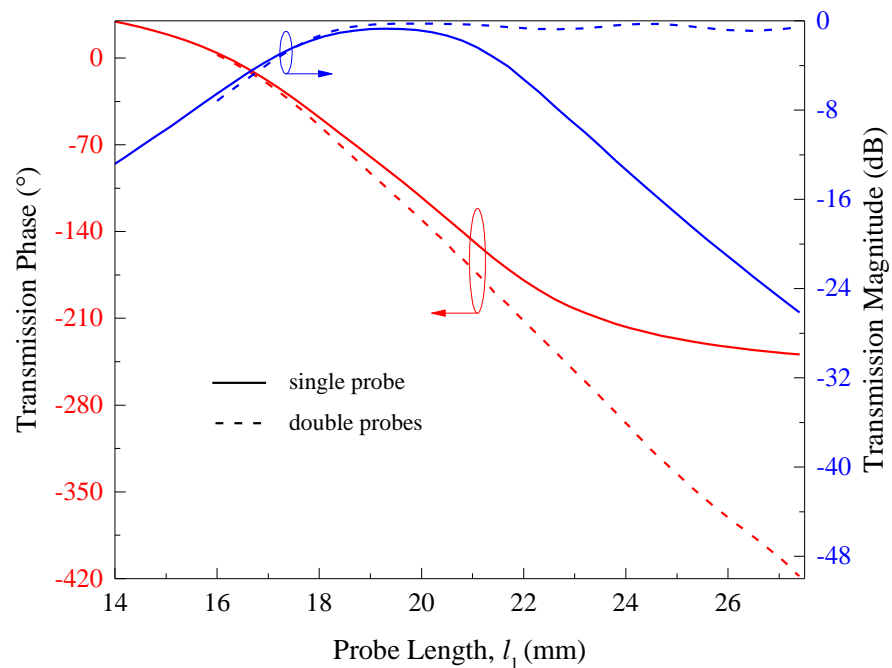


Figure 4.12: Comparison of the transmission magnitudes and transmission phases of the vertically polarized transmitarray unit elements with single and double L probes.

4.6.2 Length Difference between Long and Short Probes

By varying the probe length (l_1) from 16 mm to 27.4 mm, Figure 4.13 shows the transmission performances of the unit element when the length difference (x) between the long and the short probes is varied. Poor transmission of lower than -5.5 dB across all probe lengths is observed when the two probes are equal in length. It is also observed that the changing rate of the transmission phase curve becomes slower when the length difference between the long and the short probes increases. Figure 4.14 illustrates the radiation patterns of the vertically polarized transmitarray for different length differences between the long and the short probes. A low boresight ($\theta = 0^\circ$) antenna gain of ~ 19 dBi is obtained for the case of $x = 6$ mm.

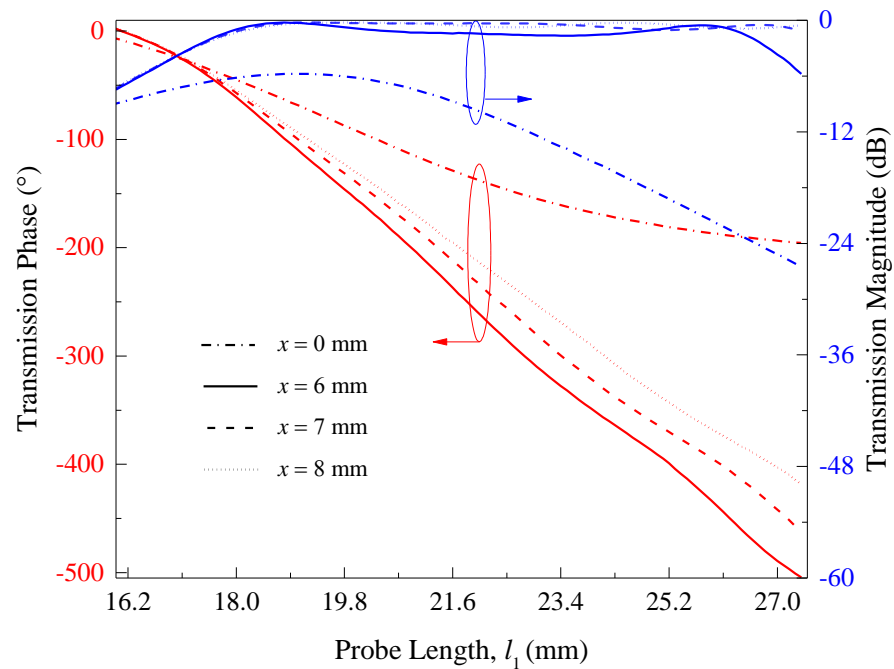
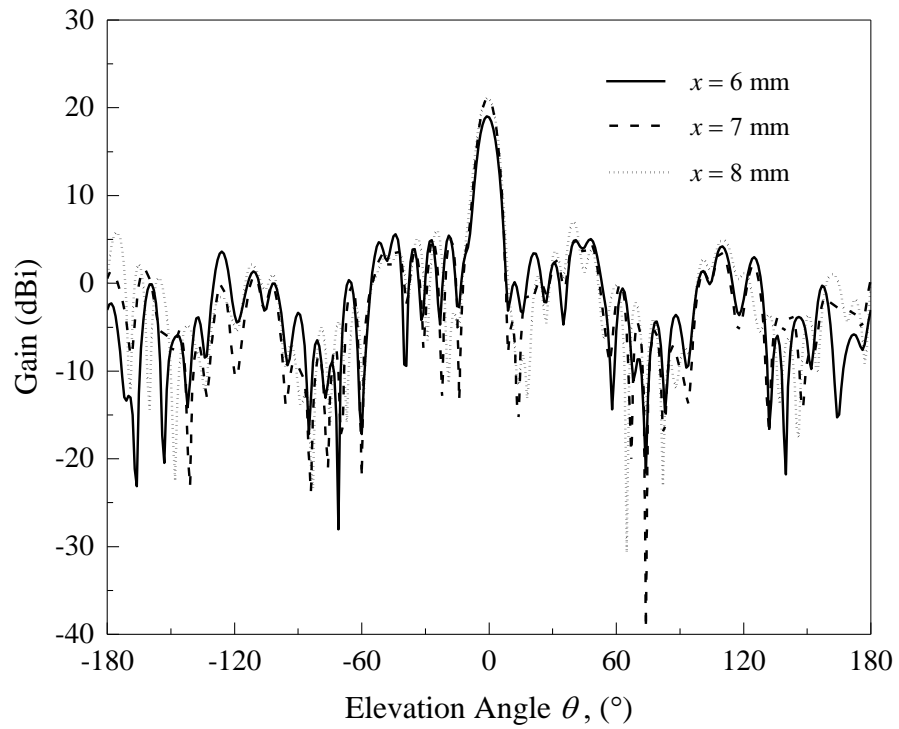
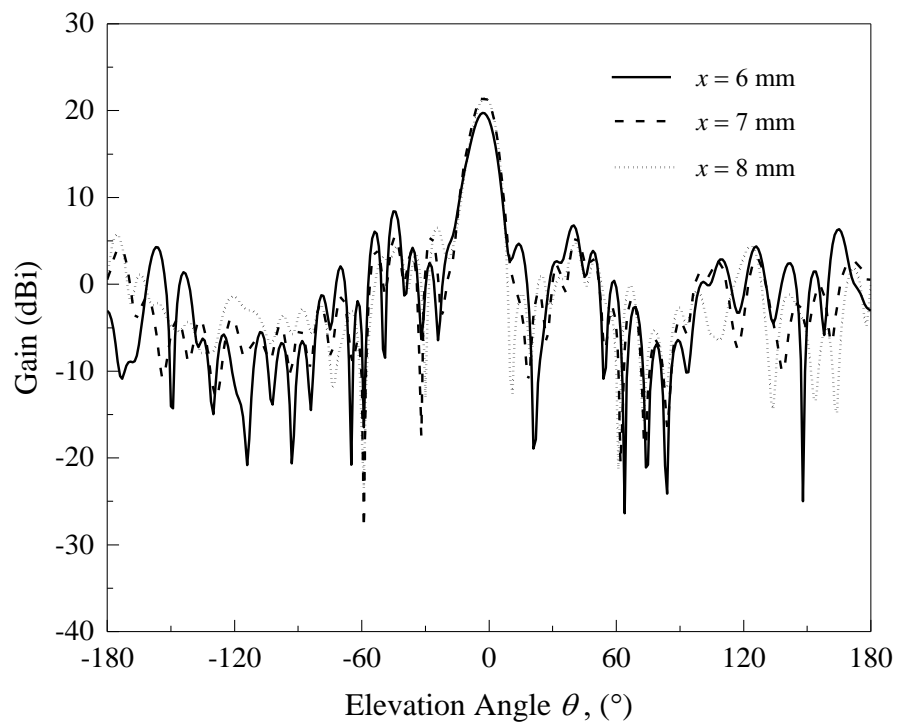


Figure 4.13: Effects of the length difference (x) between the long and the short probes on the transmission magnitude and transmission phase of the vertically polarized transmitarray unit element.



(a)



(b)

Figure 4.14: Radiation patterns of the proposed vertically polarized transmitarray for different length differences (x) between the long and the short probes at 7.8 GHz. (a) E - and (b) H - planes.

4.6.3 Probe Diameter

Effects of the probe diameter (d) are now studied and the results are shown in Figure 4.15. Poorer transmission is observed when a thicker probe is deployed. This results in a smaller transmission phase range usable for designing a full array. Change in probe diameter, however, does not affect the linearity of the transmission phase curve. The radiation performances of the full-fledged transmitarray for different probe diameters are shown in Figure 4.16. For the probe diameter of 0.5 mm, 1 mm, and 1.5 mm, a peak antenna gain of 20 dBi, 21 dBi, and 18.22 dBi is achieved, respectively. For the case of $d = 1.5$ mm, a significantly high back lobe level of ~ 10 dBi is also inspected, which results in a low front-to-back ratio of 8.22 dBi.

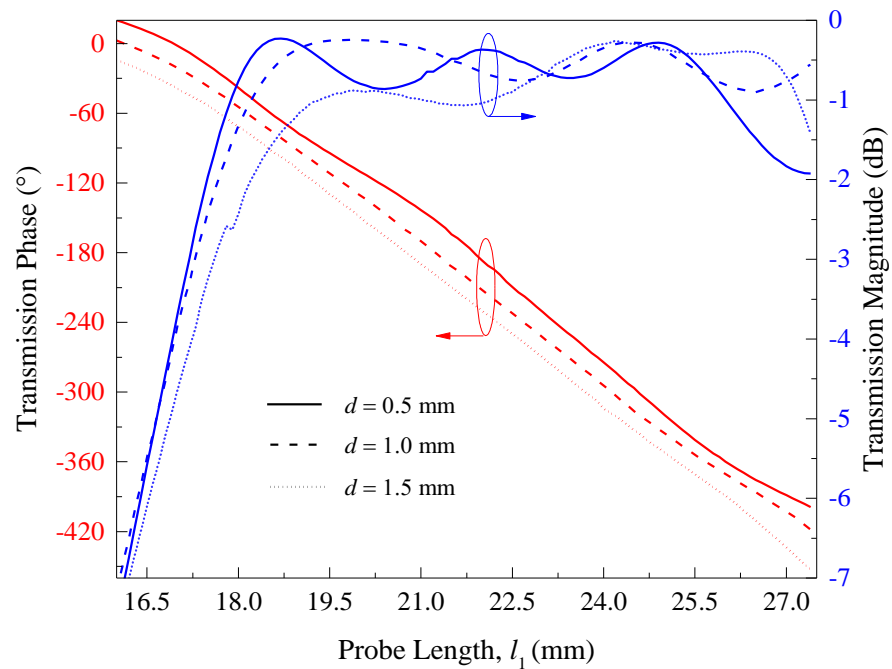
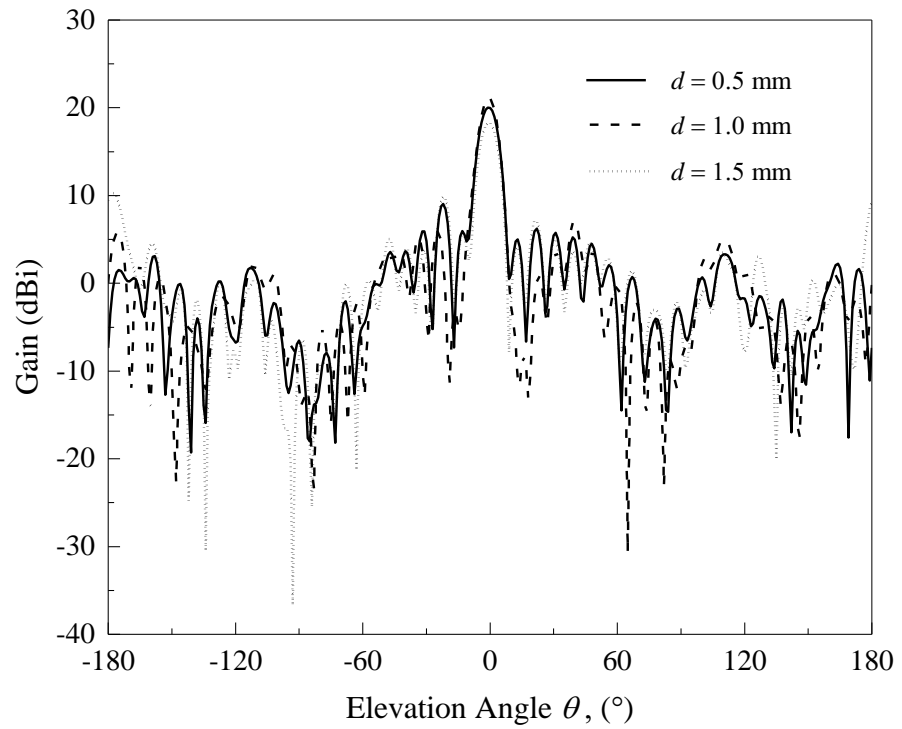
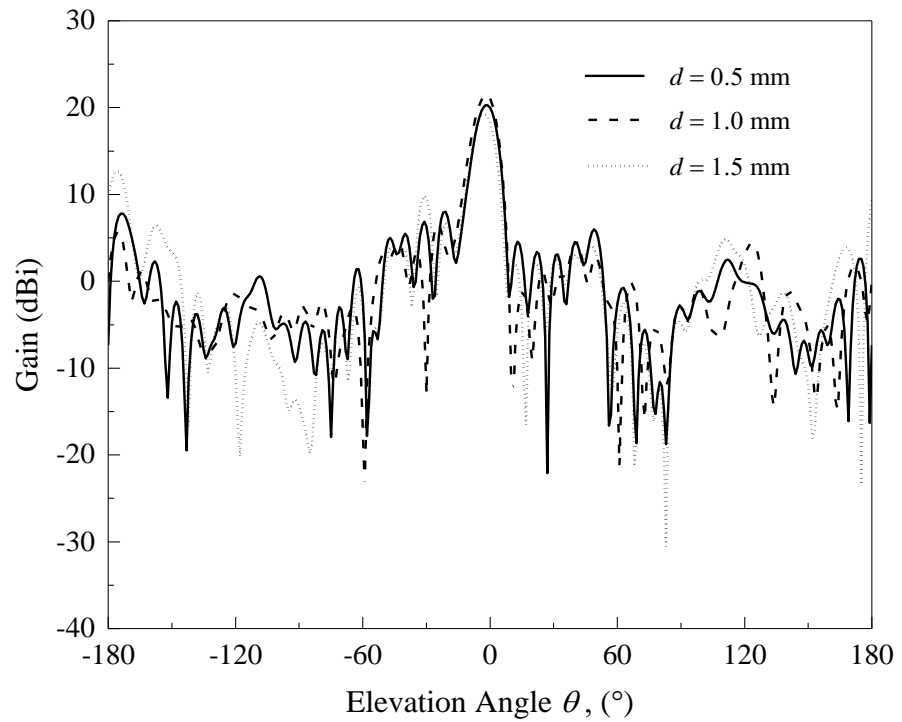


Figure 4.15: Effects of the probe diameter (d) on the transmission magnitude and transmission phase of the vertically polarized transmitarray unit element.



(a)



(b)

Figure 4.16: Radiation patterns of the proposed vertically polarized transmitarray for different probe diameters (d) at 7.8 GHz. (a) E - and (b) H - planes.

4.6.4 Probe Height

The effects of the probe height (h) are also studied. With reference to Figure 4.17, it is observed from the transmission magnitude and phase responses that probe heights of 8 mm, 10 mm, and 12 mm enable transmission phase ranges of 360.67° , 388° , and 444.64° , respectively. It is also observed that varying probe height does not affect the gradient of the transmission phase curve much. Radiation performances for different probe heights are also illustrated in Figure 4.18. It can be seen that the transmitarray performs at its best when the probe height is set to be 10 mm. High back lobe level of 11.52 dBi is observed when the probe height is increased to 12 mm.

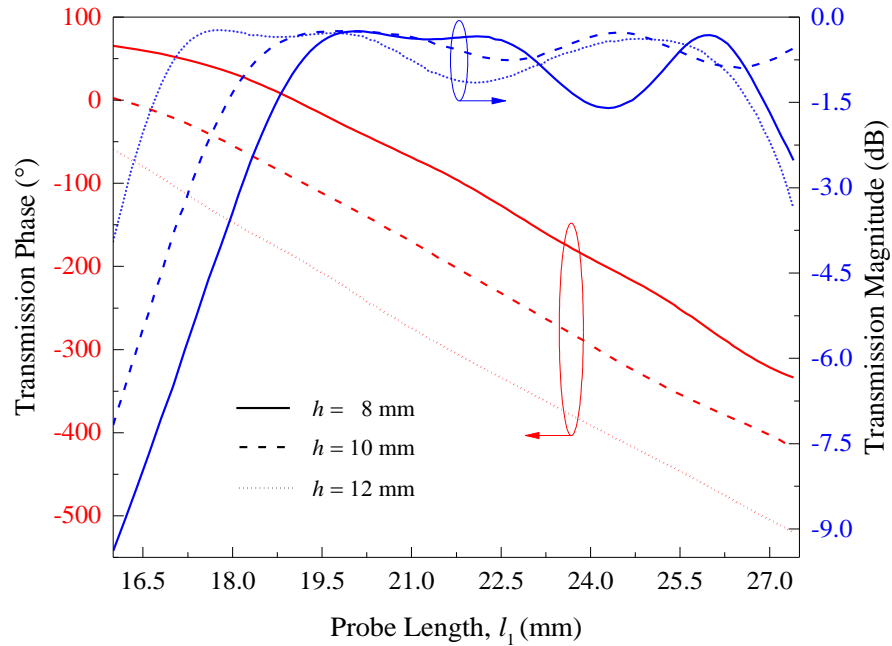
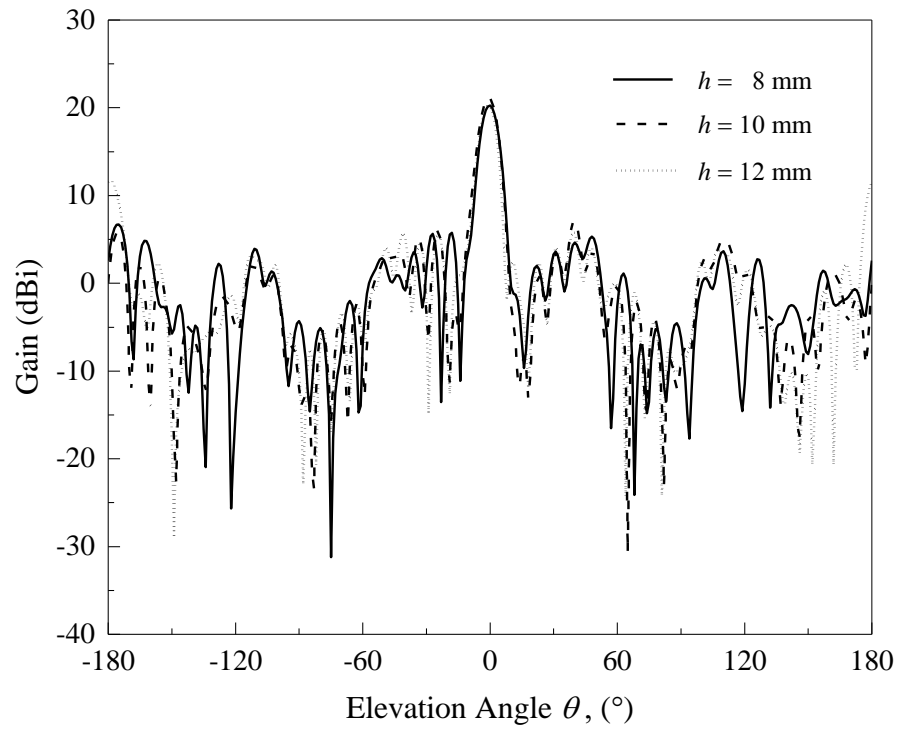
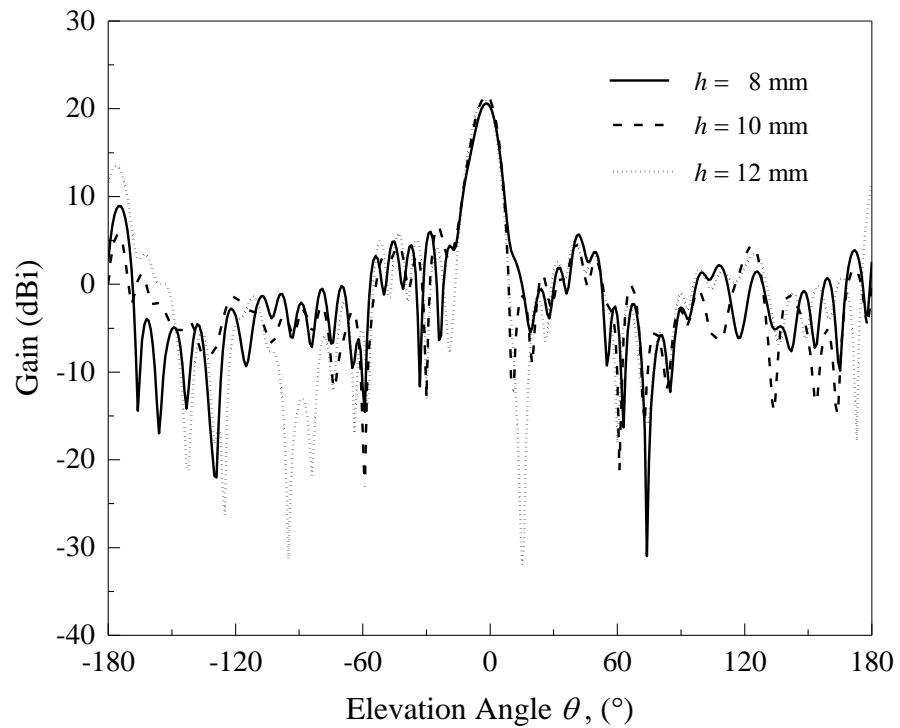


Figure 4.17: Effects of the probe height (h) on the transmission magnitude and transmission phase of the vertically polarized transmitarray unit element.



(a)



(b)

Figure 4.18: Radiation patterns of the proposed vertically polarized transmitarray for different probe heights (h) at 7.8 GHz. (a) E - and (b) H - planes.

4.6.5 Separation Distance between Long and Short Probes in x -direction

Next, the properties of the separation distance between the long and the short probes in the x -direction (G_x) are analyzed. Referring to Figure 4.19, varying G_x from 4 mm to 6 mm does not alter the changing rate and the phase range of the transmission phase curve much. The full-fledged transmitarray performances for different probe separations in the x -direction are depicted in Figure 4.20. It can be clearly seen that the transmitarray with probe separation of $G_x = 5$ mm has an antenna gain of 21 dBi, which is ~ 1 dBi and ~ 2 dBi higher than the transmitarray with probe separation of $G_x = 4$ mm and 6 mm, respectively. A back lobe level of ~ 4 dBi is also observed for the case of $G_x = 6$ mm.

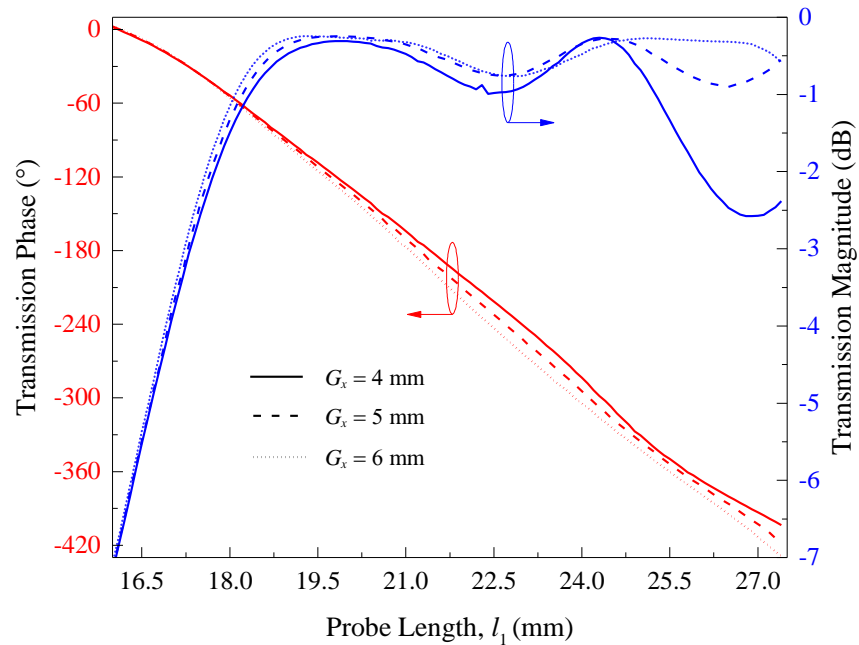
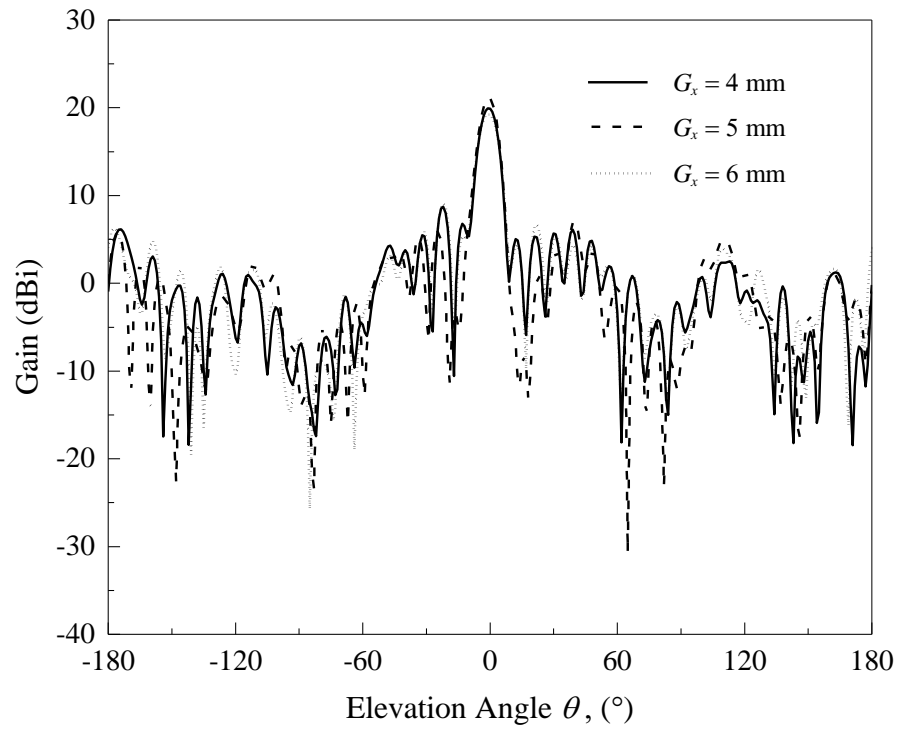
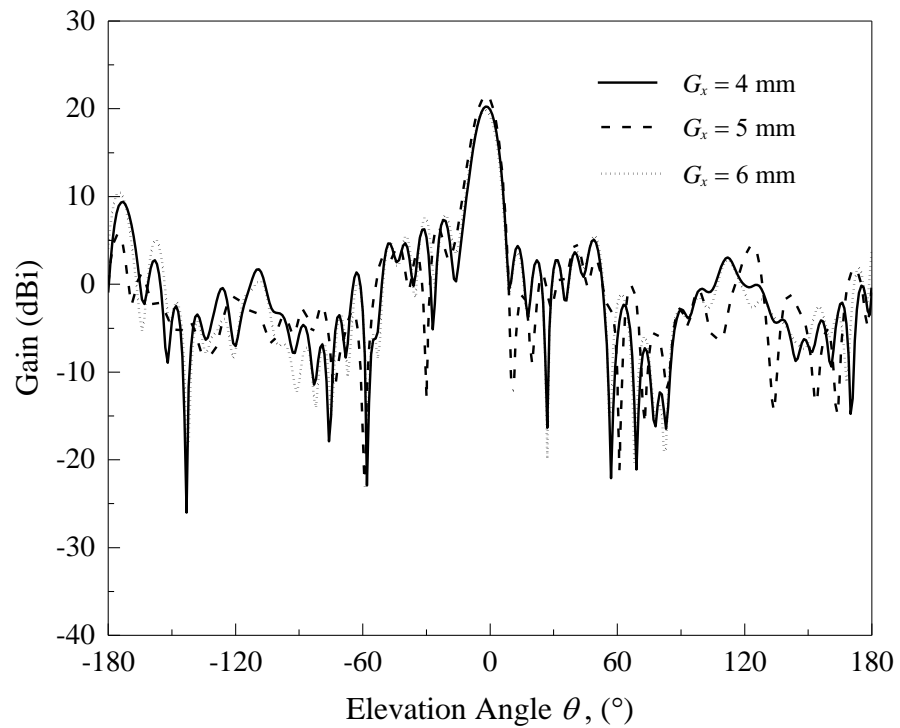


Figure 4.19: Effects of the separation distance between the long and the short probes in the x -direction (G_x) on the transmission magnitude and transmission phase of the vertically polarized transmitarray unit element.



(a)



(b)

Figure 4.20: Radiation patterns of the proposed vertically polarized transmitarray for different probe separations in the x -direction (G_x) at 7.8 GHz. (a) E - and (b) H - planes.

4.6.6 Unit Cell Size

The characteristics of the unit cell size (L), which is also the separation distance between the elements in the full transmitarray, are then studied. It is found that the element size does not affect the changing rate of transmission phase slope. For unit cell sizes of $L = 0.806\lambda$, 0.832λ , and 0.858λ at 7.8 GHz, as depicted in Figure 4.21, phase ranges of 388° , 449° , and 475.86° are obtained, respectively. The radiation performances of the transmitarray for different element spacings are illustrated in Figure 4.22. As expected, varying the element spacing affects the antenna gain of the main lobe as the optimal point of the transmitarray has shifted to lower frequency when designed with larger unit cell sizes of $L = 0.832\lambda$ and 0.858λ . It can be seen that when L is increased by 0.026λ , the boresight antenna gain reduces by ~ 1 dBi.

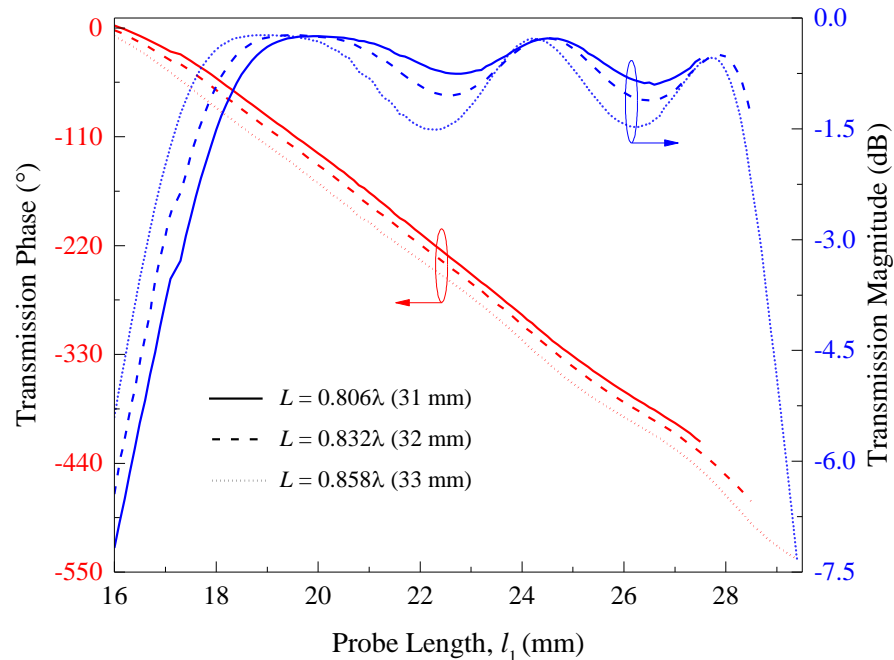
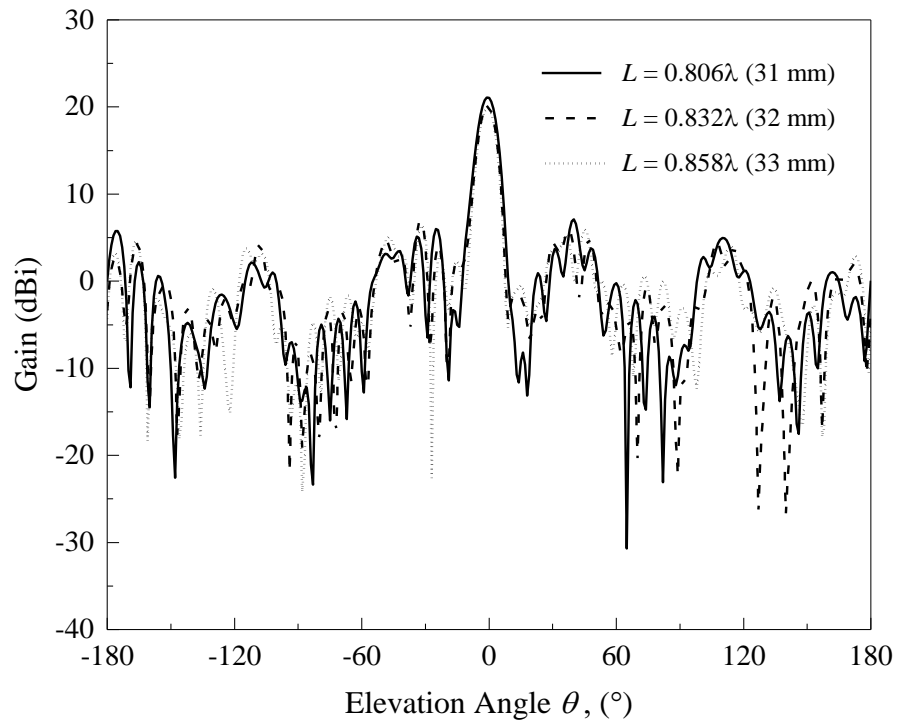
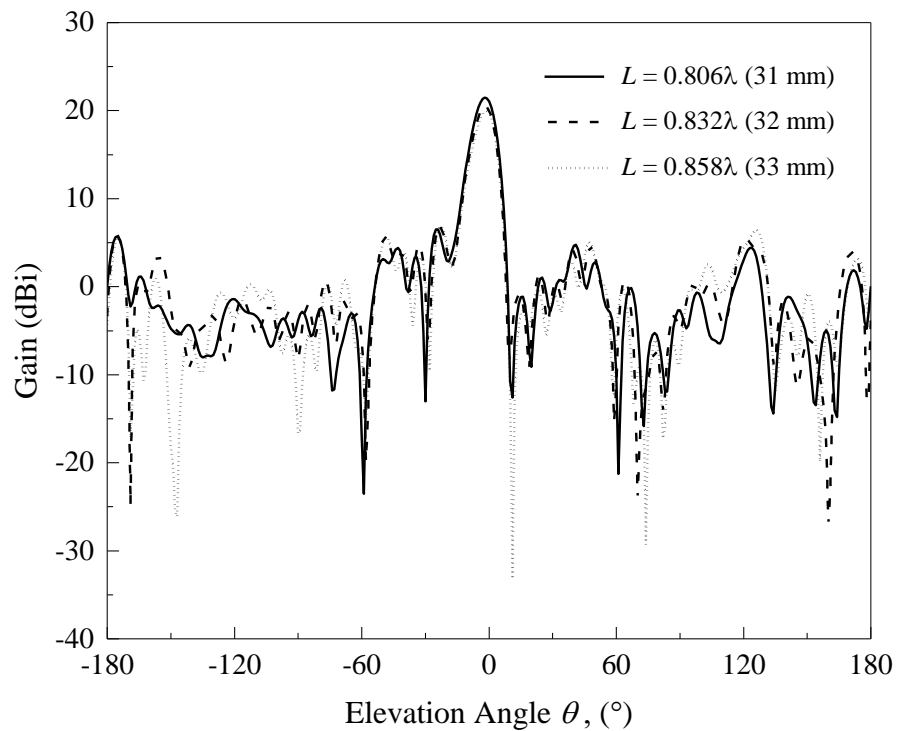


Figure 4.21: Effects of the unit element dimension (L) on the transmission magnitude and transmission phase of the vertically polarized transmitarray unit element.



(a)

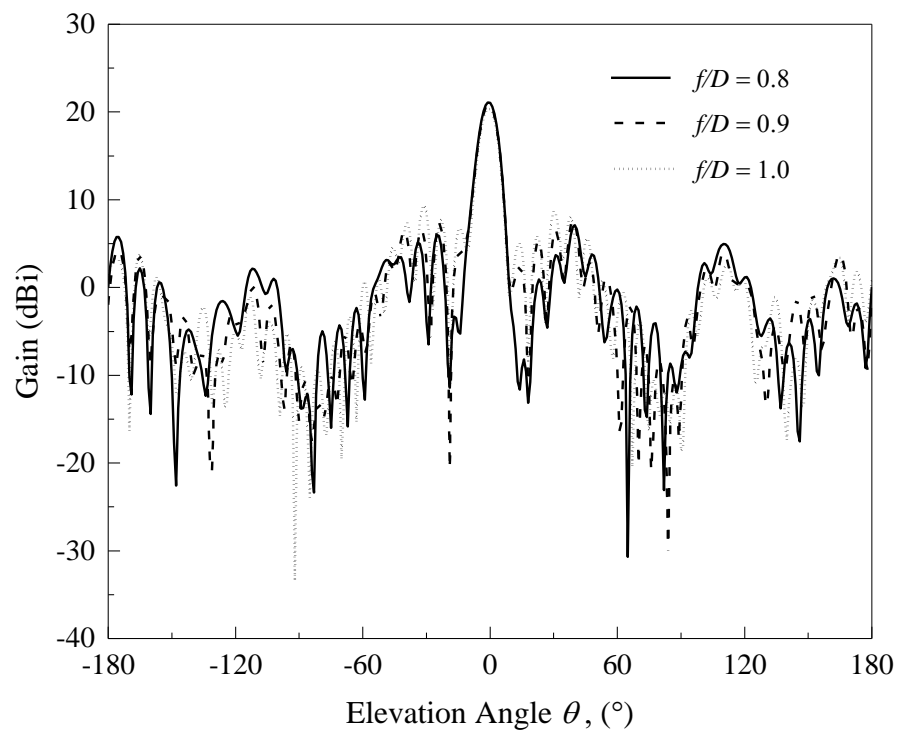


(b)

Figure 4.22: Radiation patterns of the proposed vertically polarized transmitarray for different separation distances (L) at 7.8 GHz. (a) E - and (b) H - planes.

4.6.7 f/D Ratio

With the cell size (L) and board dimension (D) kept at 0.806λ and 279 mm, respectively, the f/D ratio is varied from 0.8 to 1 and its effects are studied in Figure 4.23. It can be seen that adjusting f/D ratio does not affect the radiation performances of the transmitarray much. Only a slight increase in the side lobe level is observed when the f/D ratio is equal to 1.



(a)

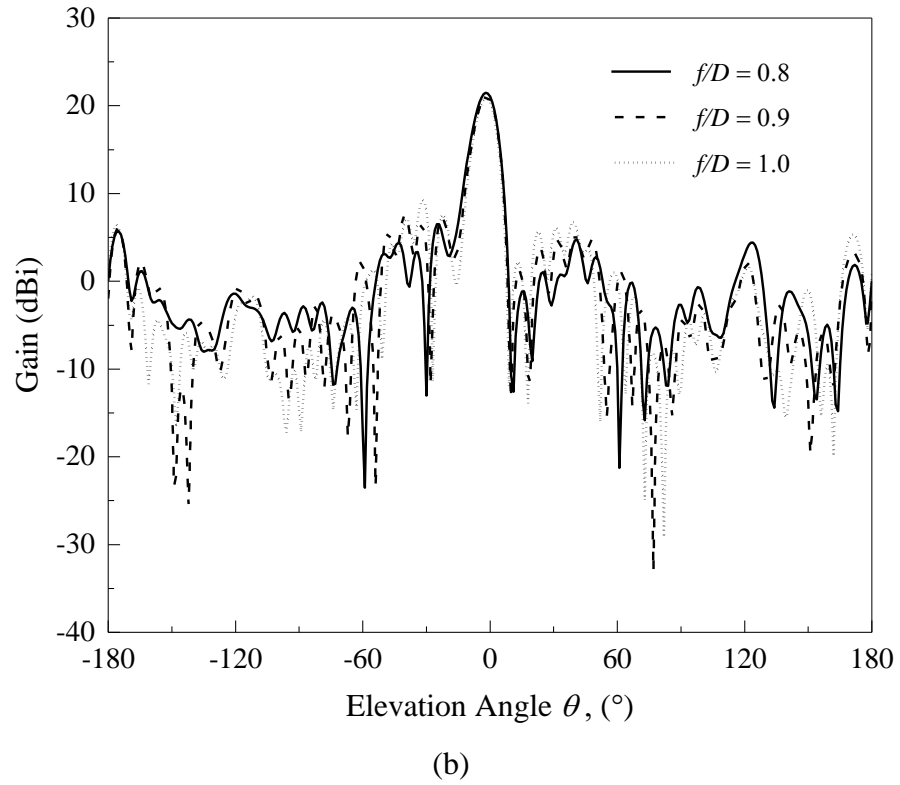


Figure 4.23: Radiation patterns of the proposed vertically polarized transmitarray for different f/D ratios. (a) E - and (b) H - planes.

4.7 Parametric Analysis for Horizontally Polarized Transmitarray

In this section, the effects of the important geometrical design parameters of the horizontally polarized transmitarray on the transmission magnitude and transmission phase as well as the radiation pattern are studied.

4.7.1 Comparison of Single and Double L Probe Elements

The performances of the unit elements with single L probe (depicted in Figure 4.24) and double L probes (depicted in Figure 4.2 (a)) are first analyzed and the results are shown in Figure 4.25. It is observed that for a transmission

magnitude of higher than -3 dB, the unit element with single L probe can only provide a phase range of up to 130.1° which is insufficient for designing the full-fledged transmitarray.

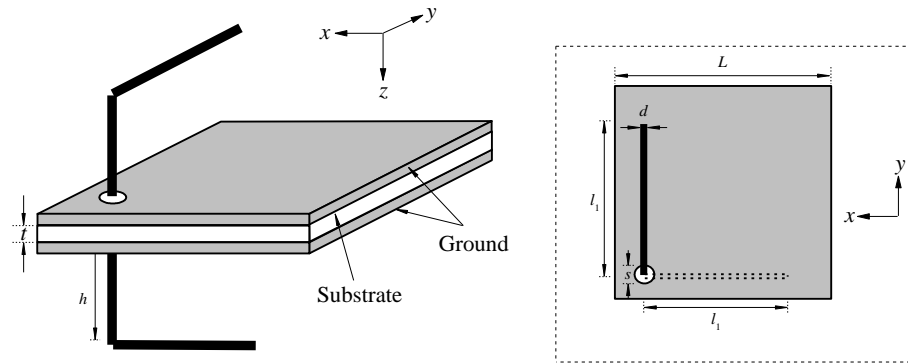


Figure 4.24: Configuration of the horizontally polarized transmitarray unit element with single L probe.

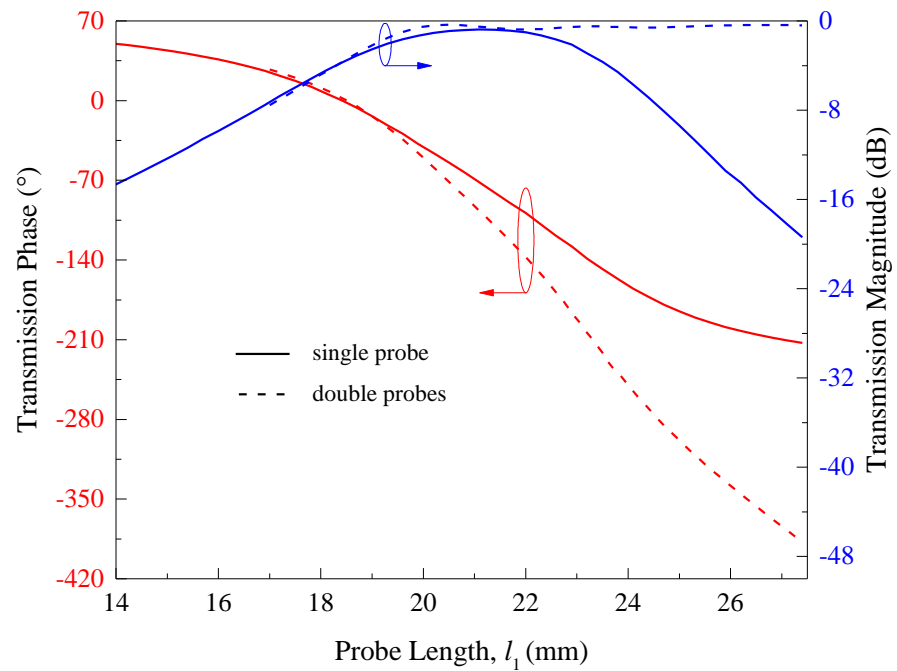


Figure 4.25: Comparison of the transmission magnitudes and transmission phases of the horizontally polarized transmitarray unit elements with single and double L probes.

4.7.2 Length Difference between Long and Short Probes

The effects of the length difference (x) between the long and the short probes are now analyzed. Referring to Figure 4.26, the changing rate of the transmission phase curve can be made slower by increasing x , but with the price of reducing the phase range. For $x = 5$ mm, certain ranges of the transmission magnitude go beyond -3 dB when the probe length (l_1) is lengthened from 21.2 mm to 23.3 mm. This has undoubtedly reduced the total usable phase range for designing the full-fledged transmitarray. With reference to Figure 4.27, high back lobe levels of ~ 7 dBi and ~ 9.5 dBi are observed when $x = 6$ mm and 8 mm, respectively. For the case of $x = 7$ mm, the back lobe level of the transmitarray is able to maintain well below 0 dBi.

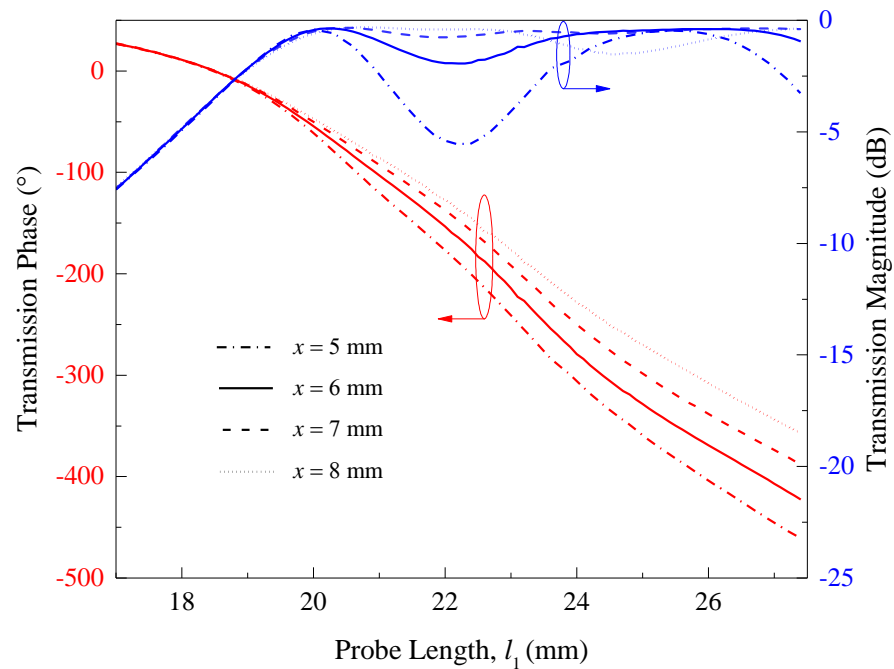
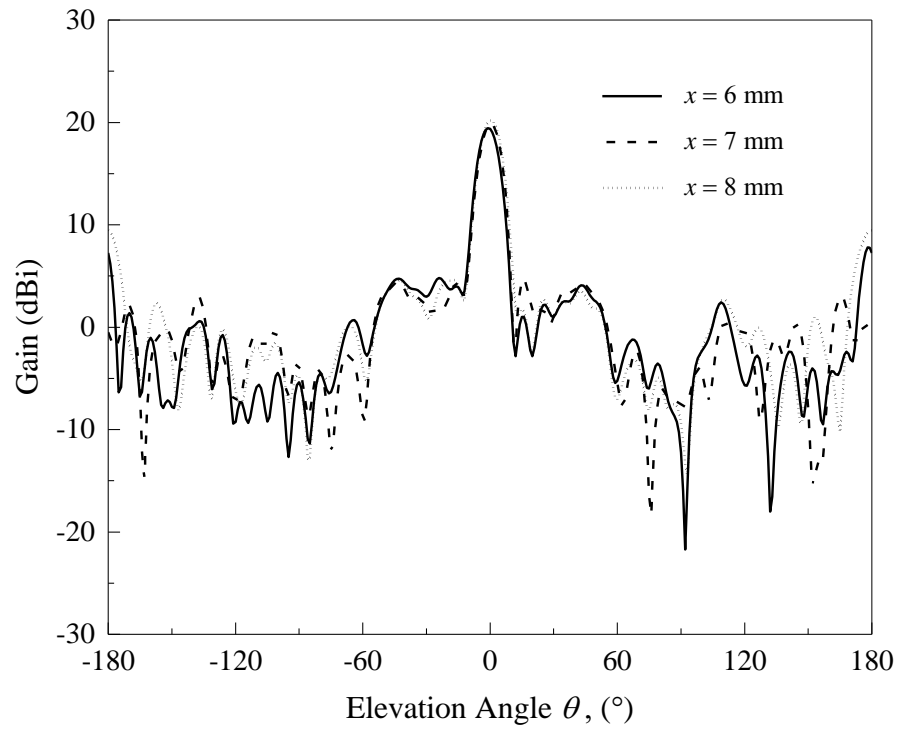
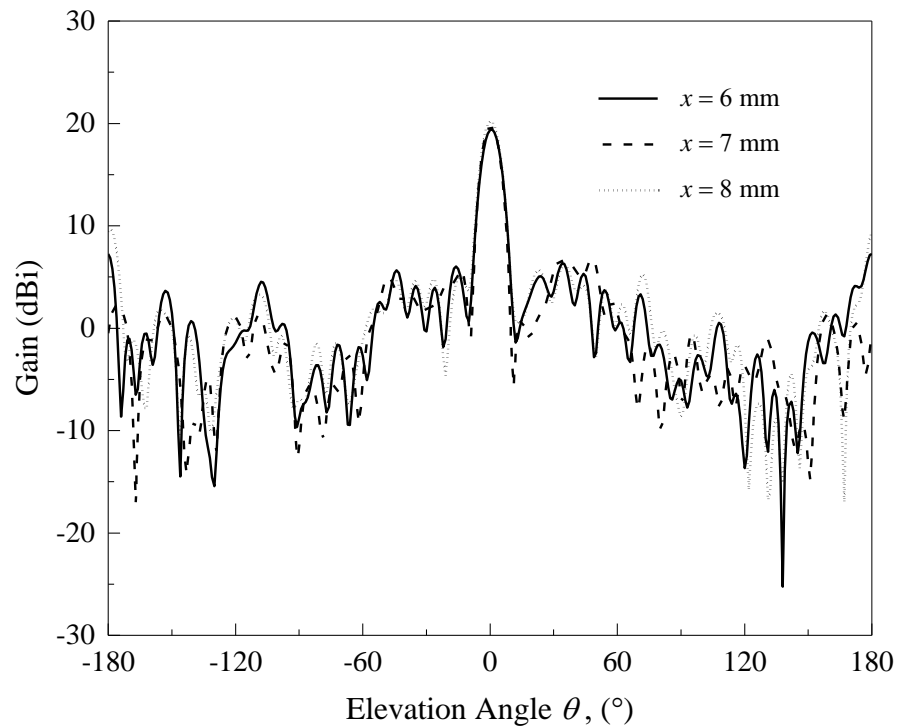


Figure 4.26: Effects of the length difference (x) between the long and the short probes on the transmission magnitude and transmission phase of the horizontally polarized transmitarray unit element.



(a)



(b)

Figure 4.27: Radiation patterns of the proposed horizontally polarized transmitarray for different length differences (x) between the long and the short probes at 7.3 GHz. (a) E - and (b) H - planes.

4.7.3 Probe Height

The effects of probe height (h) on the transmission magnitude and phase, shown in Figure 4.28, are analyzed. With $h = 6$ mm, poor transmission of lower than -3 dB is observed for all probe lengths, making this height infeasible for designing the full-fledge transmitarray. Increasing the probe height from 8 mm to 10 mm does not affect the gradient of phase curve much. Phase ranges of 353.14° and 382.89° are obtainable, respectively, for the probe heights of 8 mm and 10 mm.

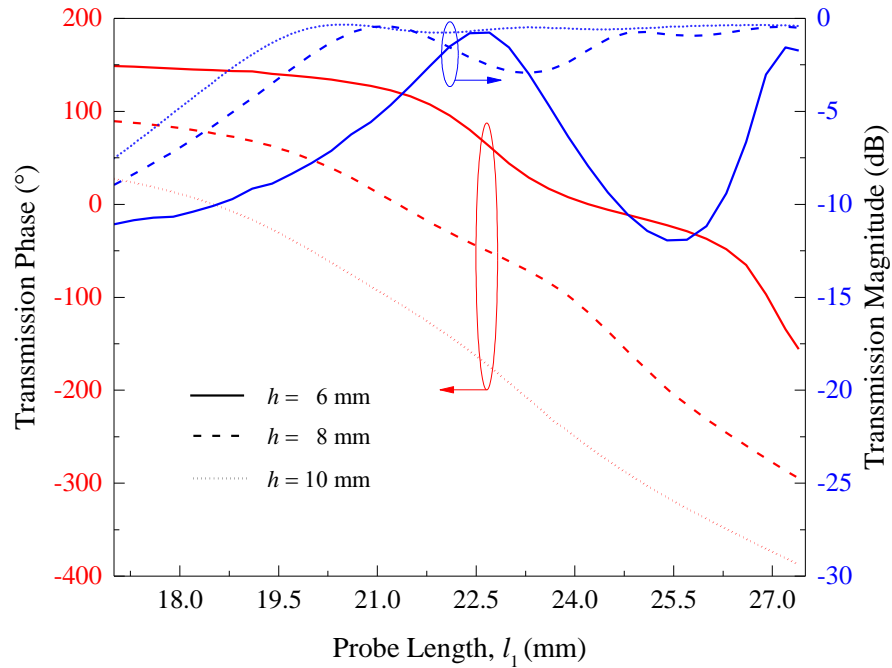


Figure 4.28: Effects of the probe height (h) on the transmission magnitude and transmission phase of the horizontally polarized transmitarray unit element.

4.7.4 Probe Diameter

The effects of the probe diameter (d) are now studied. Figure 4.29 illustrates the transmission characteristics of the unit element when the probe diameter is varied from $d = 0.5$ mm to 1.5 mm. It can be seen that the unit element with probe diameter of $d = 1$ mm has achieved a better transmission beyond the probe length (l_1) of 18.7 mm as compared to the unit elements with probe diameters of $d = 0.5$ mm and 1.5 mm. The radiation performances of the transmitarray for different probe diameters are shown in Figure 4.30. The boresight antenna gain reduces by ~ 0.5 dBi when the probe diameter is increased by 0.5 mm. For probe diameters of $d = 0.5$ mm, 1 mm, and 1.5 mm, a front-to-back ratio of 14.97 dBi, 20.33 dBi, and 8.82 dBi is obtainable, respectively.

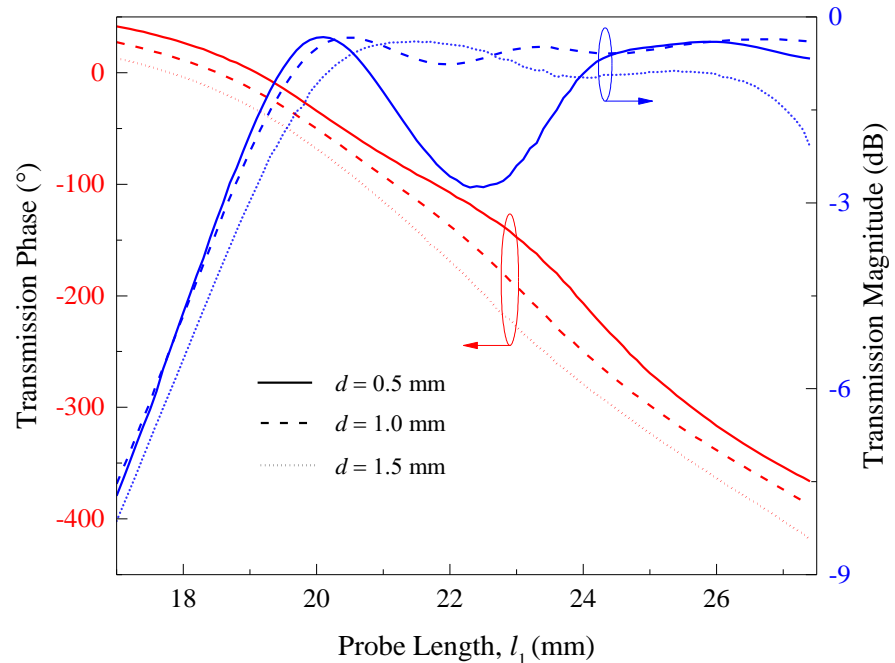
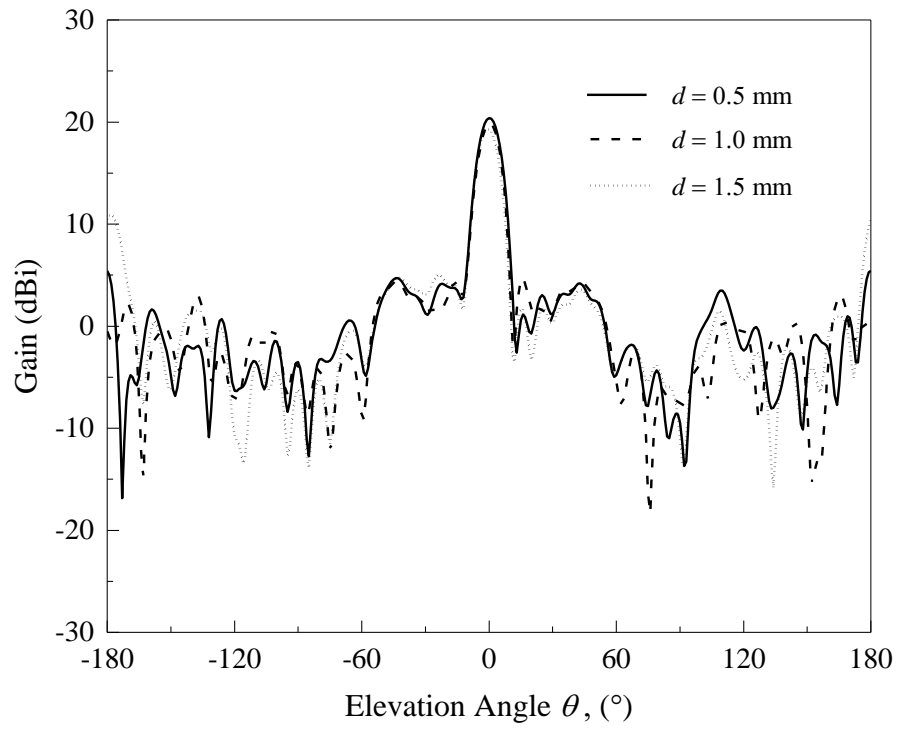
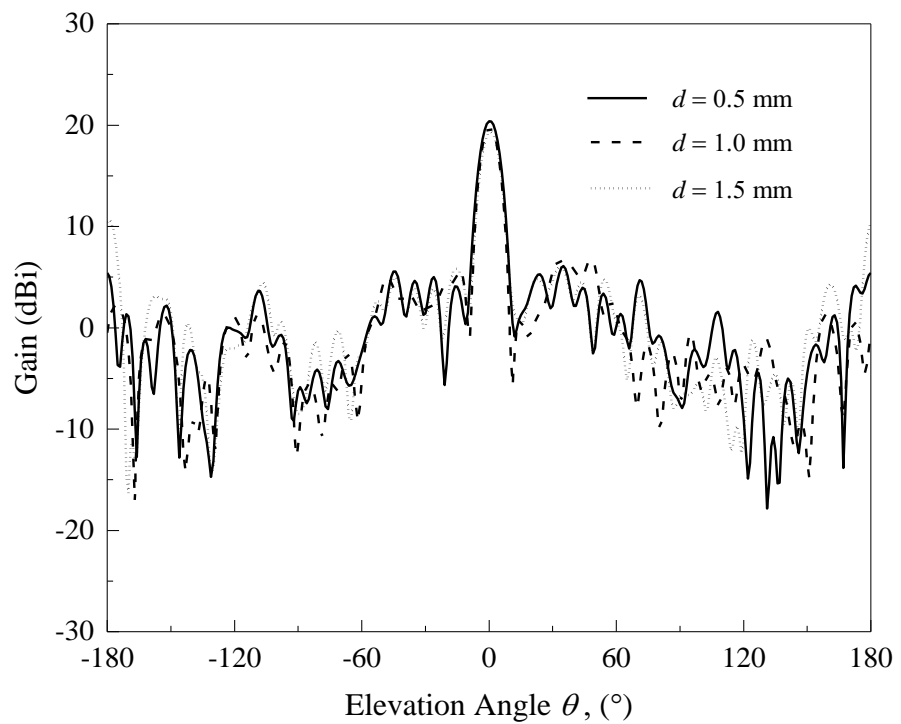


Figure 4.29: Effects of the probe diameter (d) on the transmission magnitude and transmission phase of the horizontally polarized transmitarray unit element.



(a)



(b)

Figure 4.30: Radiation patterns of the proposed horizontally polarized transmitarray for different probe diameters (d) at 7.3 GHz. (a) E - and (b) H - planes.

4.7.5 Separation Distance between Long and Short Probes in y -direction

Next, the properties of the separation distance between the long and the short probes in the y -direction (G_y) are studied. From the unit element simulation, as can be seen in Figure 4.31, adjusting G_y from 3 mm to 7 mm does not affect the gradient of transmission phase curve much. Transmission phase range of $\sim 382^\circ$ is obtained for G_y of 3 mm, 5 mm, and 7 mm. In the full-fledged transmitarray, varying the separation distance between the long and the short probes in the y -direction would, however, affect the radiation performances of the transmitarray. It is observed from Figure 4.32 that the transmitarrays which are designed with G_y of 3 mm or 7 mm have a much higher back lobe level than the one designed with G_y of 5 mm. Similar trends are found in the transmission magnitude and phase responses as well as the radiation patterns when the separation distance between the long and the short probes is varied from 3 mm to 7 mm in the x -direction (G_x).

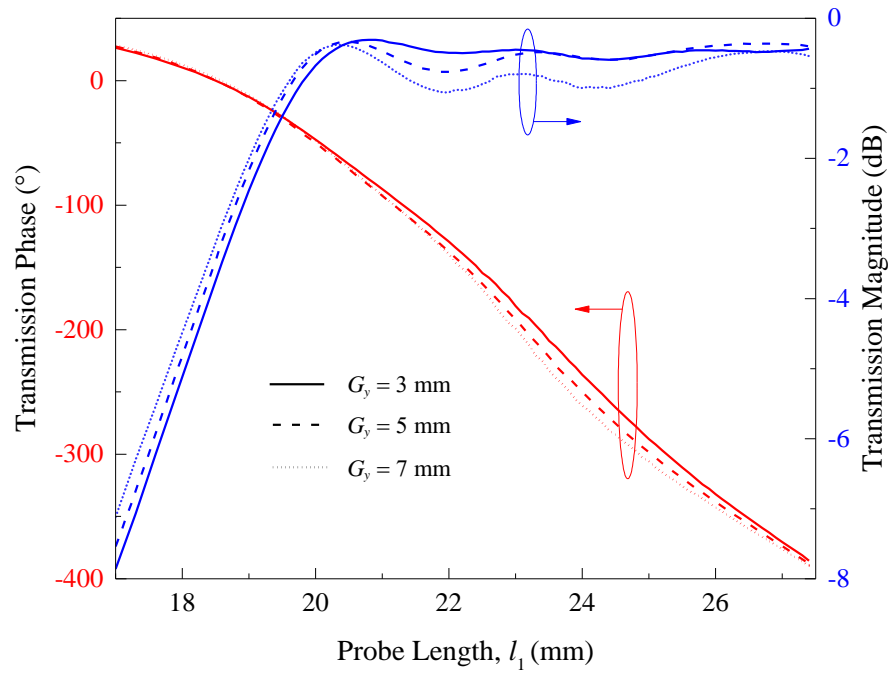
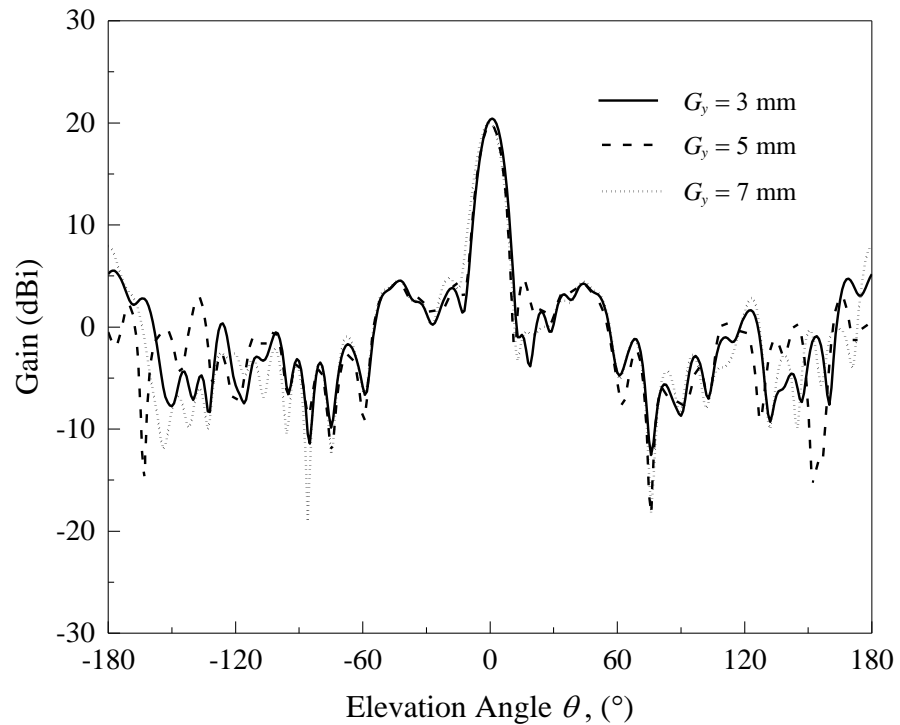


Figure 4.31: Effects of the separation distance between the long and the short probes in the y -direction (G_y) on the transmission magnitude and transmission phase of the horizontally polarized transmitarray unit element.



(a)

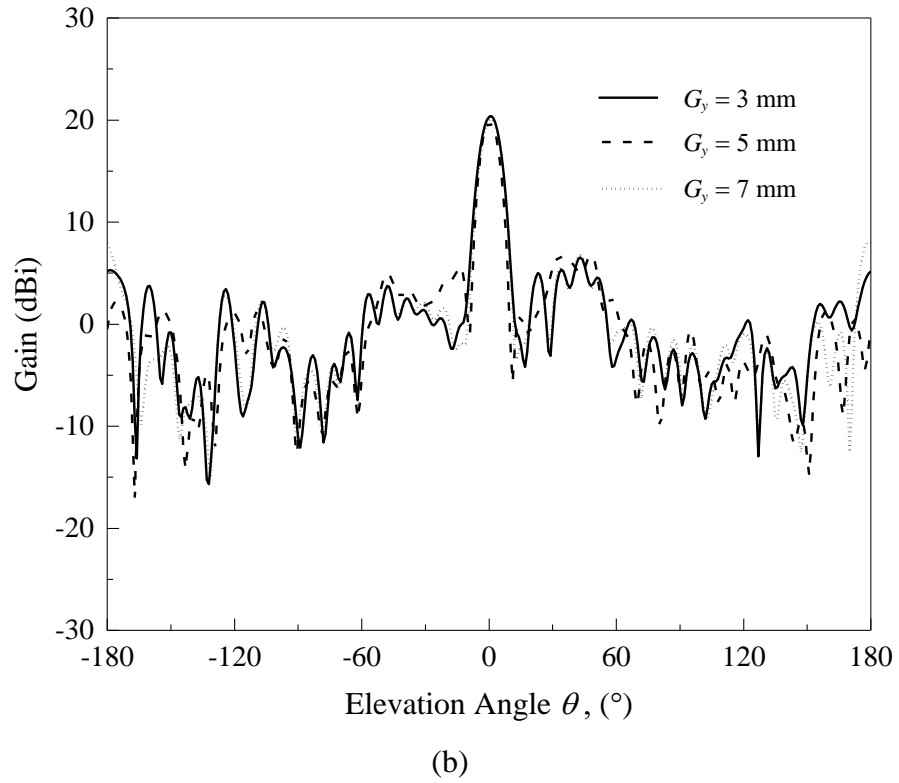


Figure 4.32: Radiation patterns of the proposed horizontally polarized transmitarray for different probe separations in the y -direction (G_y) at 7.3 GHz. (a) E - and (b) H - planes.

4.7.6 Separation Distance between Long and Short Probes

Figure 4.33 shows the element responses when the separation distances between the long and the short probes in the x - and y -directions ($G_x = G_y$) are set to be equal and varied from 3 mm to 7 mm. It can be observed that the transmission phase curve becomes steeper and the transmission phase range becomes larger when $G_x (= G_y)$ increases. The radiation performances for different probe separations are depicted in Figure 4.34. Apparently, the transmitarrays with $G_x = G_y = 3$ mm and 7 mm are unable to achieve high front-to-back ratios due to the significantly high back lobe levels. High side lobe level is also perceived for the case of $G_x = G_y = 3$ mm.

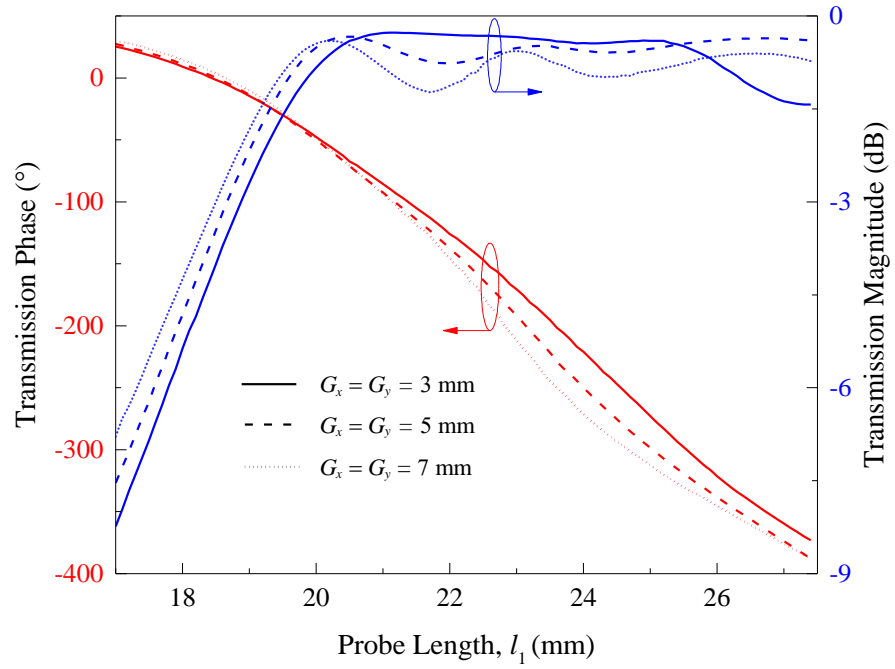
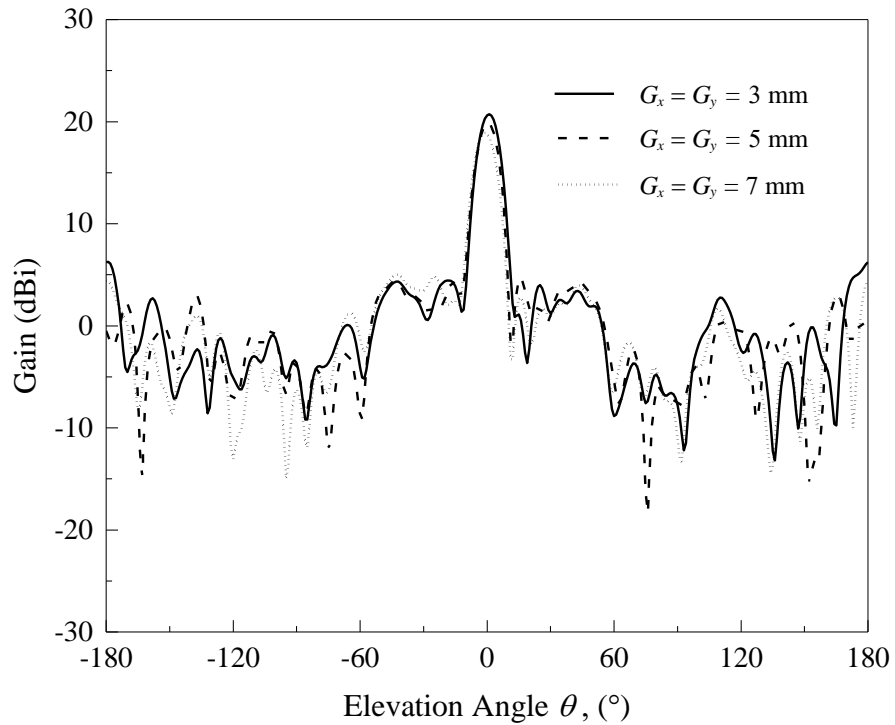


Figure 4.33: Effects of the separation distance between the long and the short probes ($G_x = G_y$) on the transmission magnitude and transmission phase of the horizontally polarized transmitarray unit element.



(a)

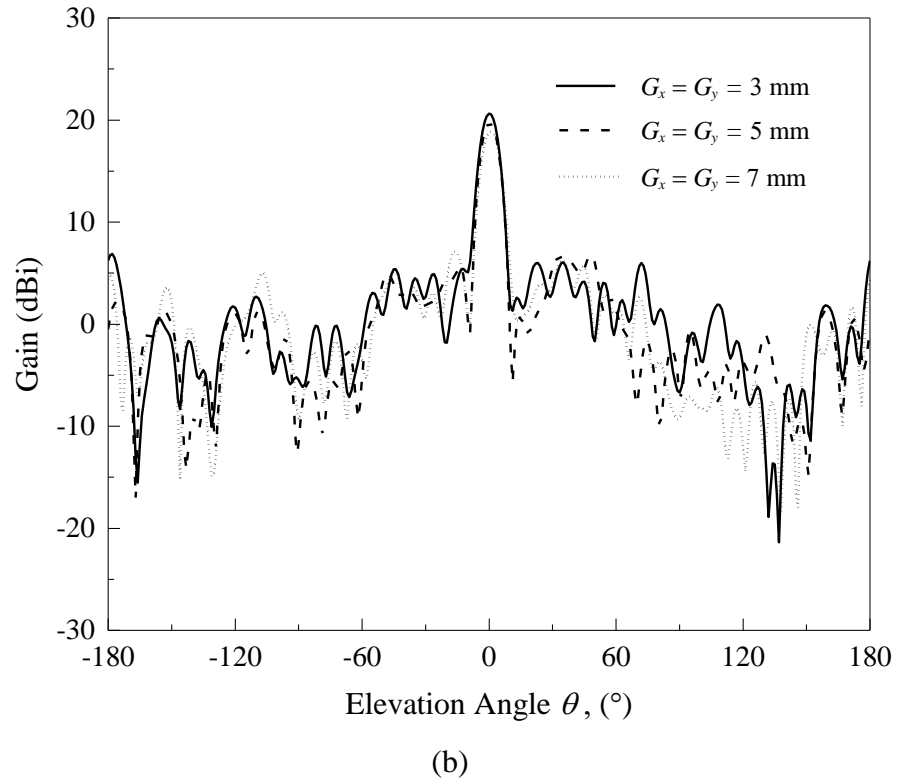


Figure 4.34: Radiation patterns of the proposed horizontally polarized transmitarray for different probe separations ($G_x = G_y$) at 7.3 GHz. (a) E - and (b) H - planes.

4.7.7 Unit Cell Size

The unit cell size (L) and the element spacing of the full-fledged transmitarray are then studied. Figure 4.35 shows the transmission magnitude and phase responses of the transmitarray element when the cell size is varied from 0.765λ to 0.814λ at 7.4 GHz. As expected, broader phase range can be achieved for a larger cell size as the probe length can be further lengthened. With reference to the figure, unit cell sizes of 0.765λ , 0.789λ , and 0.814λ have generated phase ranges of 382.89° , 428.92° , and 477.04° , respectively. Varying the cell size does not affect the gradient of the phase curve much. Figure 4.36 illustrates the radiation patterns of the transmitarray for different

element spacings at 7.3GHz. It is observed that the transmitarray with an element spacing of 0.765λ is able to achieve a higher front-to-back ratio than those for 0.789λ and 0.814λ .

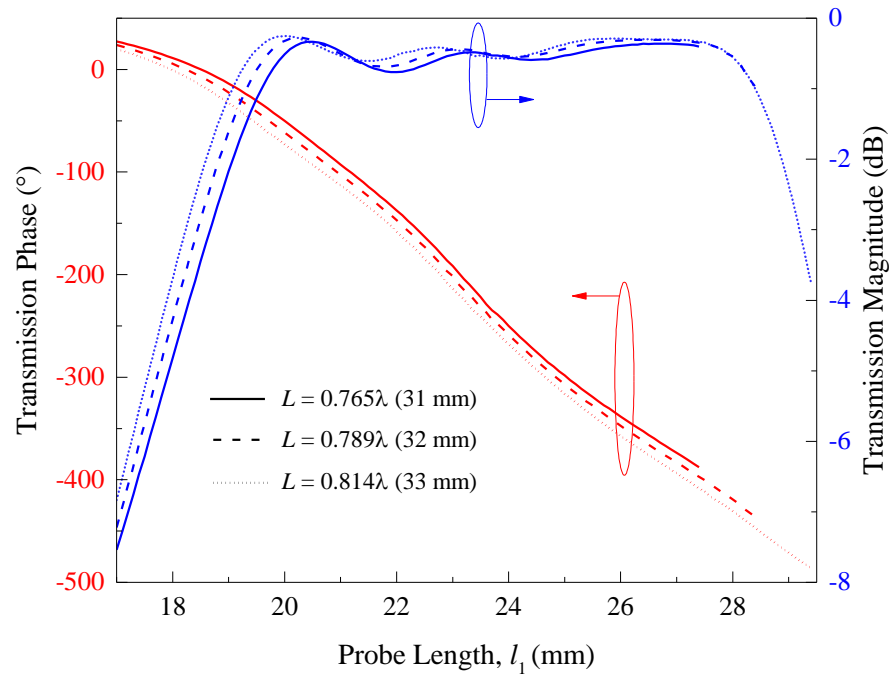
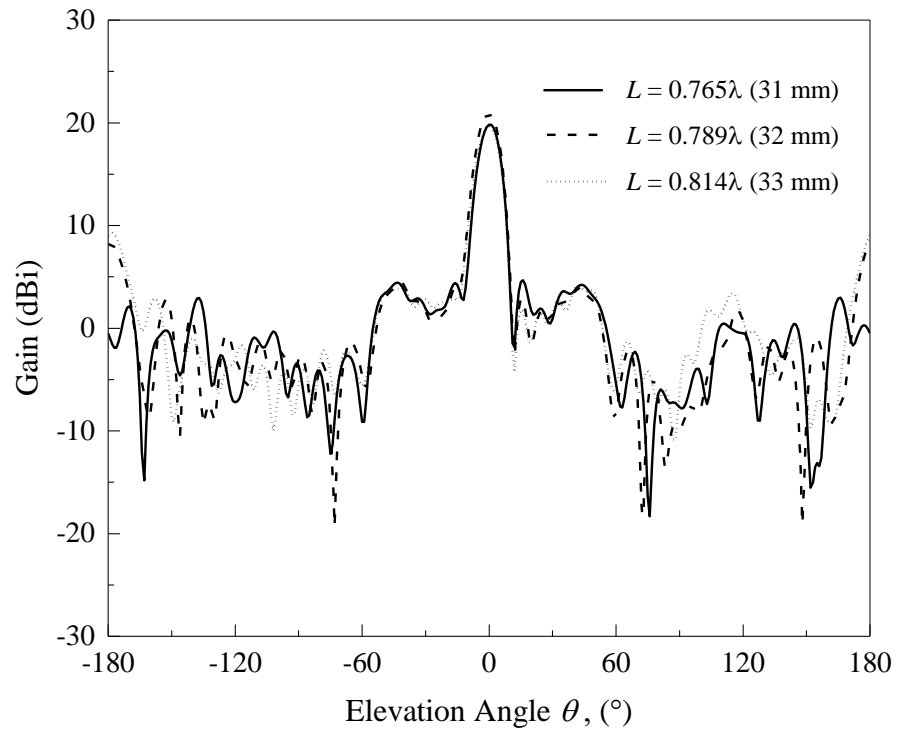
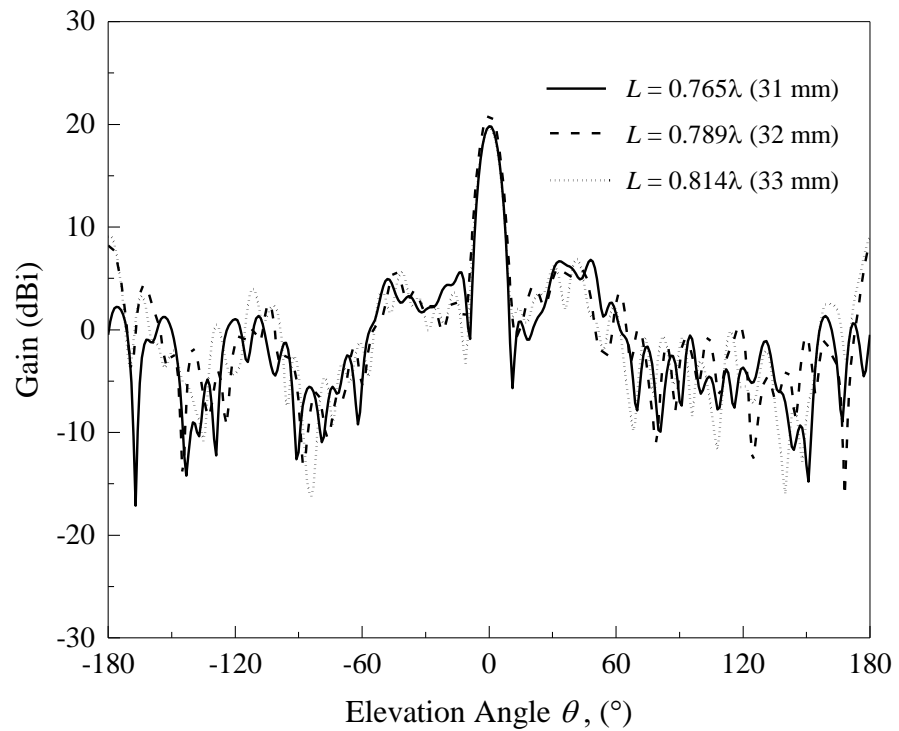


Figure 4.35: Effects of the unit element dimension (L) on the transmission magnitude and transmission phase of the horizontally polarized transmitarray unit element.



(a)

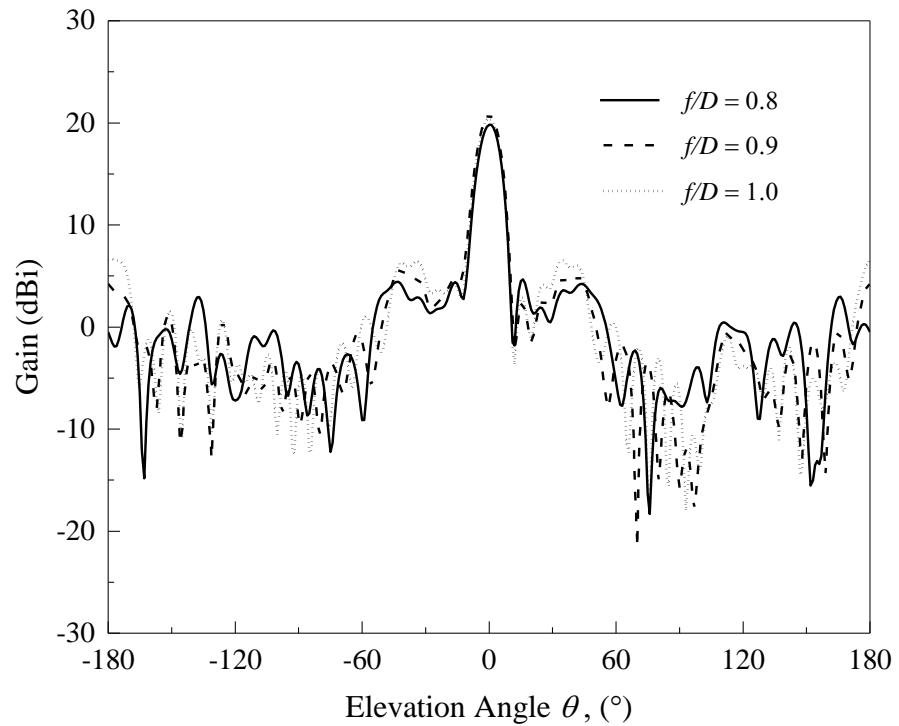


(b)

Figure 4.36: Radiation patterns of the proposed horizontally polarized transmitarray for different separation distances (L) at 7.3 GHz. (a) E - and (b) H - planes.

4.7.8 f/D Ratio

Finally, by keeping the cell size (L) at 0.765λ (31 mm) and board dimension (D) at 279 mm, the effects of f/D ratio are studied at 7.3 GHz. It can be seen from Figure 4.37 that the back lobe level and the side lobe level around the elevation angle of $\theta = -60^\circ$ to $+60^\circ$ increase when the f/D ratio is varied from 0.8 to 1. For f/D ratios of 0.8, 0.9, and 1, front-to-back ratios of 20.33 dBi, 16.62 dBi, and 13.84 dBi are obtained, respectively.



(a)

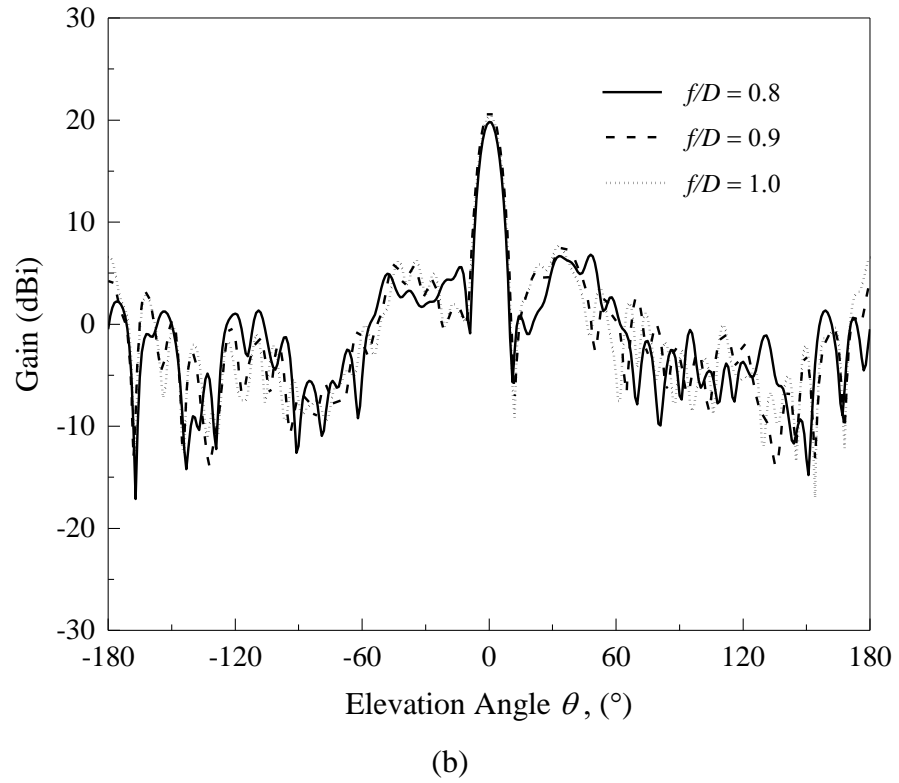


Figure 4.37: Radiation patterns of the proposed horizontally polarized transmitarray for different f/D ratios. (a) E - and (b) H - planes.

4.8 Conclusion

Two L-shaped probes are co-joined for designing the vertically and horizontally polarized broadband transmitarrays. The unit elements have achieved a linear transmission phase range of greater than 380° , and both of the full-fledge transmitarrays have generated a -1 dB gain bandwidth of more than 10%. Parametric analysis has been conducted on several essential geometrical parameters for both the vertically and the horizontally polarized transmitarrays. It is found that the unit element with only one probe has poor transmission. For the unit element with two probes, it was discovered that a length difference between the two probes has to be introduced in order to

obtain good transmission and sufficient phase range. By properly adjusting the geometrical parameters, it was shown that the side and back lobes for both the transmitarrays can be lowered down and optimized.

CHAPTER 5

SUMMARY AND DISCUSSION

In this dissertation, the L-shaped probe resonator has been employed for designing a reflectarray and two transmitarrays, operating in the C-band. Each of the antenna arrays consist of two co-joined L-shaped probes of different lengths, supported by an FR4 substrate. In the first part, the L-probe reflectarray element has achieved a linear reflection phase range of 454.2° . An 11×11 full-fledged reflectarray is able to provide an antenna gain of 20.4 dBi and a wide -1 dB gain bandwidth of 15.38%. In the second part, the concept of dual linear polarization has been realized by altering the orientation of the L-shaped probes of the transmitarray. It is presented using two transmitarrays: one of which has the transmitting wave polarized in vertical direction while the other in horizontal direction. For both transmitarray elements, a linear transmission phase range of $\sim 380^\circ$ is attained. For each of the transmitarrays, a prototype which consists of 81 elements is fabricated. Measurements show that the vertically polarized transmitarray has an antenna gain of 21.9 dBi with a broad -1 dB gain bandwidth of 11.62%; whereas the horizontally polarized transmitarray has an antenna gain of 19.1 dBi with a wide -1 dB gain bandwidth of 10.39%. Good agreement is found between the simulations and the measurements.

BIBLIOGRAPHY

Abdelrahman, A.H., Elsherbeni, A.Z. and Yang, F., 2014a. Transmission phase limit of multilayer frequency-selective surfaces for transmitarray designs. *IEEE Transactions on Antennas and Propagation*, 62 (2), pp. 690–697.

Abdelrahman, A.H., Elsherbeni, A.Z. and Yang, F., 2014b. Transmitarray antenna design using cross-slot elements with no dielectric substrate. *IEEE Antennas and Wireless Propagation Letters*, 13, pp. 177–180.

Abdelrahman, A.H. and Elsherbeni, A.Z., 2014. High-gain and broadband transmitarray antenna using triple-layer spiral dipole elements. *IEEE Antennas and Wireless Propagation Letters*, 13, pp. 1288–1291.

Abdelrahman, A.H., Nayeri, P., Elsherbeni, A.Z. and Yang, F., 2015. Bandwidth improvement methods of transmitarray antennas. *IEEE Transactions on Antennas and Propagation*, 63 (7), pp. 2946–2954.

Almajali, E., McNamara, D.A., Shaker, J. and Chaharmir, M.R., 2014. Feed image lobes in offset-fed reflectarrays: diagnosis and solution. *IEEE Transactions on Antennas and Propagation*, 62 (1), pp. 216–227.

Berry, D., Malech, R. and Kennedy, W., 1963. The reflectarray antenna. *IEEE Transactions on Antennas and Propagation*, 11 (6), pp. 645–651.

Bozzi, M., Germani, S. and Perregrini, L., 2004. A figure of merit for losses in printed reflectarray elements. *IEEE Antennas and Wireless Propagation Letters*, 3 (1), pp. 257–260.

Cadoret, D., Laisné, A., Gillard, R. and Legay, H., 2005. A new reflectarray cell using microstrip patches loaded with slots. *Microwave and Optical Technology Letters*, 44 (3), pp. 270–272.

Carrasco, E., Arrebola, M., Encinar, J.A. and Barba, M., 2008. Demonstration of a shaped beam reflectarray using aperture-coupled delay lines for LMDS central station antenna. *IEEE Transactions on Antennas and Propagation*, 56 (10), pp. 3103–3111.

Chang, D.-C. and Huang, M.-C., 1992. Microstrip reflectarray antenna with offset feed. *Electronics Letters*, 28 (16), p. 1489.

Chang, D.-C. and Huang, M.-C., 1995. Multiple-polarization microstrip reflectarray antenna with high efficiency and low cross-polarization. *IEEE Transactions on Antennas and Propagation*, 43 (8), pp. 829–834.

Chen, Q.-Y., Qu, S.-W., Li, J.-F., Chen, Q. and Xia, M.-Y., 2013a. An X-band reflectarray with novel elements and enhanced bandwidth. *IEEE Antennas and Wireless Propagation Letters*, 12, pp. 317–320.

Chen, Y., Chen, L., Yu, J.-F. and Shi, X.-W., 2013b. A C-band flat lens antenna with double-ring slot elements. *IEEE Antennas and Wireless Propagation Letters*, 12, pp. 341–344.

Clemente, A., Dussopt, L., Sauleau, R., Potier, P. and Pouliguen, P., 2012. Focal distance reduction of transmit-array antennas using multiple feeds. *IEEE Antennas and Wireless Propagation Letters*, 11, pp. 1311–1314.

Encinar, J.A., Arrebola, M., Fuente, L.F. and Toso, G., 2011. A transmit-receive reflectarray antenna for direct broadcast satellite applications. *IEEE Transactions on Antennas and Propagation*, 59 (9), pp. 3255–3264.

Encinar, J.A. and Zornoza, J.A., 2003. Broadband design of three-layer printed reflectarrays. *IEEE Transactions on Antennas and Propagation*, 51 (7), pp. 1662–1664.

Encinar, J.A. and Zornoza, J.A., 2004. Three-layer printed reflectarrays for contoured beam space applications. *IEEE Transactions on Antennas and Propagation*, 52 (5), pp. 1138–1148.

Encinar, J.A., 2001. Design of two-layer printed reflectarrays using patches of variable size. *IEEE Transactions on Antennas and Propagation*, 49 (10), pp. 1403–1410.

Friedlander, F.G., 1946. A dielectric-lens aerial for wide-angle beam scanning. *Journal of the Institution of Electrical Engineers - Part IIIA: Radiolocation*, 93 (4), pp. 658–662.

Huang, J., 1991. Microstrip reflectarray. *Antennas and Propagation Society International Symposium*, 2, pp. 612–615.

Huang, J., 1995. Analysis of a microstrip reflectarray antenna for microspacecraft applications. *TDA Progress Report 42-120*, pp. 153–173.

Jiang, M., Zhang, Y., Hong, W. and Yu, S.H., 2013. An investigation on the gain of folded reflectarray antennas with different F/Ds. *Proceedings of the International Symposium on Antennas and Propagation*, 01, pp. 164–167.

Kaouach, H., Dussopt, L., Lanteri, J., Koleck, T. and Sauleau, R., 2011. Wideband low-loss linear and circular polarization transmit-arrays in V-band. *IEEE Transactions on Antennas and Propagation*, 59 (7), pp. 2513–2523.

Karnati, K.K., Yusuf, Y., Ebadi, S. and Gong, X., 2013. Theoretical analysis on reflection properties of reflectarray unit cells using quality factors. *IEEE Transactions on Antennas and Propagation*, 61 (1), pp. 201–210.

Kelkar, A., 1991. FLAPS: conformal phased reflecting surfaces. *Proceedings of the IEEE National Radar Conference*, pp. 58–62.

Kishk, A.A., Chair, R. and Lee, K.F., 2006. Broadband dielectric resonator antennas excited by L-shaped probe. *IEEE Transactions on Antennas and Propagation*, 54 (8), pp. 2182–2189.

Lau, K.L. and Luk, K.M., 2005. A wide-band circularly polarized L-probe coupled patch antenna for dual-band operation. *IEEE Transactions on Antennas and Propagation*, 53 (8), pp. 2636–2644.

Lau, K.L. and Luk, K.M., 2007. A wideband dual-polarized L-probe stacked patch antenna array. *Antennas and Wireless Propagation Letters*, 6, pp. 529–532.

Li, Y., Bialkowski, M.E. and Abbosh, A.M., 2012. Single layer reflectarray with circular rings and open-circuited stubs for wideband operation. *IEEE Transactions on Antennas and Propagation*, 60 (9), pp. 4183–4189.

Lim, E.H., Tang, K.S. and Choo, K.L., 2012. Broadside L-shaped wire array. *Proceedings of the IEEE International Symposium on Antennas and Propagation*, pp. 1–2.

Liu, B., Wang, F., Chen, C. and Chen, W., 2014. A wideband dual-polarized L-probe proximity-fed annular ring antenna with compact size. *Asia-Pacific Microwave Conference*, pp. 336–338.

Liu, G., Wang, H., Jiang, J., Xue, F. and Yi, M., 2015. A high-efficiency transmitarray antenna using double split ring slot elements. *IEEE Antennas and Wireless Propagation Letters*, 14, pp. 1415–1418.

Luk, K.M., Mak, C.L., Chow, Y.L. and Lee, K.F., 1998. Broadband microstrip patch antenna. *Electronics Letters*, 34 (15), p. 1442.

Malagisi, C.S., 1978. Microstrip disc element reflect array. *Electronics and Aerospace Systems Convention*, pp. 186–192.

McGrath, D., 1986. Planar three-dimensional constrained lenses. *IEEE Transactions on Antennas and Propagation*, 34 (1), pp. 46–50.

Mener, S., Gillard, R., Sauleau, R., Cheymol, C. and Potier, P., 2013. Design and characterization of a CPSS-based unit-cell for circularly polarized reflectarray applications. *IEEE Transactions on Antennas and Propagation*, 61 (4), pp. 2313–2318.

Milne, R., 1982. Dipole array lens antenna. *IEEE Transactions on Antennas and Propagation*, 30 (4), pp. 704–712.

Montgomery, J.P., 1978. A microstrip reflectarray antenna element. *Antenna Applications Symposium*.

Nakano, H., Yoshida, H. and Wu, Y., 1995. C-shaped loop antennas. *Electronics Letters*, 31 (9), p. 693.

Nayeri, P., Yang, F. and Elsherbeni, A.Z., 2011. Bandwidth improvement of reflectarray antenna using closely spaced elements. *Progress In Electromagnetics Research C*, 18, pp. 19–29.

Pan, Y., Zhang, Y. and Karimkashi, S., 2012. Broadband low-cost reflectarray for multi-mission radar applications. *IEEE Radar Conference*, pp. 0613–0617.

Pham, K. et al., 2016. Design of wideband dual linearly polarized transmitarray antennas. *IEEE Transactions on Antennas and Propagation*, 64 (5), pp. 2022–2026.

Phelan, H.R., 1977. Spiraphase reflectarray for multitarget radar. *Microwave Journal*, 20, pp. 67–73.

Plaza, E.G., Leon, G., Loredó, S. and Las-Heras, F., 2014. Dual polarized transmitarray lens. *The 8th European Conference on Antennas and Propagation*, pp. 2305–2308.

Pozar, D.M. and Metzler, T.A., 1993. Analysis of a reflectarray antenna using microstrip patches of variable size. *Electronics Letters*, 29 (8), p. 657.

Pozar, D.M., Targonski, S.D. and Syrigos, H.D., 1997. Design of millimeter wave microstrip reflectarrays. *IEEE Transactions on Antennas and Propagation*, 45 (2), pp. 287–296.

Pozar, D.M. and Targonski, S.D., 1998. A microstrip reflectarray using crossed dipoles. *IEEE Antennas and Propagation Society International Symposium*, 2, pp. 1008–1011.

Pozar, D.M., 1996. Flat lens antenna concept using aperture coupled microstrip patches. *Electronics Letters*, 32 (23), p. 2109.

Qin, P.-Y., Guo, Y.J. and Weily, A.R., 2016. Broadband reflectarray antenna using subwavelength elements based on double square meander-line rings. *IEEE Transactions on Antennas and Propagation*, 64 (1), pp. 378–383.

Rahmati, B. and Hassani, H.R., 2015a. High-efficient wideband slot transmitarray antenna. *IEEE Transactions on Antennas and Propagation*, 63 (11), pp. 5149–5155.

Rahmati, B. and Hassani, H.R., 2015b. Low-profile slot transmitarray antenna. *IEEE Transactions on Antennas and Propagation*, 63 (1), pp. 174–181.

Ryan, C.G.M. et al., 2010. A wideband transmitarray using dual-resonant double square rings. *IEEE Transactions on Antennas and Propagation*, 58 (5), pp. 1486–1493.

Shaker, J., Chaharmir, M.R. and Ethier, J., 2014. *Reflectarray antennas: analysis, design, fabrication, and measurement*. London, UK: Artech House.

Shibayama, R., Deguchi, H. and Tsuji, M., 2010. Flat thin polarizer-lens based on multiple resonance behavior. *IEEE Antennas and Propagation Society International Symposium*, pp. 1–4.

Singh, A.K., Gangwar, R.K. and Kanaujia, B.K., 2013. Bandwidth enhancement of L-probe proximity-fed annular ring microstrip slot antenna. *6th IEEE/International Conference on Advanced Infocomm Technology*, pp. 195–197.

Sze, K.Y. and Shafai, L., 1999. Substrate thickness in a microstrip reflectarray. *Asia Pacific Microwave Conference*, 1, pp. 146–149.

Wang, L., Guo, Y.-X. and Sheng, W.-X., 2013. Wideband high-gain 60-GHz LTCC L-probe patch antenna array with a soft surface. *IEEE Transactions on Antennas and Propagation*, 61 (4), pp. 1802–1809.

Wang, Y., Deguchi, H. and Tsuji, M., 2012. A broadband flat lens based on aperture-coupled patch FSSs with four-pole resonant behaviour. *Proceedings of the IEEE International Symposium on Antennas and Propagation*, pp. 1–2.

Wong, H., Lau, K.L. and Luk, K.M., 2004. Design of dual-polarized L-probe patch antenna arrays with high isolation. *IEEE Transactions on Antennas and Propagation*, 52 (1), pp. 45–52.

Xu, H.-X. et al., 2016. Multifunctional microstrip array combining a linear polarizer and focusing metasurface. *IEEE Transactions on Antennas and Propagation*, 64 (8), pp. 3676–3682.

Yamauchi, R. and Fukusako, T., 2014. Circularly polarized broadband waveguide antenna using L-shaped probe. *IEEE International Workshop on Electromagnetics*, pp. 237–238.

Yamauchi, R. and Fukusako, T., 2015. Reduction of cross polarization for circularly polarized broadband waveguide antenna. *International Workshop on Electromagnetics: Applications and Student Innovation Competition*, pp. 1–2.

Yoon, J.H., Yoon, Y.J., Lee, W. and So, J., 2015. Broadband microstrip reflectarray with five parallel dipole elements. *IEEE Antennas and Wireless Propagation Letters*, 14, pp. 1109–1112.

Yu, J., Chen, L., Yang, J. and Shi, X., 2016. Design of a transmitarray using split diagonal cross elements with limited phase range. *IEEE Antennas and Wireless Propagation Letters*, 15, pp.1514–1517.

Zhang, K., Fan, Y., Xu, J. and Qu, C., 2013. Design of broadband, low cost single layer reflectarray using phoenix cell. *TENCON IEEE Region 10 conference*, pp. 1–4.

Zhao, G., Jiao, Y.-C., Zhang, F. and Zhang, F.-S., 2010. A subwavelength element for broadband circularly polarized reflectarrays. *IEEE Antennas and Wireless Propagation Letters*, 9, pp. 330–333.

Zheng, J., Hu, G., Hu, X. and Gu, J., 2014. E-shaped patch antenna using L-probe for 4G communication systems. *International Frequency Sensor Association*, 182 (11), pp. 105–110.

Zhong, X., Chen, L., Yan, S. and Shi, X., 2016. Design of multiple polarization transmitarray antenna using rectangle ring slot elements. *IEEE Antennas and Wireless Propagation Letters*, 15, pp. 1803–1806.

Zhou, M. et al., 2013. Direct optimization of printed reflectarrays for contoured beam satellite antenna applications. *IEEE Transactions on Antennas and Propagation*, 61 (4), pp. 1995–2004.

APPENDIX A

| Phase difference; Phase from S-curve; (Probe length, l_1) | Column 1 | Column 2 | Column 3 | Column 4 | Column 5 | Column 6 | Column 7 | Column 8 | Column 9 | Column 10 | Column 11 |
|--|--------------------------------|--------------------------------|---------------------------------|---------------------------------|--------------------------------|--------------------------------|--------------------------------|--------------------------------|--------------------------------|--------------------------------|--------------------------------|
| Row 1 | 333.6° -51.9° (13.8 mm) | 277.5° -108.0° (16.7 mm) | 246.0° -139.5° (17.6 mm) | 240.3° -145.2° (17.8 mm) | 260.4° -125.1° (17.2 mm) | 305.6° -79.9° (15.5 mm) | 374.9° -370.6° (23.3 mm) | 466.2° -279.3° (21.3 mm) | 577.6° -167.9° (18.3 mm) | 706.7° -38.8° (12.5 mm) | 851.4° -254.1° (20.7 mm) |
| Row 2 | 218.6° -166.9° (18.3 mm) | 159.9° -225.6° (19.8 mm) | 126.9° -258.6° (20.8 mm) | 120.9° -264.6° (20.9 mm) | 141.9° -243.6° (20.4 mm) | 189.4° -196.1° (19.0 mm) | 261.8° -123.7° (17.2 mm) | 357.0° -28.5° (11.0 mm) | 472.8° -272.7° (21.1 mm) | 606.6° -138.9° (17.6 mm) | 756.1° -349.4° (22.9 mm) |
| Row 3 | 125.4° -260.1° (20.8 mm) | 64.3° -321.2° (22.4 mm) | 30.0° -355.5° (23.0 mm) | 23.7° -361.8° (23.1 mm) | 45.7° -339.8° (22.8 mm) | 95.0° -290.5° (21.6 mm) | 170.2° -215.3° (19.5 mm) | 268.9° -116.6° (16.9 mm) | 388.5° -357.0° (23.0 mm) | 526.3° -219.2° (19.6 mm) | 679.8° -65.7° (14.8 mm) |
| Row 4 | 56.6° -328.9° (22.5 mm) | -6.4° -31.9° (11.5 mm) | -41.8° -67.3° (14.9 mm) | -48.3° -73.8° (15.2 mm) | -25.6° -51.1° (13.7 mm) | 25.3° -360.2° (23.1 mm) | 102.7° -282.8° (21.4 mm) | 204.0° -181.5° (18.7 mm) | 326.6° -58.9° (14.3 mm) | 467.5° -278.0° (21.2 mm) | 624.1° -121.4° (17.1 mm) |
| Row 5 | 14.3° -371.2° (23.3 mm) | -49.7° -75.2° (15.3 mm) | -85.9° -111.4° (16.8 mm) | -92.6° -118.1° (17.0 mm) | -69.5° -95.0° (16.2 mm) | -17.6° -43.1° (13.0 mm) | 61.2° -324.3° (22.4 mm) | 164.3° -221.2° (19.7 mm) | 288.7° -96.8° (16.3 mm) | 431.6° -313.9° (22.2 mm) | 590.2° -155.3° (18.0 mm) |
| Row 6 | 0° -385.5° (23.5 mm) | -64.6° -90.1° (16.0 mm) | -100.9° -126.4° (17.2 mm) | -107.6° -133.1° (17.4 mm) | -84.3° -109.8° (16.7 mm) | -32.1° -57.6° (14.2 mm) | 47.2° -338.3° (22.7 mm) | 150.9° -234.6° (20.0 mm) | 276.0° -109.5° (16.7 mm) | 419.6° -325.9° (22.4 mm) | 578.8° -166.7° (18.3 mm) |
| Row 7 | 14.3° -371.2° (23.3 mm) | -49.7° -75.2° (15.3 mm) | -85.9° -111.4° (16.8 mm) | -92.6° -118.1° (17.0 mm) | -69.5° -95.0° (16.2 mm) | -17.6° -43.1° (13.0 mm) | 61.2° -324.3° (22.4 mm) | 164.3° -221.2° (19.7 mm) | 288.7° -96.8° (16.3 mm) | 431.6° -313.9° (22.2 mm) | 590.2° -155.3° (18.0 mm) |
| Row 8 | 56.6° -328.9° (22.5 mm) | -6.4° -31.9° (11.5 mm) | -41.8° -67.3° (14.9 mm) | -48.3° -73.8° (15.2 mm) | -25.6° -51.1° (13.7 mm) | 25.3° -360.2° (23.1 mm) | 102.7° -282.8° (21.4 mm) | 204.0° -181.5° (18.7 mm) | 326.6° -58.9° (14.3 mm) | 467.5° -278.0° (21.2 mm) | 624.1° -121.4° (17.1 mm) |
| Row 9 | 125.4° -260.1° (20.8 mm) | 64.3° -321.2° (22.4 mm) | 30.0° -355.5° (23.0 mm) | 23.7° -361.8° (23.1 mm) | 45.7° -339.8° (22.8 mm) | 95.0° -290.5° (21.6 mm) | 170.2° -215.3° (19.5 mm) | 268.9° -116.6° (16.9 mm) | 388.5° -357.0° (23.0 mm) | 526.3° -219.2° (19.6 mm) | 679.8° -65.7° (14.8 mm) |
| Row 10 | 218.6° -166.9° (18.3 mm) | 159.9° -225.6° (19.8 mm) | 126.9° -258.6° (20.8 mm) | 120.9° -264.6° (20.9 mm) | 141.9° -243.6° (20.4 mm) | 189.4° -196.1° (19.0 mm) | 261.8° -123.7° (17.2 mm) | 357.0° -28.5° (11.0 mm) | 472.8° -272.7° (21.1 mm) | 606.6° -138.9° (17.6 mm) | 756.1° -349.4° (22.9 mm) |
| Row 11 | 333.6° -51.9° (13.8 mm) | 277.5° -108.0° (16.7 mm) | 246.0° -139.5° (17.6 mm) | 240.3° -145.2° (17.8 mm) | 260.4° -125.1° (17.2 mm) | 305.6° -79.9° (15.5 mm) | 374.9° -370.6° (23.3 mm) | 466.2° -279.3° (21.3 mm) | 577.6° -167.9° (18.3 mm) | 706.7° -38.8° (12.5 mm) | 851.4° -254.1° (20.7 mm) |

APPENDIX B

| Phase difference; Phase from phase curve; (Probe length, l_1) | Column 1 | Column 2 | Column 3 | Column 4 | Column 5 | Column 6 | Column 7 | Column 8 | Column 9 |
|--|--------------------------------|---------------------------------|---------------------------------|---------------------------------|---------------------------------|---------------------------------|---------------------------------|---------------------------------|--------------------------------|
| Row 1 | 266.9° -193.3° (20.0 mm) | 153.6° -306.6° (22.8 mm) | 69.4° -390.8° (25.1 mm) | 17.5° -82.7° (17.2 mm) | 0° -100.2° (17.7 mm) | 17.5° -82.7° (17.2 mm) | 69.4° -390.8° (25.1 mm) | 153.6° -306.6° (22.8 mm) | 266.9° -193.3° (20.0 mm) |
| Row 2 | 153.6° -306.6° (22.8 mm) | 35.0° -65.2° (16.8 mm) | -53.4° -153.6° (19.1 mm) | -108.1° -208.3° (20.4 mm) | -126.7° -226.9° (20.9 mm) | -108.1° -208.3° (20.4 mm) | -53.4° -153.6° (19.1 mm) | 35.0° -65.2° (16.8 mm) | 153.6° -306.6° (22.8 mm) |
| Row 3 | 69.4° -390.8° (25.1 mm) | -53.4° -153.6° (19.1 mm) | -145.3° -245.5° (21.3 mm) | -202.3° -302.5° (22.7 mm) | -221.6° -321.8° (23.1 mm) | -202.3° -302.5° (22.7 mm) | -145.3° -245.5° (21.3 mm) | -53.4° -153.6° (19.1 mm) | 69.4° -390.8° (25.1 mm) |
| Row 4 | 17.5° -82.7° (17.2 mm) | -108.1° -208.3° (20.4 mm) | -202.3° -302.5° (22.7 mm) | -260.8° -361.0° (24.2 mm) | -280.7° -380.9° (24.8 mm) | -260.8° -361.0° (24.2 mm) | -202.3° -302.5° (22.7 mm) | -108.1° -208.3° (20.4 mm) | 17.5° -82.7° (17.2 mm) |
| Row 5 | 0° -100.2° (17.7 mm) | -126.7° -226.9° (20.9 mm) | -221.6° -321.8° (23.1 mm) | -280.7° -380.9° (24.8 mm) | -300.8° -401.0° (25.4 mm) | -280.7° -380.9° (24.8 mm) | -221.6° -321.8° (23.1 mm) | -126.7° -226.9° (20.9 mm) | 0° -100.2° (17.7 mm) |
| Row 6 | 17.5° -82.7° (17.2 mm) | -108.1° -208.3° (20.4 mm) | -202.3° -302.5° (22.7 mm) | -260.8° -361.0° (24.2 mm) | -280.7° -380.9° (24.8 mm) | -260.8° -361.0° (24.2 mm) | -202.3° -302.5° (22.7 mm) | -108.1° -208.3° (20.4 mm) | 17.5° -82.7° (17.2 mm) |
| Row 7 | 69.4° -390.8° (25.1 mm) | -53.4° -153.6° (19.1 mm) | -145.3° -245.5° (21.3 mm) | -202.3° -302.5° (22.7 mm) | -221.6° -321.8° (23.1 mm) | -202.3° -302.5° (22.7 mm) | -145.3° -245.5° (21.3 mm) | -53.4° -153.6° (19.1 mm) | 69.4° -390.8° (25.1 mm) |
| Row 8 | 153.6° -306.6° (22.8 mm) | 35.0° -65.2° (16.8 mm) | -53.4° -153.6° (19.1 mm) | -108.1° -208.3° (20.4 mm) | -126.7° -226.9° (20.9 mm) | -108.1° -208.3° (20.4 mm) | -53.4° -153.6° (19.1 mm) | 35.0° -65.2° (16.8 mm) | 153.6° -306.6° (22.8 mm) |
| Row 9 | 266.9° -193.3° (20.0 mm) | 153.6° -306.6° (22.8 mm) | 69.4° -390.8° (25.1 mm) | 17.5° -82.7° (17.2 mm) | 0° -100.2° (17.7 mm) | 17.5° -82.7° (17.2 mm) | 69.4° -390.8° (25.1 mm) | 153.6° -306.6° (22.8 mm) | 266.9° -193.3° (20.0 mm) |

APPENDIX C

| Phase difference; Phase from phase curve; (Probe length, l_i) | Column 1 | Column 2 | Column 3 | Column 4 | Column 5 | Column 6 | Column 7 | Column 8 | Column 9 |
|--|--------------------------------|---------------------------------|---------------------------------|---------------------------------|---------------------------------|---------------------------------|---------------------------------|---------------------------------|--------------------------------|
| Row 1 | 253.2° -207.9° (21.8 mm) | 145.7° -315.4° (23.9 mm) | 65.9° -35.2° (18.1 mm) | 16.6° -84.5° (19.3 mm) | 0° -101.1° (19.7 mm) | 16.6° -84.5° (19.3 mm) | 65.9° -35.2° (18.1 mm) | 145.7° -315.4° (23.9 mm) | 253.2° -207.9° (21.8 mm) |
| Row 2 | 145.7° -315.4° (23.9 mm) | 33.2° -67.9° (18.9 mm) | -50.7° -151.8° (20.8 mm) | -102.6° -203.7° (21.7 mm) | -120.2° -221.3° (22.0 mm) | -102.6° -203.7° (21.7 mm) | -50.7° -151.8° (20.8 mm) | 33.2° -67.9° (18.9 mm) | 145.7° -315.4° (23.9 mm) |
| Row 3 | 65.9° -35.2° (18.1 mm) | -50.7° -151.8° (20.8 mm) | -137.9° -239.0° (22.3 mm) | -191.9° -293.0° (23.4 mm) | -210.3° -311.4° (23.8 mm) | -191.9° -293.0° (23.4 mm) | -137.9° -239.0° (22.3 mm) | 50.7° -151.8° (20.8 mm) | 65.9° -35.2° (18.1 mm) |
| Row 4 | 16.6° -84.5° (19.3 mm) | -102.6° -203.7° (21.7 mm) | -191.9° -293.0° (23.4 mm) | -247.5° -348.6° (24.8 mm) | -266.3° -7.4° (17.3 mm) | -247.5° -348.6° (24.8 mm) | -191.9° -293.0° (23.4 mm) | -102.6° -203.7° (21.7 mm) | 16.6° -84.5° (19.3 mm) |
| Row 5 | 0° -101.1° (19.7 mm) | -120.2° -221.3° (22.0 mm) | -210.3° -311.4° (23.8 mm) | -266.3° -7.4° (17.3 mm) | -285.3° -26.4° (17.9 mm) | -266.3° -7.4° (17.3 mm) | -210.3° -311.4° (23.8 mm) | -120.2° -221.3° (22.0 mm) | 0° -101.1° (19.7 mm) |
| Row 6 | 16.6° -84.5° (19.3 mm) | -102.6° -203.7° (21.7 mm) | -191.9° -293.0° (23.4 mm) | -247.5° -348.6° (24.8 mm) | -266.3° -7.4° (17.3 mm) | -247.5° -348.6° (24.8 mm) | -191.9° -293.0° (23.4 mm) | -102.6° -203.7° (21.7 mm) | 16.6° -84.5° (19.3 mm) |
| Row 7 | 65.9° -35.2° (18.1 mm) | -50.7° -151.8° (20.8 mm) | -137.9° -239.0° (22.3 mm) | -191.9° -293.0° (23.4 mm) | -210.3° -311.4° (23.8 mm) | -191.9° -293.0° (23.4 mm) | -137.9° -239.0° (22.3 mm) | 50.7° -151.8° (20.8 mm) | 65.9° -35.2° (18.1 mm) |
| Row 8 | 145.7° -315.4° (23.9 mm) | 33.2° -67.9° (18.9 mm) | -50.7° -151.8° (20.8 mm) | -102.6° -203.7° (21.7 mm) | -120.2° -221.3° (22.0 mm) | -102.6° -203.7° (21.7 mm) | -50.7° -151.8° (20.8 mm) | 33.2° -67.9° (18.9 mm) | 145.7° -315.4° (23.9 mm) |
| Row 9 | 253.2° -207.9° (21.8 mm) | 145.7° -315.4° (23.9 mm) | 65.9° -35.2° (18.1 mm) | 16.6° -84.5° (19.3 mm) | 0° -101.1° (19.7 mm) | 16.6° -84.5° (19.3 mm) | 65.9° -35.2° (18.1 mm) | 145.7° -315.4° (23.9 mm) | 253.2° -207.9° (21.8 mm) |